Testing models of cortical area MT

TESTING MODELS
OF CORTICAL AREA MT

VALERIO MANTE

MAY-SEPTEMBER, 2000

DIPLOMA THESIS

AT THE INSTITUTE OF NEUROINFORMATICS,

ETH/UNI ZURICH,

SWITZERLAND

PROF. RODNEY J. DOUGLAS

SUPERVISED BY DR. MATTEO CARANDINI

Acknowledgments

My greatest thanks go to Matteo Carandini. He spent many hours in discussions on this thesis, and was always available for explanations and help. I guess he is close to being the perfect supervisor. I have learned a lot from him already during these few months and it has been a great pleasure to work with him.

Thanks also to Najib Majaj, for some crucial advice during the writing of the thesis, but mostly for the opportunity to work on a little part of the incredible data collected by he and his colleagues. I really had an easy job compared to the nights he spent watching hundreds of stimuli.

Finally, thanks to Rodney Douglas and Kevan Martin and to all the members of the Institute of Neuroinformatics. The very pleasant atmosphere during these months at the institute had an important part in convincing me to remain loyal to my home country for some more time.

ABSTRACT

The visual motion of rigid objects can be analyzed through two stages, one that responds to the oriented image components, and one that finds the motion consistent with these components (method of intersection of constraints). These stages are considered to correspond to two classes of neurons in cortical area MT. Neurons are commonly classified by comparing their direction tuning for a plaid (composed of two drifting sinusoidal gratings) with the predictions of two *abstract models*. The response of the "component-direction-selective" model is just the sum of the responses to the plaid components alone. By contrast, the "pattern-direction-selective" model predicts the same direction tuning for gratings and plaids, and computes the direction of a plaid with the intersection of constraints method.

More recently Simoncelli and Heeger (1998) proposed physiologically more detailed models (hereafter the *SH models*) for both type of MT cells. In these models, MT cells combine the output of appropriate model V1 cells selected by an intersection of constraints rule. These models account qualitatively for a wide range of phenomena, but both their large number of parameters and the fact that their response is not given in a closed equation form make them difficult to fit to data.

We have tested all these models by fitting large data sets obtained by Majaj, Carandini & Movshon (1998) in area MT of paralyzed, anesthetized macaques. Stimuli included drifting gratings and plaids with (1) variable direction of the two components; (2) variable direction of the first grating and variable contrast of the other. The abstract models were extended with a simple form of contrast-dependence and with a contrast-gain control mechanism acting through divisive inhibition (normalization), while closed form equations were developed for a reduced form of the SH models.

The abstract model for component-direction selective cells extended with a contrast gain control correctly predicted the responses of a subset of cells. By contrast, even though it had the largest number of free parameters, the abstract model for pattern-direction selective cells was generally inferior to all the other models. This was particularly evident for those stimuli in which gratings had different contrasts. However, these data sets are possibly strongly influenced by contrast adaptation in area V1, an effect that has not been modeled in this study.

Our results support the SH models, which together correctly predicted the responses of a large fraction of cells. The predictions of the abstract and the SH models for component-direction selective cells were similar if both were provided with a gain control. On the other hand, on a subset of cells, the SH model for pattern-direction selective cells performed better than all the other models.

Our results further confirm that stimuli often used for the classification of MT cells may be inadequate. Indeed, the predictions of the SH pattern-direction selective and component-direction selective models are substantially different only for slow moving gratings, not for fast moving gratings.

1 Introduction

Motion is one of the most important features in a visual image, and allows us to infer fundamental information about the world surrounding us. For example, from the analysis of visual motion we get information about the boundaries, the movement and the rigidity of objects in the scene, we can locate them in a three-dimensional space, and we can deduce our self-motion inside this space.

In macaque monkeys cortical area MT plays a central role in the perception of motion. Area MT contains a large number of cells that are selective for the motion of a pattern ("pattern" cells), unlike earlier stages involved in motion processing, where the cells are selective to the motion of the oriented components in the image ("component" cells). Movshon et al. (1983) distinguished these "component" and "pattern" cells by comparing the cell responses to gratings and to plaids. These authors have introduced two simple *abstract models* to test the hypothesis of the existence of cells truly selective to a pattern as whole. These models predict that for a "component" cell the response to a plaid is just the sum of the responses to the individual gratings. On the other hand a "pattern" cell shows the same direction tuning for gratings and for plaids. A possible computation underlying "pattern" cells is the method of intersection of constraints.

To better understand the computations underlying the responses of MT cells, we have analyzed large data sets of extracellular recordings in MT, recently measured by Majaj, Carandini and Movshon (1999). The stimuli used in the experiments are the superposition of two sinusoidal gratings, and explore a much wider range in stimulus space than earlier studies. In particular, these measurements allowed us to analyze the response of MT cells in the transition from a plaid to a grating. This transition has been measured either by progressively changing the orientation of the gratings or by progressively reducing the contrast of one of the gratings.

We have compared the data with the predictions of different models for component- and pattern-selective cells. To assess the ability of these models to explain the measured responses, we have also fitted the models to the data. The original abstract models proposed by Movshon et al. (1983) can be directly used to predict the responses only to a small subset of the stimuli analyzed in this study. Therefore we had to extend the original abstract models to our larger stimulus set. For instance, the contrast of the gratings composing our stimuli can vary in a wide range, unlike the situation in Movshon et al. (1983). Because the original abstract models are not provided with a dependence on the stimulus contrast, we had to extend them with such a dependence to be able to compare the predictions of the models over the entire set of stimuli. As in the original abstract models, for "pattern" cells we have chosen intersection of constraints

as the method underlying the computation of direction and speed. We have then used these extensions of the original models by Movshon et al. (1983) to fit our data.

In a second step we have further extended the abstract models by introducing a contrast gain control stage acting through divisive inhibition. We have derived a simple expression for the normalization signal that is common for all the stimuli. The resulting normalization signal is a function of the contrasts of the gratings and the angle between the gratings. Thus it considers the fact that the energy of two superimposed gratings abruptly changes when the two gratings have exactly the same orientation. This normalization stage added new important properties to the models and in particular allowed better predictions of the cell responses in experiments that involved different grating contrasts.

In addition to these abstract models, we have also considered more recent models. Simoncelli and Heeger (1998) have proposed models for pattern- and component-selective cells that compute the response to a visual stimulus in two stages. The first stage may correspond to primary visual cortex (V1), while the second stage takes place in area MT. Again the method of intersection of constraints (IOC) plays an important role for the responses of a model “pattern” cell. Indeed, the signals coming from the first stage of the computation are combined in MT following the rules of IOC.

These models by Simoncelli and Heeger (1998) have a large number of free parameters and their response is not given in a form that is suitable to fit the models to the data. Therefore we had to simplify the models and to derive closed equation forms of their responses. We have then used this reduced form of the original models to fit our large data sets.

2 Visual Motion

Images are the result of the projection of the three-dimensional world on the retina. Motion in the world may change the resulting light intensity distribution on the retina. In this chapter we will consider algorithms that use these changes in the intensity distribution to compute an approximation of the motion field called **optical flow**. We will distinguish three different approaches:

1. Gradient based techniques
2. Spatio-temporal filtering techniques
3. Frequency domain approaches

We will follow the arguments of Simoncelli (1993) and see that all these apparently different approaches are essentially equivalent, in the sense that they are all composed of the same three stages. First a linear filtering (convolution), then a quadratic combination of the outputs of the linear stage, and finally a combination of the second stage outputs to estimate the velocity vector in a certain point. The main difference in the three approaches lies in the choice of the initial linear operators. At the end of the chapter we will discuss “intersection of constraints”, another method for the estimation of the velocity of an object. Again we will see that there is a strong link between this method and optical flow algorithms.

2.1 Optical Flow

Motion in the 3D-world usually results in changes in the 2D-intensity distribution on the retina. This temporal variation of the light intensity distribution f(x,y,t) is the main source of information for the computation of the motion field. The reconstruction of the original motion from the variations of f(x,y,t) are however not trivial. We have necessarily to make some approximations about the changes in the light intensity that are usually a good approximation in local regions of space.

Optical flow algorithms try to measure the apparent motion of local regions of image intensity patterns. The underlying assumption is that intensity patterns are always preserved. Several problems arise form this approach that is common to all the algorithms that we will discuss in this chapter. Here some examples of these problems:

- **Underconstrained regions**: in some situations, there is not enough information to determine a unique velocity for a given region. This happens in two cases, as shown in Figure 1A. First, in regions where the light intensity is constant. In this case, even if the object as a whole is moving, the optical flow in the considered region will be zero (“blank wall” problem). Second, when the intensity distribution in the considered local region is one-dimensional (i.e. varies only in one direction), then

only the component of the velocity perpendicular to the orientation of the intensity distribution will be constrained ("aperture problem"). In both cases the problem can usually be solved by choosing a larger local region for the computation of the velocity vector in the considered point.

- **Non-motion intensity changes**: when the overall lighting in the image is changing, then the basic assumption of intensity conservation is false. This is also the case when the reflectance of the considered object is changing, for example because of a change in orientation with respect to the light source.
- **Non-translational motions**: violations to the assumption of purely translational motions arise for example in regions that lie on an occlusion boundary (Figure 1B) or when two patterns are moving transparently one over the other (Figure 1C). In this case the problem is that a single velocity vector is not enough to describe the motion in the considered region.

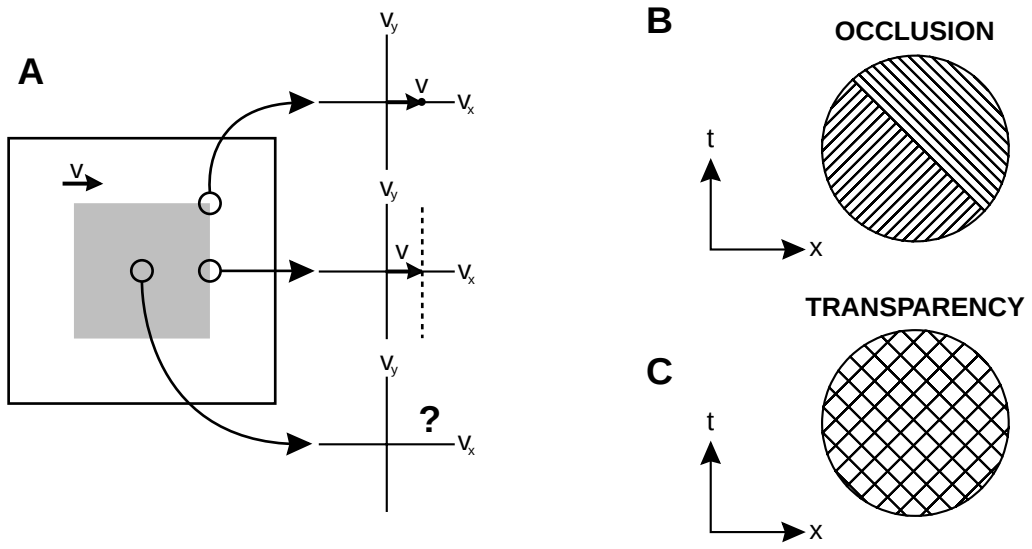

Figure 1, Motion signals in an image. A: a square moving with constant speed v. An optical flow algorithm acts on local regions in the image, illustrated as circles. Regions of constant intensity don't allow any prediction about the underlying motion. One-dimensional stimuli constrain the velocity to a line, the constraint line. Only at the corners of the square the velocity can be determined. B & C : situations for which the motion field representation (i.e. only one velocity per point) is inadequate. B: a rightward moving pattern is occluded by leftward moving pattern. C: two patterns moving in opponent directions move transparently one over the other. The figure is taken from Simoncelli (1993).

2.2 Optical Flow Algorithms

2.2.1 Differential Techniques

A first approach for the computation of the optical flow is given by differential techniques. The standard assumption underlying differential techniques is that all changes in the intensity distribution f(x,y,t) are due to rigid translations of local intensities:

$$f(x,y,t) = f(x + v_x \cdot \Delta t, y + v_y \cdot \Delta t, t + \Delta t)$$

where (v_x,v_y) is the velocity vector in the point (x,y). Taylor expansion of the right side of this equation gives:

$$f(x + v_x \cdot \Delta t, y + v_y \cdot \Delta t, t + \Delta t) \approx f(x,y) + \frac{\partial f}{\partial x} v_x + \frac{\partial f}{\partial y} v_y + \frac{\partial f}{\partial t} = f(x,y) + \vec{f}_s \cdot \vec{v} + f_t$$

where $\vec{f}_s = (f_x, f_y)$ is the spatial gradient of f, and subscripts indicate the variable with respect to which we have derived. By combining this two equations we obtain the **gradient constraint equation**:

$$\frac{\partial f}{\partial x} v_x + \frac{\partial f}{\partial y} v_y + \frac{\partial f}{\partial t} = 0 \qquad (1)$$

Equation (1) is insufficient for computing the optical flow, because it provides a single linear equation for two variables. Because its solutions (v_x,v_y) lie on a line in the two-dimensional velocity space the equation constrains only the normal velocity. The normal velocity is the component of the velocity parallel to the spatial gradient of the considered local intensity patch.

One possibility to find a unique velocity in each point is to combine the information given by equation (1) locally. The idea is to find the velocity (v_x,v_y) most consistent with all the normal constraints given by equation (1) in a small region around the point of interest. The underlying assumption is that all points in this region share a common velocity. We can introduce a function E of the form:

$$E(\vec{v}) = \sum_i w_i \left[\vec{f}_s(x_i, y_i, t) \cdot \vec{v} + f_t(x_i, y_i, t) \right]^2$$

where we are summing over a local region defined by the positive weights w_i , and we are assuming that the intensity f is sampled in the positions (x_i,y_i). To find the velocity $\vec{v}$ most consistent with the individual gradient constraint equations, we have to find a minimum of $E(\vec{v})$, i.e. the gradient of $E(\vec{v})$ must be zero:

$$\vec{\nabla}_{\vec{v}} E(\vec{v}) = 0 \quad \Rightarrow \quad M\vec{v} = \vec{b}$$

with:

$$M = \begin{pmatrix} \sum f_x^{\,2} & \sum f_x f_y \\ \sum f_x f_y & \sum f_y^{\,2} \end{pmatrix} \quad \vec{b} = \begin{pmatrix} \sum f_x f_t \\ \sum f_y f_t \end{pmatrix} \tag{2}$$

where we have written $\sum$ instead of the weighted sum $\sum_i w_i$.

As we can see, if the matrix M is invertible, it is possible to find a unique velocity by combining locally the gradient constraints. It is possible to show that in the two underconstrained cases, i.e. when f is one-dimensional or constant, the matrix M is singular, and we can't find a unique velocity.

2.2.2 Spatio-Temporal Filtering Techniques

Another approach for the computation of the optical flow is based on linear filters oriented in space-time. The basic observation underlying this approach is that motion corresponds to orientation in x-y-t space. This fact is illustrated in Figure 2 for a vertical dark bar moving with constant speed on a uniform background. Because the stimulus is one-dimensional, i.e. constant along the y-direction, it is enough to consider the (x,t) components of the light intensity distribution f(x,y,t). In this representation the moving bar is represented by a line, with the inverse of the slope proportional to the normal velocity of the bar.

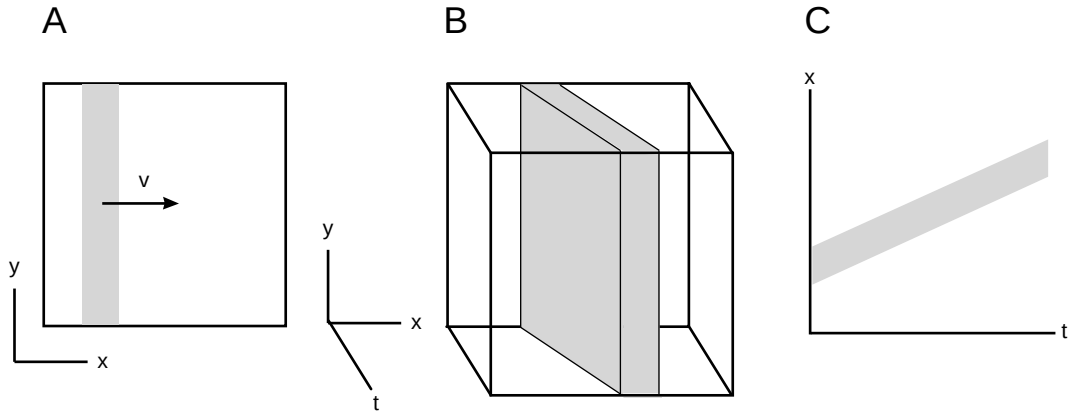

Figure 2, Motion and orientation in space-time, for a dark bar moving on a uniform background. The plots show the intensity distribution f(x,y,t) in different subspaces of the space-time (x,y,t). The stimulus is one-dimensional, so the (x,t) representation in C contains al the information about the intensity distribution. From Carandini et al. (1999).

To detect the moving bar it is possible to use an oriented filter that is matched to the velocity of the bar. One possible form for such a filter is shown in Figure 3 together with the varying output of the filter for two different directions of motion of the bar.

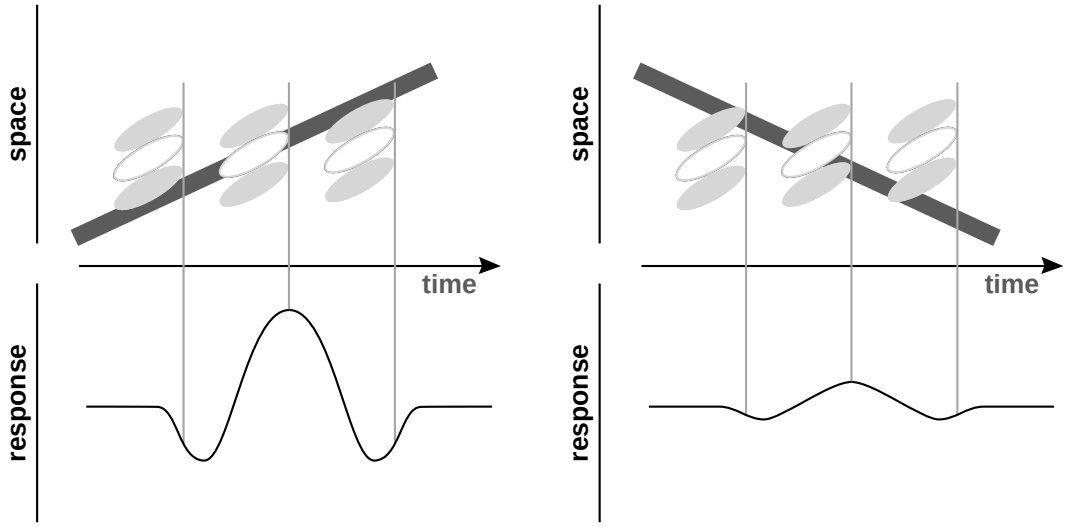

Figure 3, Time varying response of a linear filter oriented in space-time. The response is given by the convolution of the stimulus with the filter. For a causal filter, only events in the past contribute to the response in the present. Dark areas indicate inhibitory regions, light areas indicate excitatory regions. The response amplitude is large for a stimulus aligned to the filter (i.e. the stimulus is moving in the preferred direction of the filter with the best speed). From Wandell (1995).

Some problems arise if we try to use directly the output of the linear filter to estimate velocity. First, the amplitude and sign of the response vary in time (Figure 3). For example, if the stimulus consists of a sinusoidal grating, the response will also vary sinusoidaly in time. As a result, the instantaneous response cannot be used directly as a measure of velocity. Second, the sign of the response depends on the contrast of the stimulus, so that for example a black bar and a white bar moving in the same direction will elicit inverted responses. And third, in two dimensions the filter response depends on the orientation of the stimulus.

The two first problems can be partially solved by combining the outputs of more than one filter, as proposed by Adelson and Bergen (1985). The idea is to sum the squared responses of a pair of filters with the same amplitude responses, but with phases that are shifted by 90 deg. Such a pair of filters is called a **quadrature pair**. An example of a quadrature pair is given by two Gabor functions (i.e. the product of a sinusoid with a gaussian), one with cosine (even) phase, the other with sine (odd) phase. If we consider one-dimensional stimuli, it is enough to consider one spatial dimension, and an example of a quadrature pair is given by:

$$G_e = \cos(\omega_x x + \omega_t t)\cdot \exp\left(-\frac{{\omega_x}^2 + {\omega_t}^2}{2\sigma^2}\right) \text{ and } G_o = \sin(\omega_x x + \omega_t t)\cdot \exp\left(-\frac{{\omega_x}^2 + {\omega_t}^2}{2\sigma^2}\right) \quad (3)$$

The sum of the squared outputs of the even- and odd-symmetric filters is independent on the sign of the contrast, and is constant in time for a drifting sinusoidal intensity

distribution, as shown in Figure 4. As we will see in the section on frequency approaches, the sum of the squared outputs of a quadrature pair can be considered as an estimate of the local energy of the stimulus in the spatio-temporal frequency band determined by the amplitude responses of the two filters. Because of this property, models based on a similar combination of squared outputs are called **energy models.**

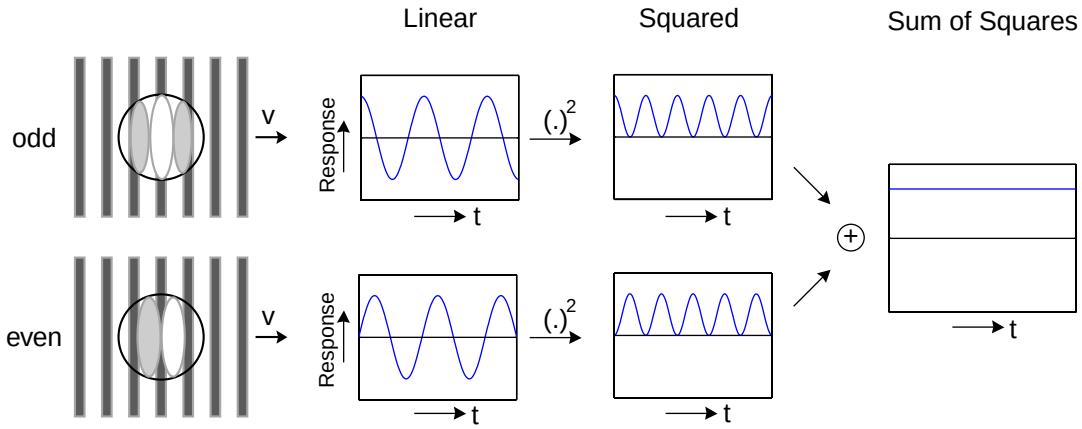

Figure 4, Combination of the squared outputs of a quadrature pair. The response of a linear filter to a sinusoid is again a sinusoid. The sum of the squared responses of the quadrature pair is constant in time for a sinusoidal input.

The output of such a motion detector is independent on the sign of the contrast, but does still depend on the amplitude of the contrast. For example, the detector will give a weak response for a stimulus moving too fast or too slow with respect to the preferred speed of the detector, but also if the contrast amplitude of the stimulus is very. As a result, the detector confounds velocity with contrast. Adelson et al. (1986) have also proposed a mechanism for computing a signal monotonically related with speed that is independent on the contrast amplitude. In one dimension this mechanism performs the following computation:

$$v \sim \frac{\sum\left(R_o^{\,2} + R_e^{\,2}\right) - \sum\left(L_o^{\,2} + L_e^{\,2}\right)}{\sum\left(S_o^{\,2} + S_e^{\,2}\right)} \qquad (4)$$

where R indicates the output of a filter tuned for rightward motion, L for leftward motion and S for stationary stimuli. The subscripts e and o indicate even or odd symmetric filters. Equation (1) combines the outputs of two quadrature pairs tuned for opposite directions, and discards the effects of contrast by normalizing with the response of a quadrature pair tuned to stationary stimuli.

In summary, we have seen that the optical flow can be computed in three stages: first a convolution with oriented filters, then the combination of the squared linear outputs

estimates the local energy of the stimulus, and finally a combination of the second stage outputs measures the local velocity.

2.2.3 Derivatives as Oriented Filters

In the two previous sections, we have considered two apparently very different methods for the estimation of the optical flow: methods using derivatives in space-time and methods based on linear filters oriented in space-time. Now we will follow the arguments in Simoncelli (1993) to see that, upon close examination, these two approaches are essentially equivalent.

The first observation is that a derivative is a linear shift invariant operator, and we can therefor see it as a convolution operation. Consider a one-dimensional function f(x), sampled in the set of points {n}. The derivative is an operator that acts on continuous functions. Before applying it to f, we have to interpolate the sampled function to make it a continuous function. We can do this by performing a convolution of the sampled version of f with a continuous interpolation function G(x). We will call this function a prefilter. When we apply the derivative on the interpolated version of f, and consider only the values of the derivatives at the original sampling points {n}, we obtain:

$$\frac{d}{dx} f(x) = \frac{d}{dx}\left[\sum_m f(m) G(x-m)\right]_n = \sum_m f(m) \frac{dG}{dx}(n-m)$$

and we see that the derivative of f is given by the convolution of f with a derivative kernel, in this case G_x. This shows that a derivative can be seen as a filtering operation.

The second observation is that for a circularly symmetric filter function G the resulting derivative kernel is an oriented operator in space-time. Consider the x-y-t space, and a unit vector $\hat{u}$ in it. The derivative in the $\hat{u}$-direction can be written as:

$$f_{\hat{u}} = \left(\hat{u} \cdot \vec{\nabla}\right) f = \hat{u} \cdot \begin{pmatrix} f_x \\ f_y \\ f_t \end{pmatrix} \qquad (5)$$

where $\vec{\nabla}$ is the spatio-temporal gradient operator:

$$\vec{\nabla} = \begin{pmatrix} \partial_x \\ \partial_y \\ \partial_t \end{pmatrix}$$

It is easy to see that, for a circularly symmetric prefilter, the function $\left(\hat{u} \cdot \vec{\nabla}\right) f$ is oriented perpendicularly to the direction $\hat{u}$.

The standard motion gradient equation (1) can now easily be written as a convolution with an oriented filter, just by observing that :

$$v_x f_x + v_y f_y + f_t = \left(\hat{u}(v) \cdot \vec{\nabla}\right) f$$

where:

$$\hat{u}(\vec{v}) = \left(v_x, v_y, 1\right)^T$$

The elements of M and $\vec{b}$ in equation (2) can be written as a local average of the square of a directional (derivative) filter, or the difference of two such squares, just as in the Adelson and Bergen's formulation in equation (4). For a detailed discussion see Simoncelli (1993).

We can conclude that the derivative and oriented filtering approaches are equivalent, in the sense that they consist of the same three stages of linear filtering, squaring and combing the outputs of squared filters.

2.2.4 Frequency-Domain Approaches

As a last approach for the estimation of the optical flow, we will consider methods based on a frequency domain description as discussed by Watson and Ahunada (1983).

Basic Observations

Consider the Fourier transform of an arbitrary function f(x,y,t) in space-time:

$$F(\vec{k}, \omega) = \int d\omega d\vec{k} \cdot f(\vec{r}, t) e^{i\vec{k}\vec{r} - i\omega t}$$

where $\vec{r} = (x, y)$, $\vec{k} = (k_x, k_y)$ are the spatial frequencies and ω is the temporal frequency.

Now consider an intensity distribution f(x,y,t) that undergoes rigid translation with constant velocity $\vec{v}$, so that f can be written as:

$$f(x, y, t) = f(x - v_x \cdot t, y - v_y \cdot t, t = 0)$$

In this particular case we find that:

$$F(\vec{k}, \omega) = f(\vec{k}) \delta(\vec{k} \cdot \vec{v} - \omega)$$

The Dirac-delta function δ is different from zero only when:

$$k_x v_x + k_y v_y = \omega \qquad (6)$$

This is the equation of a plane in frequency space. As a result, the power of an intensity distribution undergoing rigid translation lies on a plane in frequency space. If we consider the equation of the plane in the form:

$$w(\vec{v}) \cdot \begin{pmatrix} \vec{k} \\ \omega \end{pmatrix} = 0 \qquad (7)$$

it is clear that the defined plane goes through the origin and is perpendicular to the vector $w = (v_x, v_y, -1)^T$. These issues are discussed in detail for example by Watson and Ahumada (1983).

Transfer function of oriented filters

In the previous sections we have considered linear filters oriented in space-time. As an example for these kind of filters, we have seen Gabor-functions (equation (3)) and spatio-temporal derivatives of a circularly symmetric prefilter function (equation (5)). These are linear shift-invariant operators, and their response is given by the convolution of the filter with the intensity distribution f(x,y,t). Instead of computing the filter response using the space-time representation, we can use the frequency space representation, i.e. the Fourier transform of the filters and of f(x,y,t).

As an example of oriented filter we can consider a three-dimensional Gabor filter. The equation of this filter is a straightforward generalization of the two-dimensional case in equation (3), just with two spatial frequencies k_x and k_y instead of one. This filter is clearly tuned for the orientation and spatial frequency of the stimulus, because of the underlying spatial sinusoid. The transfer function is significantly different from zero only in two regions of the frequency space in symmetric positions with respect to the origin. As a result, the filter has a preferred spatial frequency k_0, a preferred direction of motion θ and a preferred temporal frequency ω_0, where:

$$\vartheta = \arctan\left(\frac{k_y}{k_x}\right) \quad \text{and} \quad {k_0}^2 = {k_x}^2 + {k_y}^2$$

The link between an amplitude response of this form and the selectivity for a sinusoidal grating with a particular spatial frequency, orientation and speed is easily understood when we consider the Fourier transform of a drifting sinusoid. We can write the equation of a drifting sinusoid in space-time as:

$$\sin\left(\vec{k}_s \cdot \vec{x} - \omega_s \cdot t\right) = \frac{1}{2i}\left(e^{i\vec{k}_s \cdot \vec{x} - i\omega_s \cdot t} - e^{-i\vec{k}_s \cdot \vec{x} + i\omega_s \cdot t}\right)$$

where $k_s = |\vec{k}_s|$ is the spatial frequency, ω_s is the temporal frequency of the sinusoid. Just by applying the definition, we obtain the Fourier transform of the sinusoid:

$$F(\vec{k},\omega) \propto \left[\delta(\vec{k}-\vec{k}_s)\cdot\delta(\omega-\omega_s) - \delta(\vec{k}+\vec{k}_s)\cdot\delta(\omega+\omega_s)\right]$$

and we see that the power of the sinusoid is different from zero only in the points $(\vec{k}_s,\omega_s)$ and $(-\vec{k}_s,-\omega_s)$.

However, the normal velocity of a sinusoid eliciting the highest filter response depends on the spatial frequency. It is easy to see that the normal velocity of the sinusoid is given by:

$$v = \frac{\omega_s}{k_s} \tag{8}$$

Because the preferred temporal frequency of the filter is always ω_0, independently of the spatial frequency k_s of the sinusoid the preferred normal velocity of the sinusoid is:

$$v_{pref} = \frac{\omega_0}{k_s}$$

a function of k_s.

Heeger (1987) proposed to compute the optical flow by interpolating the energy distribution of the stimulus with a plane. The best fitting plane corresponds to the velocity most consistent with the one-dimensional motions in the image. Again these methods are strongly related to those we have already seen. Simoncelli (1993) shows that, in the case of constant weights w_i (i.e. a global computation of velocity), the basic gradient solution of equation (2) operates as a regression algorithm, seeking the plane that best accounts for the derivative measurements.

Quadrature pairs

In the case of a local computation of the velocity we need a local estimate of energy. One possibility for these estimate is to use the output of a quadrature pair. In space-time, we have defined a quadrature pair as two linear filters with the same amplitude responses, but with phases that are shifted of 90 deg. The sum of squared responses of such a pair gives a response to drifting sinusoidal gratings that is constant in time and independent of the contrast polarity of the stimulus, as we have already seen in the model proposed by Adelson (1985). In fact the response of this mechanism is proportional to the energy of the sinusoid.

Usually, energy and phase of a function f(x) are defined through the Fourier transform F(k) of the function. We can write F(k) as:

$$F(k) = A(k) \cdot e^{i\Phi(k)}$$

$$A^2(k) = \mathrm{Re}^2\big(F(k)\big) + \mathrm{Im}^2\big(F(k)\big), \qquad \Phi(k) = \arctan\frac{\mathrm{Im}\big(F(k)\big)}{\mathrm{Re}\big(F(k)\big)}$$

where A^2 is the energy of the function, Φ the phase. The real and imaginary parts of the Fourier transform F(k) are given by:

$$\mathrm{Re}\big(F(k)\big) = \int dx f(x)\cos(kx), \qquad \mathrm{Im}\big(F(k)\big) = \int dx f(x)\sin(kx)$$

where we integrate over the whole space.

To compute motion locally using energy models like those described in this chapter, we need a local estimate of stimulus energy. We cannot use the Fourier transform for that, because it is defined globally. But in analogy to the global definition of energy and phase, we can define them locally with the response of a quadrature pair. The expressions of the real and imaginary parts of the Fourier transform can be interpreted as a projection of the function f(x) on two base functions, i.e. cos(x) and sin(x). For a local estimate of energy and phase, instead of using the projections on this two basis functions, we will use the projections on a quadrature pair localized in space.

In frequency space a quadrature pair is characterized by the following expression:

$$G_2(k) = -i \cdot sign(k) \cdot G_1(k)$$

where G_1 and G_2 are the transfer functions of the two filters forming the quadrature pair. This definition of local energy and local phase will give the correct result for a sinusoidal input signal, i.e. they will correspond to the squared amplitude and the phase of the sinusoid.

2.3 Intersection of Constraints

In this chapter we have discussed three different algorithms for the computation of the optical flow, and we have seen that they are in many aspects equivalent. To conclude this discussion we will consider a different approach for the computation of visual motion called intersection of constraints, and relate this method to the optical flow algorithms previously discussed.

As we have seen in previous sections, only the normal velocity of a one-dimensional stimulus is constrained by observations. All the velocities consistent with the observed normal velocity of the stimulus lie on a line in velocity space, called constraint line. However, it is possible to infer the velocity of a rigidly moving object by combining the

constraint lines of its one-dimensional components, or more precisely by looking for the intersection of all constraint lines. If the stimulus motion consists of a rigid translation, then all the constraint lines will cross in a single point, which corresponds to the velocity of the stimulus as a whole. This velocity is the only one consistent with the normal velocities of all the components. This procedure is called intersection of constraints (IOC), and is illustrated for the example of a plaid in Figure 5.

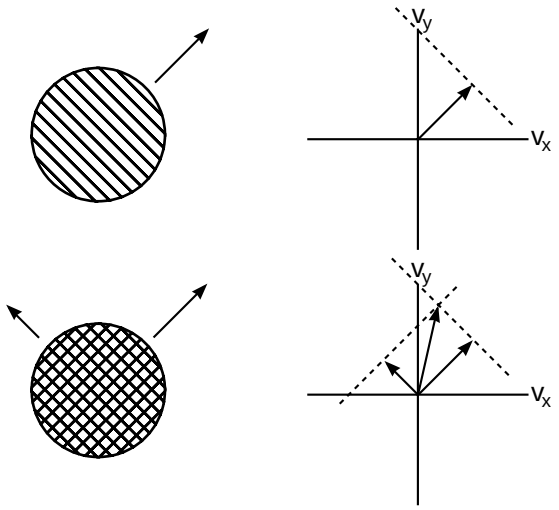

Figure 5, The computation of motion with intersection of constraints. Top: the motion of a one-dimensional stimulus is constrained to a line in velocity space, the constraint line. Bottom: for a rigidly translating stimulus the constraint lines of all one-dimensional components have a common point, corresponding to the velocity of the stimulus.

Intersection of constraints is not only useful for simple stimuli like a plaid. In fact, every image, through Fourier transform, may be seen as composed of one-dimensional stimuli, the Fourier components of the image. By applying IOC to the Fourier components of the image, we can deduce the velocity of the image as a whole. This observation is of crucial importance for biological systems like humans, because there is evidence that the visual system performs a local decomposition of the image in Fourier components in the first stages of the image analysis. If the mechanisms responsible for the computation of the velocity field use the outputs of these first stages, they could do it with IOC.

We can now easily understand the relation between IOC and the frequency domain approaches for the computation of the optical flow. Remember that the power of a rigidly translating intensity distribution lies on a plane, so that the temporal and spatial frequency of the Fourier components of the image are connected through equation (6). We can write this equation in a slightly modified form:

$$\hat{k} \cdot \vec{v} = \frac{\omega}{k}$$

where $\vec{v}$ is the velocity of the intensity distribution and $\hat{k}$ is a unit vector perpendicular to the orientation of the considered sinusoid. By using the expression for the normal velocity in equation (8), we see that the velocity of the whole image lies on the constraint line of every single one-dimensional component, so that it is given by the intersection of all these lines.

3 Physiology

It is widely held that the brain contains specific mechanisms for the processing of motion, and that this processing occurs in a motion pathway consisting of at least two stages. The primary visual cortex (V1) constitutes the first stage, and the outputs of V1 are sent to the second stage, i.e. the middle temporal (MT or V5) visual area.

Neurons in area V1 are selective for orientation and direction of motion of the stimulus (see for example Hubel and Wiesel 1962), and have small receptive fields. V1 cells respond to the oriented component in the image lying in their receptive field and moving with their preferred direction and orientation. Therefore, the output of V1 consists of local information about the motion of one-dimensional components of the image. These one-dimensional features need to be integrated over different orientations and over space by a later stage. We have already seen this problem in the previous chapter, for example in Figure 1, where the circles indicating the local regions of motion processing can be taken to indicate the receptive fields of different V1 neurons.

A candidate site for the integration of the local one-dimensional motion features is primate area MT. Many neurons in MT are tuned for retinal image velocity: they respond vigorously to a visual stimulus moving in a particular direction with a particular speed, and are somewhat indifferent of the stimulus' spatial pattern (Movshon et al., 1983). Moreover it has been possible to establish a strong link between neural activity in MT and perception of motion (for example Newsome et al. 1988; Britten et al. 1992; Salzman et al. 1992).

In this chapter we want to review some of the models that have been proposed for the response properties of neurons in V1 and MT. We will first introduce a linear model of V1 neurons extended with a rectification and normalization stage. Then we will consider some important properties of MT neurons, in particular the distinction in pattern-direction-selective cells and component direction selective cells. And finally we will review the models of MT cells recently proposed by Simoncelli and Heeger.

3.1 Cortical Area V1

V1 cells are selective for many characteristics of the visual stimulus, such as position, orientation, spatial and temporal frequency and direction of motion. For a review of the selectivity of V1 neurons see for example De Valois and De Valois (1988). V1 simple cells have been defined by Hubel and Wiesel (1962) as those neurons in V1 that respond either to the onset or the offset of the stimulus, but not to both. About 50% of V1 cells are simple cells. Many properties of V1 simple cells, and in particular their selectivity for orientation and spatial frequency, can be explained by a linear model (Heeger, 1992b; Heeger, 1992a). Some nonlinearities of V1 simple cells can be

explained by a rectification stage (Movshon et al., 1978). However, some important violations of linearity cannot be explained only with rectification. Examples of such nonlinearities are the responses saturation for high contrasts, and the fact that responses to an optimally oriented stimulus can be diminished by superimposing an orthogonal stimulus, which would be ineffective in driving the cell when presented alone (cross orientation inhibition, see Carandini et al. 1999).

It is possible to extend the linear model to account for these nonlinearities, without affecting the power of the original model in explaining the linear properties of V1 simple cells. The first necessary extension to the linear model is a rectification stage, that is a threshold in the transformation of the membrane potential into firing rates (Movshon et al., 1978). The second is a gain control mechanism acting through divisive inhibition from a population of other V1 cells (normalization). This extended linear model is shown in Figure 6. For the full description of the model and the ability in explaining qualitatively and quantitatively V1 simple cell responses see Heeger (1992a), and also Carandini et al. (1997) and (1999).

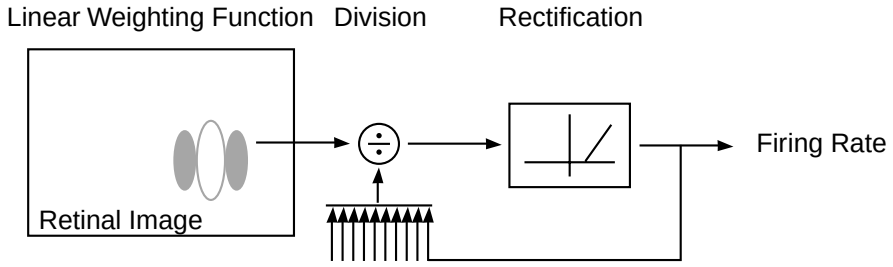

Figure 6, Linear model of V1 simple cells extended with rectification and normalization. From Carandini et al. (1999).

3.1.1 Linear Model

As in the previous section, we can describe the image on the retina as an intensity distribution f(x,y,t). This representation ignores the color of the stimulus and assumes monocular vision. Because we will consider only stimuli with constant mean intensity m, we can take light adaptation into account by considering the local contrast f:

$$f(x,y,t) = \frac{l(x,y,t) - m}{l(x,y,t)}$$

where l(x,y,t) is the luminance distribution. We use the term contrast for the maximal absolute value of f in a grating.

We can approximate the cell as a linear system at the level of the membrane potential. In this approximation, the membrane potential is given by:

$$L(t) = \int dxdyd\tau W(x, y, t) f(x, y, t - \tau)$$

where the weighting function W(x,y,t) is the impulse response of the cell. This weighting function W determines the selectivity of the cell, for example to the orientation and velocity of the stimulus.

3.1.2 Rectification

While the membrane potential of a simple cell may be a linear function L(t) of the stimulus intensity, the firing rate that the cell gives as an output must be nonlinear. Indeed, firing rates can have only positive values, while the linear response can be either positive or negative. Moreover, the spontaneous firing rate (corresponding to the resting potential) of V1 cells is very low, so that they cannot encode negative values of L(t).

The transformation of membrane potentials into firing rates can be approximated by rectification: the firing of the cell is proportional to the difference between the potential L(t) and a threshold potential V_{thres} when $L(t) > V_{thres}$, and is zero for $L(t) < V_{thres}$.

Complex cells

Complex cells have similar selectivity as simple cells, in particular they are selective for spatio-temporal orientation. However their responses are relatively independent of the precise stimulus position in the receptive field (Hubel and Wiesel, 1962). It is widely believed that complex cells are constructed from linear subunits, and that the subunit outputs are rectified before being combined into the complex cell response. In particular, it has been proposed that complex cells act like energy mechanisms that compute the sum of the squared outputs of a quadrature pair (Adelson and Bergen, 1985). Or, instead of summing the squared output of a quadrature pair, it is equivalent to sum the half-squared responses (first rectification, then squaring) of four cells with the same amplitude responses but with phases displaced by 90, 180 and 270 degrees (Heeger, 1992a).

For small responses the operation of rising the rectified linear response to a power $n > 1$ can be seen as an approximation of performing a rectification with a particular $V_{thres} > V_{rest}$. The approximation is even more precise when we consider also normalization. This means that complex cells, if they sum the rectified responses of underlying linear subunits, act like approximated energy mechanisms.

3.1.3 Normalization

Rectification of the linear responses cannot account for all nonlinearities of V1 neurons, like saturation of responses for high contrasts and cross-orientation inhibition. Different authors have proposed that these nonlinearities could be explained by a normalization stage. Heeger (1992b) proposed the following form for the normalized complex cell response C_i :

$$C_i(t) = k \frac{E_i(t)}{\sigma^2 + \sum_j E_j(t)} \qquad (9)$$

where σ is the semisaturation contrast, E_i is the non-normalized response of the considered complex cell and the sum is performed over a population of complex cells (normalization pool). The non-normalized complex cell response is given by the sum over the half-squared responses of four simple cells with the right phase relations, as described above:

$$E_i(t) = 1/4\left[A_i^{0}(t) + A_i^{90}(t) + A_i^{180}(t) + A_i^{270}(t)\right]$$

The sum in the denominator of equation (9) is proportional to the local energy of the image in a certain spatio-temporal frequency band, which is composed by the responses of all cells in the normalization pool. For gratings the local energy is proportional to the contrast c, so that the model correctly predicts the measured contrast responses (for example Sclar et al. 1990) of the form:

$$R = R_{\max} \frac{c^n}{\sigma^n + c^n} + M$$

where R is the evoked response, M is the spontaneous firing rate and R_{max} is the maximal attainable response. The mean value of n for V1 cells is close to n = 2, as it would be for ideal energy mechanisms (Sclar et al., 1990).

Carandini et al. (1997) have derived closed form equations for the responses of a biophysical implementation of the normalization model. Their model is able to fit large sets of stimuli, in particular the responses to plaids with variable contrast of the component gratings. The model response to a grating alone was given by:

$$amplitude(R) = \left\lfloor amplitude(L) \frac{c}{\sqrt{\sigma(f)^2 + c^2}} \right\rfloor^n \qquad (10)$$

where L is the response of the linear stage of the cell to a grating with unit contrast, $\sigma(f)$ is a function of the temporal frequency and n is the exponent of the rectification

stage. The response to a plaid composed of two gratings of contrast c_1 and c_2 is given by:

$$amplitude(R) \propto \left\lfloor \frac{amplitude(c_1 L_1(t) + c_2 L_2(t))}{\sqrt{\sigma(f)^2 + c_1^{\,2} + c_2^{\,2}}} \right\rfloor^n \qquad (11)$$

where L_1 and L_2 are the linear responses of the cell to the individual gratings at unit contrast.

Equations (10) and (11) do not become identical when $c_1 = c_2$. As a result, these equations are not consistent in the limit of two gratings with progressively smaller difference in the direction of motion. Let d_1 and d_2 be the direction of motion of the two gratings composing the plaid. In the limit $|d_1-d_2| \rightarrow 0$ the equation for the plaid responses should go into the response for a grating alone with contrast $c = c_1+c_2$. This is not the case for this expressions of plaid responses, that has been deduced for the case $|d_1-d_2| >> 0$. We will consider this problem again later, and introduce an expression for the normalization signal valid for all possible values of d_1 and d_2.

3.2 Cortical Area MT

According to the models discussed in the previous sections, neurons in V1 are selective only for one-dimensional components of the image. They are neither able to track the velocity of two-dimensional features, like a cross, nor to integrate the motion of the local one-dimensional components to the unique motion of an object as a whole. The situation is different in MT. In addition to a population of cells that are only selective to the motion of the components of an image, in MT there are also cells that are selective to the velocity of a stimulus as a whole. These two populations of cells have been distinguished on the basis of their responses to different set of stimuli. Movshon et al. (1983) have compared the responses of MT cells to gratings and to plaids, and were able to identify two classes of cells, called respectively pattern-direction selective cells and component-direction selective cells. Albright (1984) has used two different sets of stimuli, i.e. drifting spots and flashed bars, and again could identify two classes of cells, called type I and type II cells. Rodman and Albright (1989) have subsequently shown that the two different criteria identify the same set of cell populations in MT.

In this section we will consider the methods used for the characterization of pattern-direction and component-direction selective cells and discuss some of the difficulties inherent in these methods. We will discuss these concepts on the data sets collected by Majaj, Carandini and Movshon (1999). However, we will need only a small subset of the full data (see chapter 4).

3.2.1 Pattern and component cells

Movshon et al. (1983) have measured the responses of neurons in MT to two different set of stimuli: sinusoidal gratings and plaids (i.e. the superposition of two sinusoidal gratings). It is possible to define the preferred direction of motion of a cell as the direction for which a drifting grating evokes the largest response. Movshon et al. (1983) pointed out that a cell that is selective for the one-dimensional components of an image, like simple and complex cells in V1, should respond to a plaid only when one of the component gratings is moving in the preferred direction of the cell. They called this behavior **component-direction-selectivity**. On the other hand, a cell that is selective for the velocity of a pattern as whole should respond when the plaid is moving in the preferred direction, independently of the motion of the individual components. This behavior is called **pattern-direction-selectivity**. As we have seen, the velocity of the plaid can be defined with intersection of constraints. Whenever speaking of the direction of motion or speed of a plaid, we will refer to these quantities as those obtained with the method of intersection of constraints (IOC), and we will often speak of "component cells" and "pattern cells" to refer to component-direction-selective and pattern-direction-selective cells.

This distinction allows us to characterize cells by comparing the measured responses to plaids with the responses of a hypothetical pattern-direction-selective cell (a pattern cell) and a hypothetical component-direction-selective cell (a component cell). These hypothetical responses can be constructed with two simple models on the basis of the measured responses to gratings. The direction tuning for plaids of a model pattern cell is the same as the measured direction tuning for gratings. The direction tuning for plaids of a model component cell is just the sum of the direction tunings for the two gratings presented alone. The measured spontaneous firing rate is subtracted from the responses before summing them, and is added again after the sum.

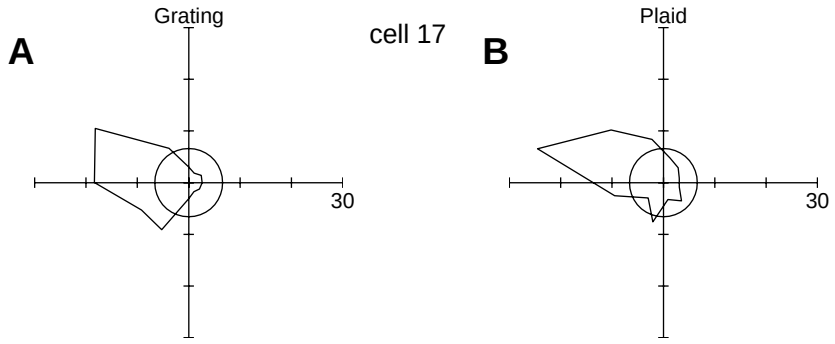

Figure 7, Polar representation of the measured direction tuning curves for gratings and plaids. The circle in both plots indicates the spontaneous firing rate of the cell.

In Figure 7 we show an example of the measured direction tuning for gratings and plaids. The responses are plotted in a polar representation: the distance of a point from the origin represents the firing rate in spikes per second, while the angle represents the direction of motion of the grating or plaid. The circles indicate the measured spontaneous firing rate of the cell.

We can now use the measured direction tuning for gratings to predict the model responses of a model component cell and of a model pattern cell to plaids and compare them with the measured direction tuning for plaids. This procedure is illustrated in Figure 8 for the same cell as in Figure 7. This cell is classified as pattern-direction-selective, because the direction tuning for plaids and for gratings are very similar, and in particular the direction tuning for plaids is not bimodal, as we would aspect for a component cell.

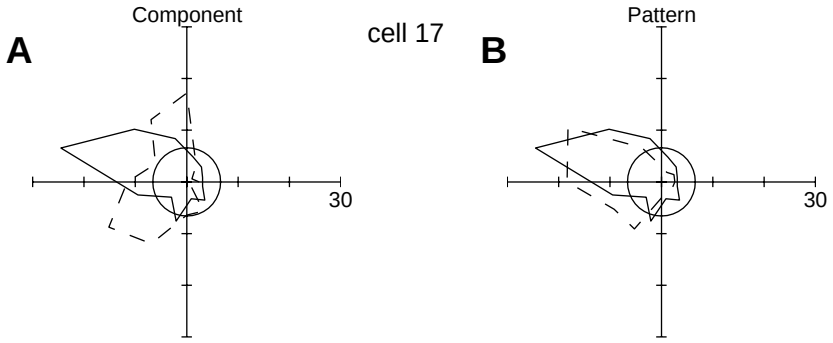

Figure 8, Comparison of the measured direction tuning for plaids with the predictions of the component and pattern models for a pattern cell. Rp = 0.87, Rc = -0.36.

An example of a component-direction-selective cell is shown in Figure 9.

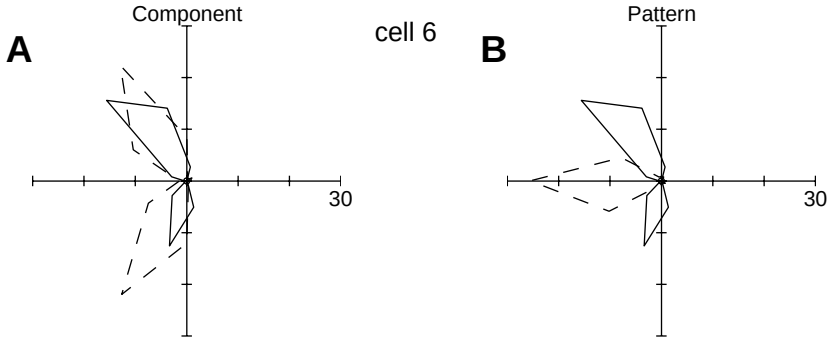

Figure 9, Comparison of the measured direction tuning for plaids with the predictions of the component and pattern models for a component cell. Rp = -0.30, Rc = 0.86.

3.2.2 Cell classification

We can now use this simple models for pattern and component cells to classify the measured cells, following the method proposed by Movshon et al. (1983). The idea is to

compute cross-correlations between the direction tuning for plaids and the tunings predicted by the models. To discard the effect of a possible correlation between the model responses we can compute partial correlations of the form:

$$R_p = \frac{r_p - r_c r_{pc}}{\sqrt{\left(1 - r_c^{\,2}\right)\left(1 - r_{pc}^{\,2}\right)}}$$

$$R_c = \frac{r_c - r_c r_{pc}}{\sqrt{\left(1 - r_p^{\,2}\right)\left(1 - r_{pc}^{\,2}\right)}}$$

where R_p and R_c are the partial correlations for the pattern and component predictions, r_p is the correlation of the data with the pattern prediction, r_c is the correlation of the data with the component prediction and r_{pc} is the correlation of the two predictions. The partial correlations for our population of 19 cell are shown in Figure 10A.

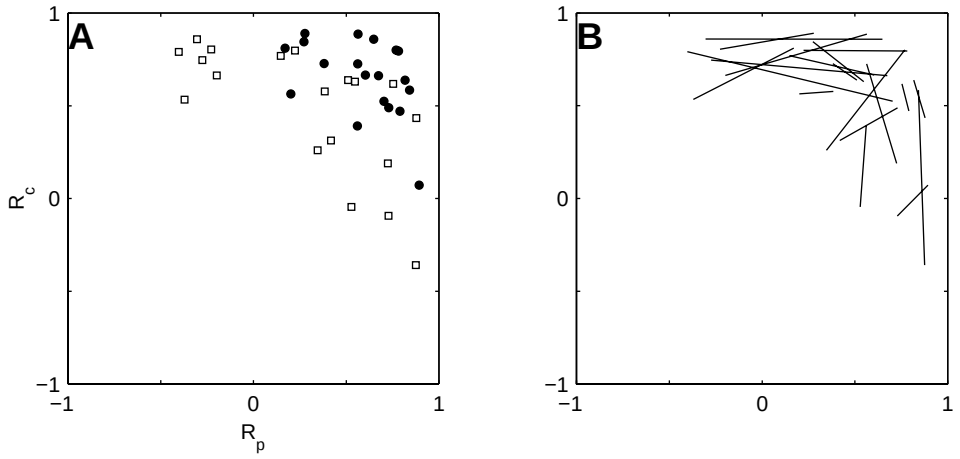

Figure 10, Influence of the plaid angle on the categorization. A: partial correlations of the pattern and model predictions for a plaid angle of 120 deg (black circles) and 150 deg (white squares). B: Each line connects the two points of (A) corresponding to the same cell, and thus illustrates the shift in the partial correlations due to the change of plaid angle.

The choice of the plaid angle to use for the computation of the partial correlations is somehow arbitrary. It is clear that for plaid angles that are much smaller than the direction tuning width for gratings we wouldn't see anymore the bimodality in the plaid-direction-tuning of a component cell. This should not be the case for the direction tuning curves shown until now, which have all been measured with a plaid angle of 120 degrees. However, to investigate the influence of the plaid angle on the classification of the cells, we have computed the partial correlations both with plaids of 120 degrees and plaids of 150 degrees. The result of the classifications are shown in Figure 10.

For most cells the partial correlations differ significantly for the two plaid angles. Following the methods of Movshon et al. (1983), the fraction of cells that are not classified decreases. On the other hand, the measurements with the 150 degree plaid do

generally not change the classification of cells that can be classified as “pattern” of “component” cells already with a plaid angle of 120 degrees. An example of the direction tunings for a cell that instead is classified in a completely different way with the two plaid angles is shown in Figure 11. This cell has direction tuning for gratings with a full width at half maximum of approximately 60 degrees. Even if in this case both plaid angles of 120 and 150 deg are large enough for the test, classification changes for the two different angles.

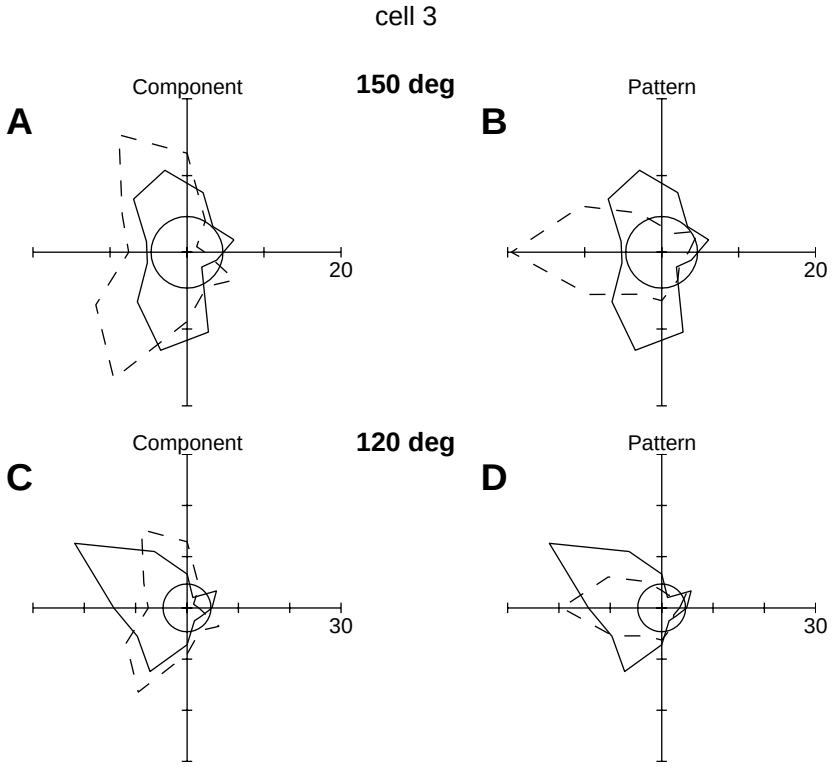

Figure 11, Dependence of the direction tuning for plaids on different plaid angles. The plaid angle affects also the categorization of the cell in pattern or component on the basis of the correlation between the model responses and the measurements. For a plaid of 150 deg : R_p = -0.4, R_c = 0.79; for a plaid of 120 deg : R_p = 0.70, R_c = 0.52 .

Some of the recorded cells show a bimodal direction tuning for gratings, as shown in Figure 12.

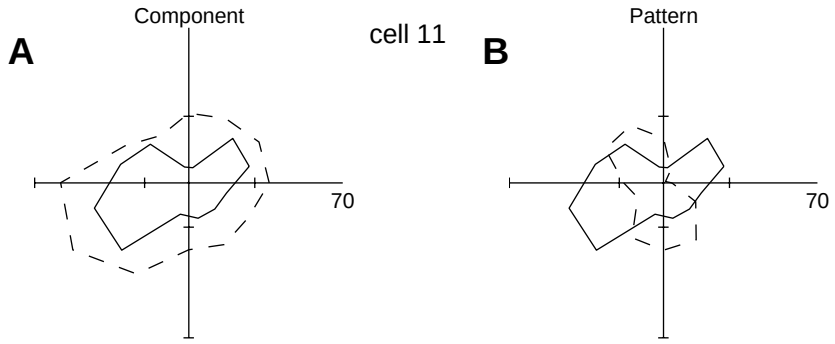

Figure 12, Example of a cell with a bimodal direction tuning for gratings, represented by the dashed line in B. The measured direction tuning for gratings is also the response predicted by the pattern model. The partial correlations for this cell are R_p = -0.20, R_c = 0.66.

As pointed out by Albright (1984), an hypothetical pattern-direction-selective detector that performs some form of intersection of constraints and that has a preferred velocity would produce a bimodal direction tuning for a grating moving slower than the preferred speed of the detector. The two peaks correspond to the directions of motion for one-dimensional components moving at this lower speed match the preferred velocity of the pattern-selective mechanism, as illustrated in Figure 13. There are many different velocities consistent with the measurable normal velocity of a one-dimensional stimulus (A). For a plaid (B), there is unique velocity v_s consistent with both normal velocities v_1 and v_2 of the components. A detector performing IOC with a preferred velocity $v_{pref} = v_s$ will respond to a grating alone when the grating is moving either with normal velocity v_1 or v_2. As a result, the direction tuning of such a detector measured with slow moving gratings will be bimodal. The cell in Figure 12 is thus a candidate for being truly pattern-velocity selective. However, on the basis of the partial correlations of the pattern and component model predictions, the cell would not be classified as pattern-velocity selective.

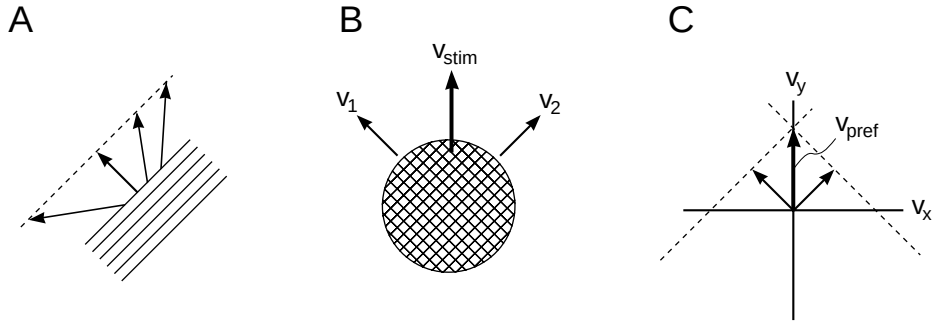

Figure 13, A motion detector performing IOC has bimodal direction tuning for slow moving gratings. See text for details.

By itself, bimodality in the direction tuning for slow moving gratings could be a good cue in the characterization of pattern cell. However, if we want to use the correlation

methods presented in the previous section, we have to chose a grating speed that is equal or higher than the preferred speed of the cell we are studying. As we will se, in our experiments the speed of the gratings is the same for the measurement of the direction tuning for gratings and for the direction tuning for plaids. Because of that, for grating speeds that are equal or larger than the preferred speed of the cell, the speed of the resulting plaid will always be larger then the preferred speed of the cell. Rodman and Albright (1989) avoided this problem by changing the grating speed so that the resulting speed of the stimulus as a whole (i.e. a grating alone or a plaid) was always the same.

To make quantitative predictions about the responses of a detector, it is not enough to say that the detector is performing intersection of constraints. IOC allows us to make some qualitative predictions about “good” stimuli and “bad” stimuli, but it doesn’t tell anything about the size of the responses to these stimuli. In particular we can’t say much about the response of a hypothetical pattern-motion selective detector to a plaid composed of two gratings both moving with the preferred speed of the cell, i.e. a plaid moving “too fast”. But we will now review a model of pattern-motion-selective neurons that allows us to make such quantitative predictions.

3.3 Simoncelli-Heeger Model

Simoncelli and Heeger have recently proposed a model for MT neurons based on a two stage processing (1998). The two stages correspond to areas V1 and MT. Both stages compute a weighted sum of their inputs followed by rectification and normalization. The V1 receptive field weights are designed for orientation and direction selectivity, while the MT receptive field weights are designed for velocity selectivity. Local image velocity is represented as a distribution of MT neuronal responses.

The model for pattern selective cells

The input to the model consists of a time-varying intensity distribution f(x,y,t), and the output is given by firing rates of a population of MT neurons.

The first stage, i.e. area V1, contains simple and complex cells. The computation of simple cells is the same as in Figure 6: the output of the linear stage is rectified with half-squaring and is normalized through divisive inhibition from a population of V1 cells. Complex cells are modeled as energy operators, i.e. they sum simple cell outputs to obtain a measure of the local energy in the stimulus in a given frequency band.

In the second stage, i.e. area MT, a velocity-selective cell is constructed by linearly combining the outputs of a set of direction selective V1 complex cells whose preferred space time orientations are consistent with the preferred velocity of the pattern cell, as

illustrated in figura. The output of the linear stage is again half-squared and normalized by the responses of a population of other MT pattern cells. This mechanism for velocity selectivity is a neuronal implementation of the intersection of constraints. It allows quantitative predictions about the responses to all stimuli, in particular to stimuli not moving with the preferred velocity.

We can also consider the details of the mechanism in frequency space. We have already seen in the previous chapter that this implementation of IOC corresponds to a sum of V1 complex cell outputs with receptive fields lying on a plane in frequency space. The orientation of the plane in frequency space determines the preferred velocity of the cell, see equation (7). Summation is over orientation, spatial frequency and spatial position. In addition to this excitatory input coming from a plane in frequency space, the cell has also an inhibitory input from complex cells with frequency-space receptive fields that are far away from the plane.

The model of component selective cells

Simoncelli and Heeger have also proposed a model for component-direction selective cells. This “component” model consists of the same stages as the model for “pattern” cells, with the only difference lying in the linear combination of complex cell outputs. The model component cells combine V1 afferents over spatial position and spatial frequency, but not over orientation. Instead of lying on a plane, the underlying complex cells have bands lying on a line through the origin. Thus, the resulting “component” cell is orientation- and speed-tuned, but with broad spatial frequency bandwidth. The preferred speed is determined by the slope of the line in frequency space.

Some predictions

We are particularly interested in the classifications in “component” and “pattern” cells predicted by the Simoncelli and Heeger models. Following the methods introduced by Movshon et al. (1983), we have therefore to compare the predicted direction tunings for both gratings and plaids. We will see that, depending on the components speed, the Simoncelli-Heeger pattern model can predict responses typical of a “pattern” cell or of a “component” cell.

Because the model for pattern-direction selective cells implements IOC, it predicts a bimodal direction tuning to gratings moving slower than the preferred speed of the cell (Figure 13). We can also explain this behavior in the frequency domain description. Consider the plane in frequency space corresponding to a cell with preferred speed v_p. The energy of a grating is different from zero only in two points in frequency space, that are symmetric around the origin. When only the direction of motion of the grating

changes, both points describe a circle centered in the temporal frequency axis and lying on a plane perpendicular to it. Depending on the speed v_g of the grating (i.e. on the spatial frequency, equation (8)) these circles will cross the plane in two points ($v_g < v_p$), one point ($v_g = v_p$) or no point ($v_g > v_p$). This is shown in Figure 14A for the case of a cell with preferred velocity parallel to the y-direction.

In the framework of this model, without considering quantitative details, we can already make some qualitative predictions about the response of a pattern cell to plaids with different velocities. For example, consider the case of a plaid moving with the preferred speed of the cell. In this case the speed of the component gratings is necessarily lower that the preferred speed of the cell. There will be exactly one direction (i.e. the direction parallel to the preferred velocity) for which the energies of both gratings lie in the plane. We have already seen this when considering IOC in frequency space. This unique direction is the one that elicits the maximal response, i.e. the direction tuning for plaids is unimodal. Thus the model cell is classified as a "pattern" cell when the speed of the plaid as a whole corresponds to the preferred speed of the model.

In the case of a plaid composed of gratings moving as fast or faster than the preferred speed of the cell, we will measure a direction tuning for the plaid typical of component direction-selective cells. This is illustrated in Figure 14. When the direction of the plaid changes, the energies of the gratings describe a circle that has only one point that is closest to the plane. The cell will give a large response when one of the two gratings' energy lies on that point. In Figure 14B this is the case for grating 2, in Figure 14B for grating 1. If the plaid angle is large enough, this will produce bimodal direction tuning for plaids, with the two maxima of the tuning in symmetric positions around the direction of maximal response to a grating alone. As a result, the cell shows selectivity to the motion of the individual components, and not to the plaid as a whole.

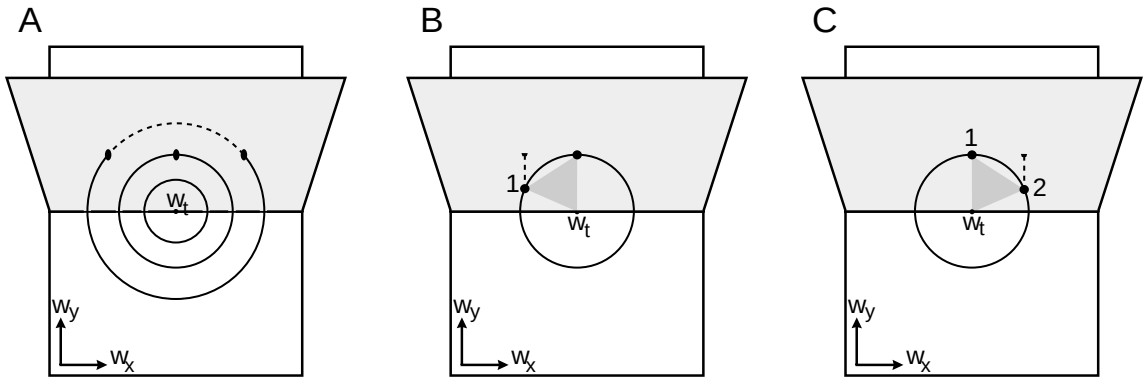

Figure 14, Explanation of the different direction tunings for plaids and gratings in the Simoncelli-Heeger model for pattern-direction selective cells. The A: bimodality in the direction tuning for gratings. B and C: a Simoncelli-Heeger model pattern cell shows component character for a grating moving faster then the preferred speed of the cell. B and C show the same plaid for two different directions of motion. The view is from the positive temporal frequency axes, and only the positive temporal frequencies are shown. See text for details.

The consequence of this important dependence of the tuning characteristics of a SH-model cell is that, to be able to identify correctly such a cell as pattern-motion selective with the methods previously described (Movshon et al., 1983), we have to use different grating speeds in the measurement of the direction tuning for the plaid and for the grating alone, as it has been done by Rodman et al. (1989). The resulting speed of the plaid must be the same as the speed of the gratings alone, and higher than the preferred speed of the cell, to avoid a bimodal tuning curve for gratings.

Another characterization

Another approach to the characterization of pattern and component direction selective cells is to directly use the speed dependence of the direction tunings to characterize the cells. Okamoto and Kawakami (1999) used this approach and measured the speed dependence of the direction tunings for spots and bars. They also compared the measured direction tunings with the predictions of a model for component- and pattern-direction selective neurons.

The Okamoto-Kawakami model (OK-model) is an implementation of intersection of constraints, and is in many aspects similar to the SH-model. There are however at least two important differences. First, directional selective simple cell responses in V1 are obtained with a correlation (i.e. a multiplication) of non directional-selective simple cells responses, so that it is not anymore possible to associate a linear weighting function to the direction selective cell. However it would be easy to modify this stage into an Elaborated Reichardt Detector, which then would be equivalent to a filtering approach, as discussed by van Santen and Sperling (1985). Second, at no level of the computation the OK-model does consider a gain control mechanism, like a normalization stage.

Despite this differences, the two models give similar qualitative predictions for the speed dependence of the direction tunings. In both models the direction tuning of a component direction selective cell is bimodal for high speed random dots, but unimodal for low speed random dots and gratings at all speeds. For pattern direction selective cells the direction tuning is bimodal for slow speed gratings, but unimodal for fast moving gratings and dots at all speeds. This is easily understood by considering the frequency domain description of the SH-model and the possible configurations between the “receptive field” of the MT cell (i.e. a plane or a line) and the energy distribution of the stimulus. These different tuning characteristics have recently been measured by Okamoto et al. (1999).

4 Data Sets

In the previous chapter we have tried to classify the cells in the measured population into “component” and “pattern” cells, by simply comparing the direction-tunings for plaids and gratings. However, we have seen that for a putative Simoncelli-Heeger pattern cell the classification would depend on the speed of the gratings, and thus would be ambiguous. A possibility to obtain a better understanding of the cell characteristics could be to analyze the responses to larger sets of stimuli.

We have analyzed large data sets obtained by Majaj, Carandini and Movshon (1999) in macaque area MT. These authors recorded the response of MT cells to stimuli produced by superimposing two sinusoidal gratings optimized in spatial- and temporal-frequency. Stimuli were presented through a circular window that was optimized in position and size to match the receptive field of the recorded cell. These authors recorded the cell responses for much larger sets of stimuli as the ones considered until now. In particular, they have studied how the cells respond when a plaid is progressively modified until it becomes a plaid. This transition form a plaid to a grating can be achieved either by progressively reducing the angle between the gratings or by progressively reducing the contrast of one of the gratings while holding fixated the directions of motion. The two resulting data sets used by Majaj et al. (1999) consist of stimuli differing only in two parameters. In the first set the authors varied the directions of motion of the two component gratings. In the second set they varied the contrast of one grating and the direction of motion of the other. These stimuli were presented in 2-4 successive repeats. Within each repeat the stimuli were presented in a random order.

To analyze these measurements we simply took the mean firing rate as a measure of neuronal responses. We call the responses obtained with the first set “direction-direction” experiments and the responses obtained with the second set “direction-contrast” experiments.

We will describe the details of these experiments in this chapter. Moreover, we will try to establish a link between some examples of measured direction-direction and direction-contrast responses and the definitions of “pattern” and “component” cells described in the previous chapter.

4.1 Direction – Direction Experiments

In direction-direction data, the two superimposed sinusoidal gratings have equal contrast c = 0.5. The directions of each grating are varied independently in steps of 30 degrees over a range of 360 degrees, resulting in a set of 12*12 = 144 stimuli.

Every stimulus consisting of gratings with different directions appears twice in a set. Indeed, the stimulus where grating 1 is moving in direction d1 and grating 2 in

direction d2 is physically identical to the one where grating 1 moves in direction d2 and grating 2 in direction d1. The remaining stimuli are sums of identical gratings with contrast c = 0.5, i.e. they are gratings with contrast c = 1.

In addition to the 144 stimuli needed for the direction-direction experiment, the stimulus sets included a blank stimulus (uniform gray screen) and a the stimuli for the measurements of a direction tuning curve for each of the gratings alone (12 directions of motion). This gives a total of 169 stimuli.

All the stimuli used for a direction-direction experiment are shown in Figure 15A. The component gratings are shown in the first column on the left and the last row on the bottom. Both components have contrast c = 0.5. The bottom-left corner corresponds to a blank stimulus. The other stimuli in the experiment are the all the possible combinations of the two components. The resulting stimulus can be again a drifting grating, a plaid or a flickering grating. The speed and direction of the resulting pattern as computed with intersection of constraints is shown in Figure 15B. Each arrow in the figure is the velocity of the pattern in Figure 15A in the corresponding position.

We now reconsider in detail the properties of the stimuli in Figure 16 and Figure 17. A subset of the stimuli used in the direction-direction experiment are shown in Figure 16A. The complete experiment involves plaids, drifting gratings and counterphase (flickering) gratings. The location of these stimuli on the plane is shown in Figure 16B.

The two parameters that vary in the direction-direction experiments, i.e. the directions of motion of the of the two gratings, are the coordinates plotted in Figure 16. However, it is easy to transform these coordinates into variables that describe the resulting plaid, namely the angle between the gratings and the direction of motion of the plaid, as obtained with intersection of constraints. The variation of these variables in the direction-direction plane is shown in Figure 17.

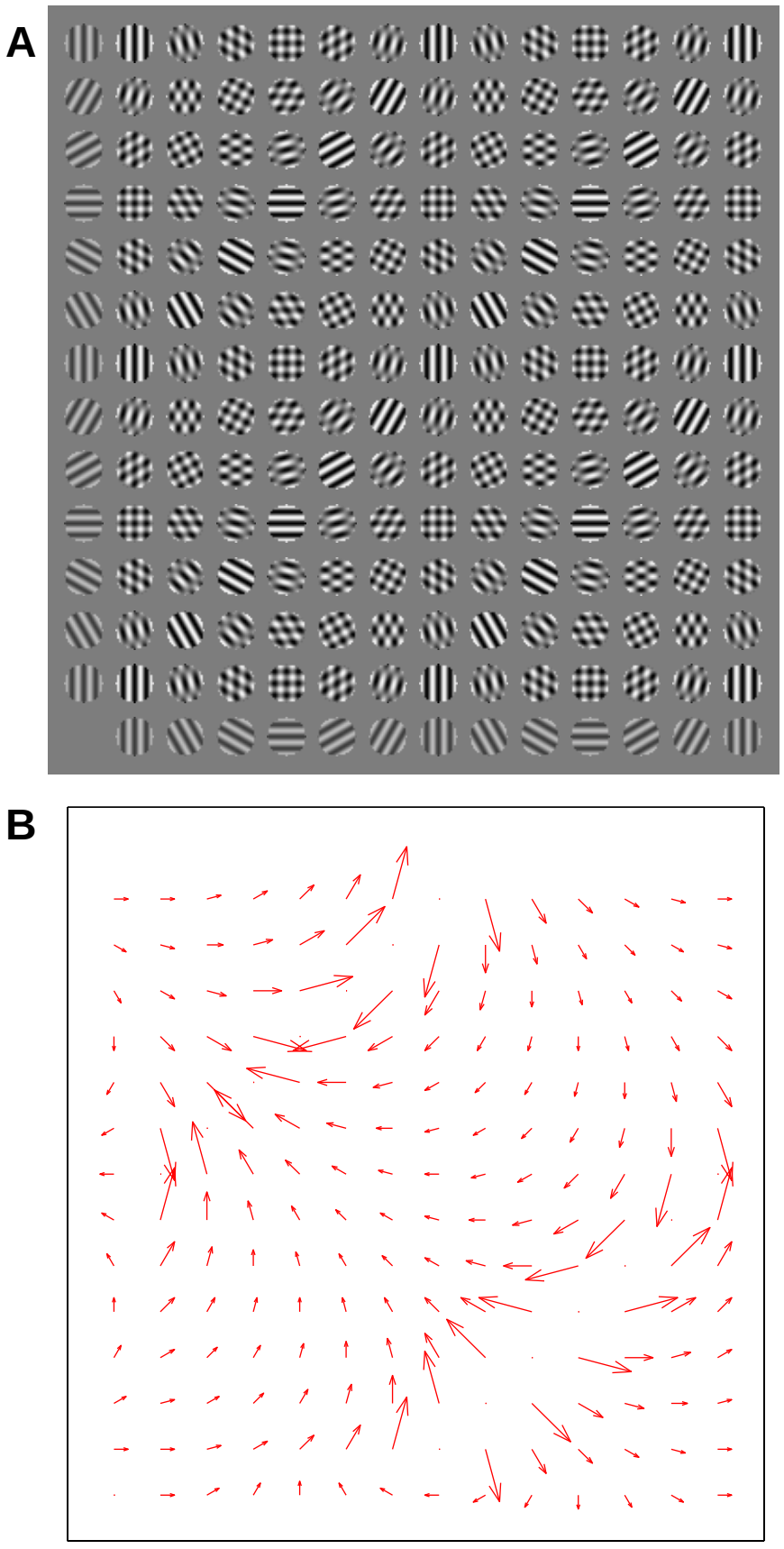

Figure 15, Stimuli in a direction-direction experiment. A: snapshots of all the non blank stimuli. B: speed and direction of the resulting pattern, computed with intersection of constraints.

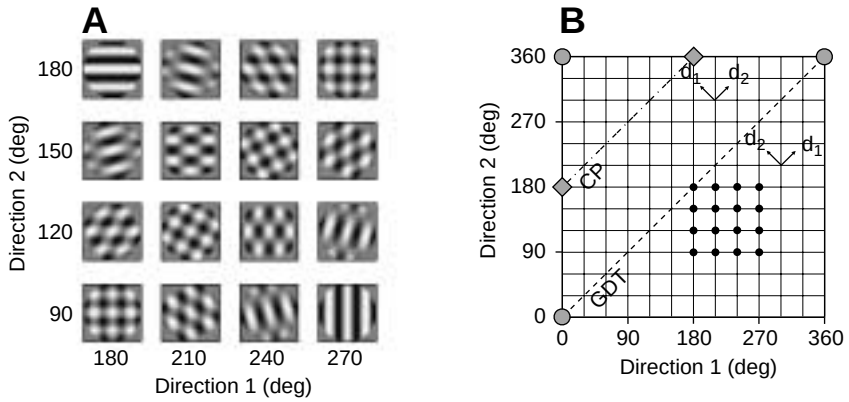

Figure 16. Properties of the stimuli in a direction-direction experiment. A: snapshots of the stimuli used for the direction-direction experiements. The stimulus in the top left is a drifting grating with c = 1, while the stimulus in the bottom-right is a counterphase grating. B: the full set of stimuli in an experiment. The stimuli shown in A are marked with black dots. Points lying in symmetric positions with respect to the GDT-line (grating direction tuning) are physically identical. The CP-line represents counterphase gratings. The three points marked with the gray circle correspond to a grating with direction d = 0, while the two points marked with the gray squares correspond to a counterphase grating with orientation 180 deg.

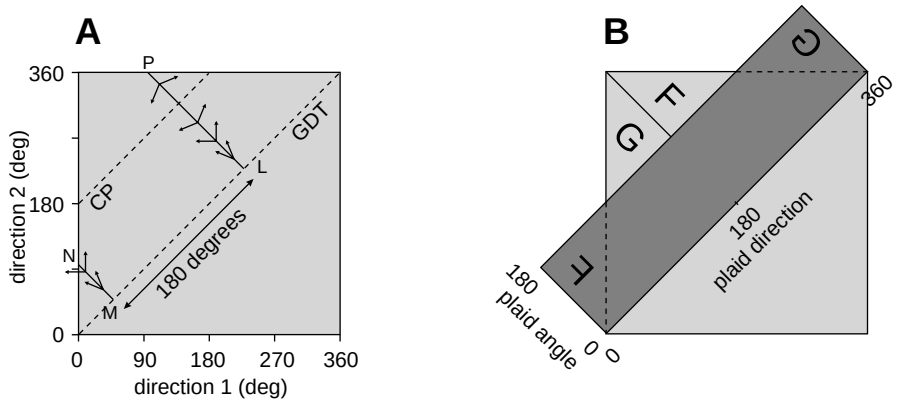

Figure 17, Grating variables vs. plaid variables. A: points L and M correspond to drifting gratings with c = 1, moving in opposite directions. When moving from L to P the direction of motion of the plaid is constant, while the angle (e.g. the speed) increases when coming closer to the CP-line (corresponding to flickering stationary gratings). When passing the CP-line, the direction of motion of the plaid flips to the opposite, while the speed of the plaid decreases again when moving towards P and then from N to M. Notice that P and N are the same point. B: The dark rectangular region represents the direction-direction plane as a function of the variables of the plaid. The dark region has been constructed by transforming and moving the two triangles marked with F and G. The same could be done with the other half of the direction-direction plane, which contains identical stimuli.

Examples of cell direction-direction responses are illustrated in Figure 18. The response of an ideal component cell to a drifting plaid is just the sum of the responses to the component gratings alone. The cell in Figure 18A is a candidate for being a component cell. It has a large response whenever one of the gratings moves in the preferred direction, which is close to 180 deg.

The direction tuning of a pattern cell for a plaid is the same as the direction tuning for a grating alone. As we have seen in previous chapters, the abstract model proposed by

Movshon et al. (1983) doesn't allow to make precise quantitative predictions about the response of a cell to different plaid velocities. However, the ideal pattern cell should respond to the variables of the plaid as given by IOC and not to the variables of the grating. In Figure 17 we have shown how the variables of the plaid are related to the variables of the gratings in the direction-direction plane. The cell in Figure 18B is a candidate for an ideal pattern-direction selective cell. It responds maximally to a plaid moving in the preferred direction of the cell with a speed larger than the speed of the component gratings. Moreover, it doesn't show the cross-shaped response that would be typical for a component-selective cell.

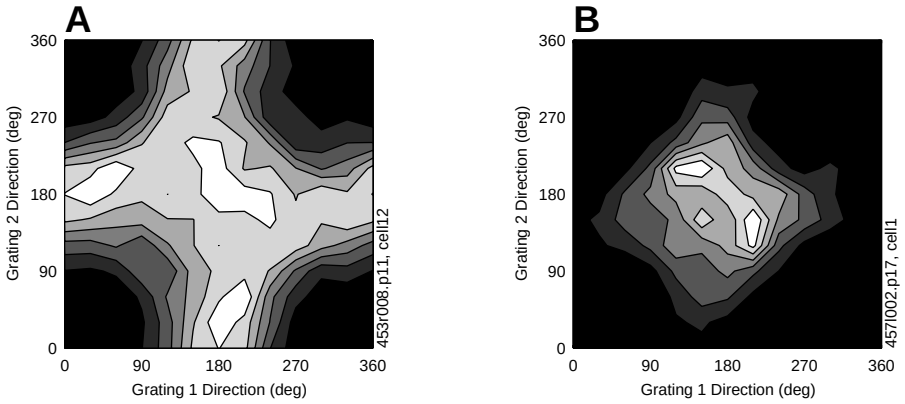

Figure 18, Two examples of measured direction-direction data. The cell in (A) could correspond to an ideal "component" cell while the cell in (B) could correspond to an ideal "pattern" cell. See text for details.

4.2 Direction – Contrast Experiments

The stimuli in the second experiment also consist of two superimposed gratings. The contrast of the first grating is fixed to c = 0.5 while the direction of motion changes in steps of 30 degrees over a range of 360 degrees. The direction of motion of the second grating is fixed to the measured preferred direction of the cell, while the contrast is variable and can take 7 values between c = 0 and c = 0.5. This gives a total of 7*12 = 84 stimuli.

This set of 84 stimuli has been enlarged with a contrast response function for a grating moving in the measured preferred direction of the cell. The contrast values used to determine the contrast response function are the same 7 values as used for the direction-contrast experiment. This gives a total of 91 stimuli. All the stimuli are shown in Figure 19. As in the direction-direction experiment, the stimuli are composed of two gratings. The first grating is shown in the first column on the left for all the possible contrasts, while the second grating I shown in row on the bottom, for all the possible directions. The bottom-left corner corresponds to a blank stimulus, and all the other stimuli are given by the superposition of the two component gratings.

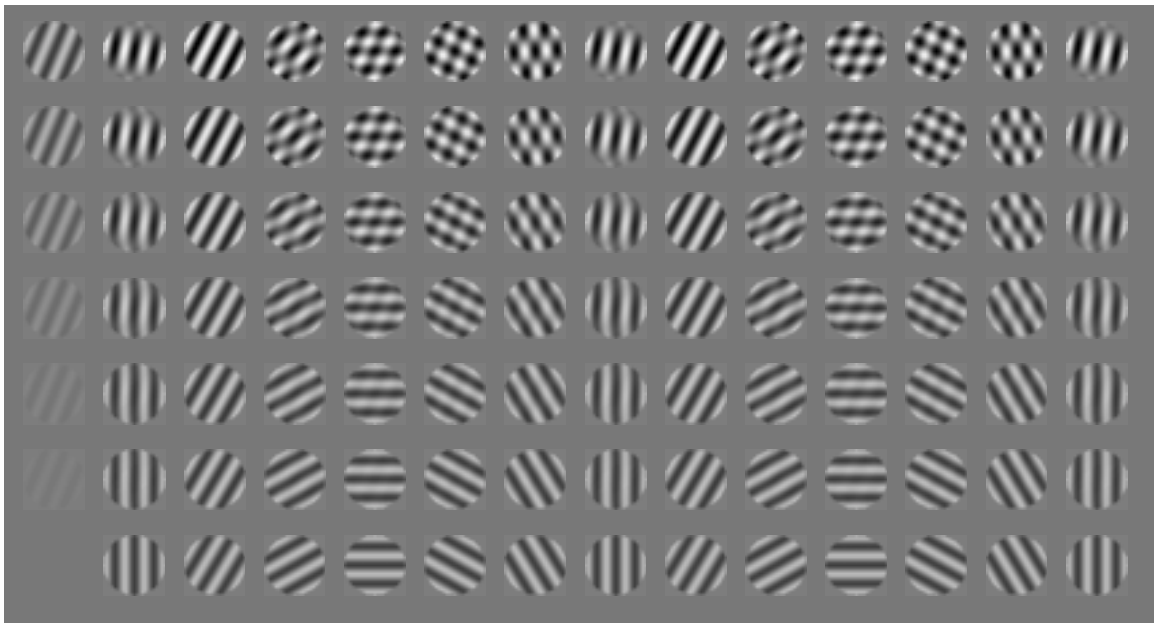

Figure 19, Stimuli in a direction-contrast experiment.

Two examples for the results of a direction-contrast experiment are shown in Figure 20. Notice that the horizontal line in the direction-contrast plane corresponding to c_2 = 0.5 corresponds to a line in the direction-direction plane determined by the direction of grating 1.

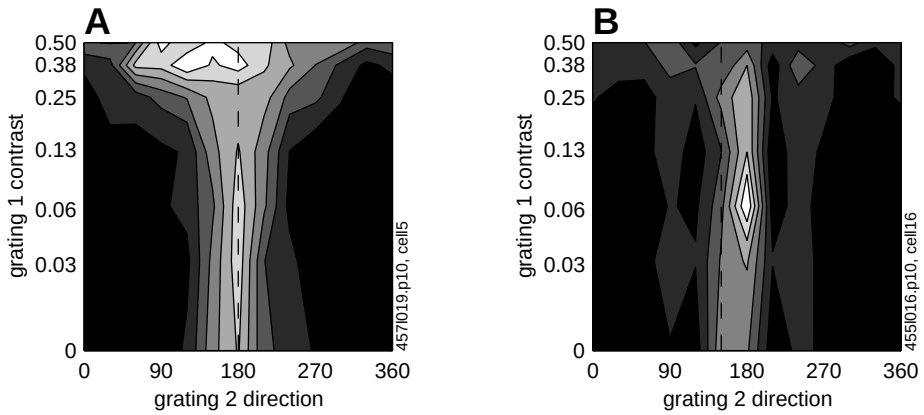

Figure 20, Example of measured direction-contrast responses. The dashed line indicates the direction of grating 1. The cell in B shows over saturation of the response for high contrasts.

5 Models of MT responses

Here we consider the predictions of different models for the responses to the large data sets presented in the previous chapter. We considered three types of models:

1. **Abstract models**
2. **Abstract models with normalization**
3. **Simoncelli-Heeger (SH) models**

The first are extensions of the models for component- and pattern-selectivity proposed by Moshon et al. (1983). The seconds are the abstract models extended with a normalization stage to obtain a more realistic representation of contrast. The last are simplified implementations of the models for component and pattern cells proposed by Simoncelli and Heeger (1998). In the following sections we will define the model responses and discuss the predictions of the different models. We will consider the fits of the data only in chapter 7.

5.1 Abstract Models

The abstract component model and the abstract pattern model are extensions of the models for component- and pattern-selectivity proposed by Moshon et al. (1983). We have discussed the original models in section 3.2.1. The extension of the original models is necessary to allow predictions of the responses to our larger set of stimuli. Moreover we have provided the models with a rectification stage. These extended models allow us to make a quantitative analysis of our set of stimuli, without any knowledge about the detailed neuronal mechanism underlying the selectivity of the cells.

5.1.1 Abstract Component Model

The abstract component model responds to the components in the stimulus independently: the variables determining the response are the variables of the components, in this case contrast and direction of motion of the components.

We define the response of the component model to a drifting grating or plaid as:

$$R = \lfloor b + g \cdot \left(c_1 L(d_1) + c_2 L(d_2)\right) \rfloor^m \qquad (12)$$

where $c_1L(d_1) + c_2L(d_2)$ is the output of the linear stage of the model. L is the direction tuning of the cell for a grating at full contrast. b determines the response baseline, g determines the response gain of the cell, and c_{50} is the semisaturation contrast. The

variables are the contrasts c_1 and c_2 and the directions d_1 and d_2 of the component gratings.

We take the response of the linear stage to a drifting grating as a function of the direction of motion d to be the sum of two gaussians with peaks 180 degrees apart:

$$L = \exp\left(-\left\langle d - d_p \right\rangle^2 / 2w_d{}^2\right) + r_n \exp\left(-\left\langle d - d_p - 180 \right\rangle^2 / 2w_d{}^2\right)$$

Here w_d is the direction-tuning width, d_p is the preferred direction of motion of the cell, and r_n is the response to the nonpreferred direction. The angled brackets indicate that all the directions are given modulo 360 deg. Two examples of L(d) for different values of w_d and r_n are shown in Figure 21.

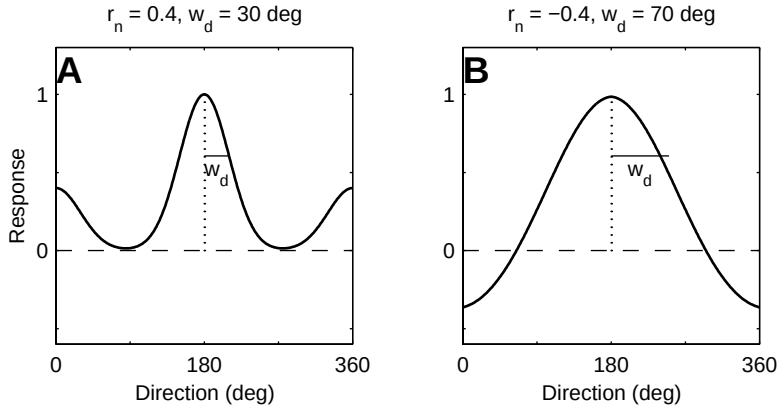

Figure 21, Direction tuning of the linear stage of the component and pattern models. A: Example for the direction tuning for r_n = 0.4 and w_d = 30 deg. B: Example for the direction tuning for r_n = -0.4 and w_d = 70 deg.

The abstract component model has 6 free parameters, listed in Table 1.

Table 1, parameters of the abstract component model

b	Baseline
g	Gain
m	Exponent
d_p	Preferred direction
r_n	Response in nonpreferred direction
w_d	Direction tuning width

Now let's look at the characteristics of the responses predicted by the abstract component model. The model is selective for the component gratings, and, for m = 1, the response to a plaid is just given by the sum of the responses to the components. A first consequence is that the maximal response to the direction-direction stimuli is obtained when both gratings are moving in the preferred direction, that is for a grating with c = 1 moving in the preferred direction. A second consequence is the symmetry of

the responses across the two lines corresponding to $d_1 = d_p$ and $d_2 = d_p$. This is shown for some examples in Figure 22. The figures show the effect of changing the response in the nonpreferred direction r_n or the exponent of rectification m. Compare these predictions with the cell in Figure 18A, which shows the same cross-shaped response typical for a component-selective mechanism.

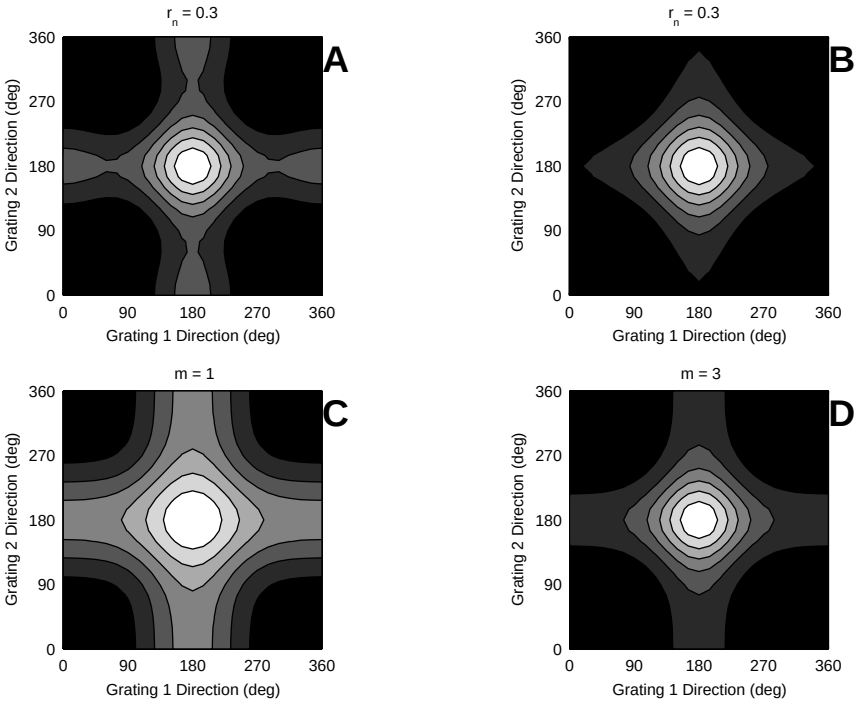

Figure 22, Predictions of the abstract component model for direction-direction stimuli. Every horizontal pair of figures represents the model responses with the same parameters except one. n is the exponent of rectification, r_n is the response in the nonpreferred direction. For all the figures the preferred direction of the cell is $d_p = 180$.

Some examples for direction-contrast data are shown in Figure 23. The direction of grating 1 is fixed and is indicated by the dashed line. The response increases for increasing values of c_1, independently of d_2. The responses are (even) symmetric around the line $d_2 = d_p$. We will see that this symmetry disappears when adding normalization to the model.

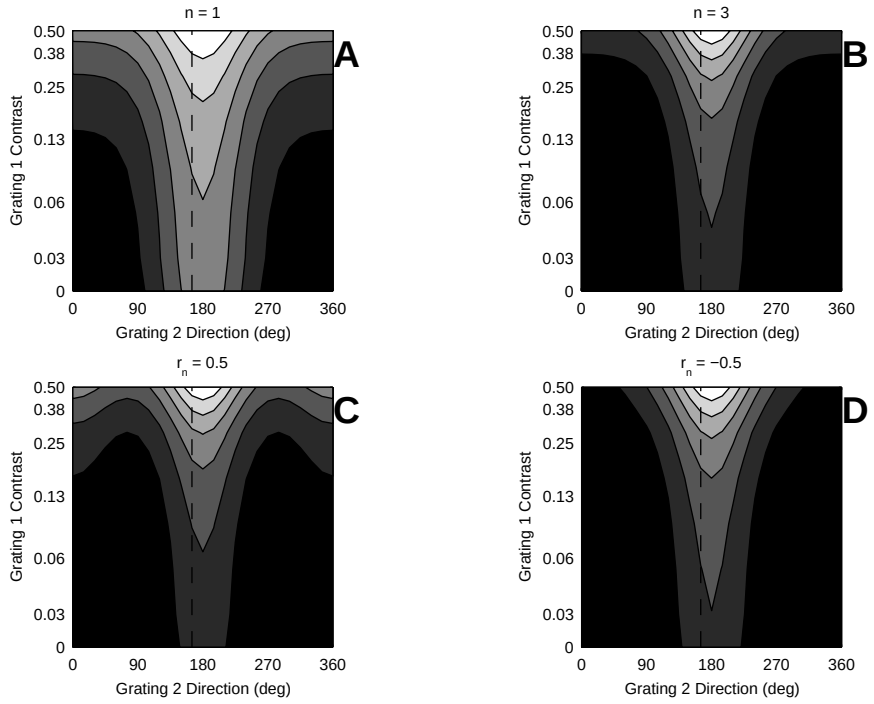

Figure 23, Predictions of the abstract component model for direction-direction stimuli. Every horizontal pair of figures represents the model responses with the same parameters except one. n is the exponent of rectification, r_n is the response in the nonpreferred direction. For all the figures the preferred direction of the cell is $d_p = 180$. The vertical dashed line indicates the (fixed) direction of grating 1. In all the figures the preferred direction of the cell is $d_p = 180$.

5.1.2 Abstract Pattern Model

The response of the abstract pattern model does not depend on the individual motions of the components in the stimulus, but only on the motion of the resulting pattern. The variables determining the response of the model are the variables of the pattern as a whole. In the case of a grating these are the contrast c, the direction of motion d and the normal speed s of the grating. In the case of a plaid the variables are the direction of motion d and the speed s of the plaid obtained with intersection of constraints. The question about how the brain actually performs intersection of constraints is not answered in this abstract model. For the contrast of a plaid we take the sum of the contrasts of the component gratings.

We define the response of the abstract pattern model to a grating or plaid as:

$$R = \lfloor b + g \cdot (c_1 + c_2) F(s) L(d) \rfloor^m \qquad (13)$$

where F is the speed tuning of the cell and L is the direction tuning. L is the same function of stimulus direction as in the abstract component model (Figure 21). F is a

gaussian function of the speed v of the stimulus, centered on the preferred speed v_p and with tuning width w_s:

$$F(s) = \exp\left(-\frac{(v - v_p)^2}{2{w_s}^2}\right)$$

The speed tuning F is shown in Figure 24 for two different values of w_s.

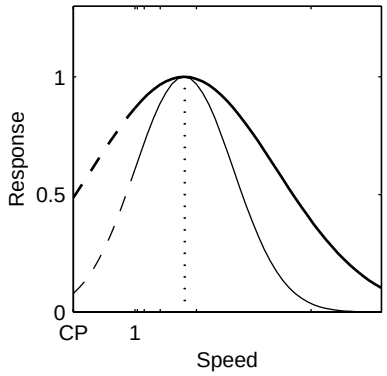

Figure 24, Speed tuning for the abstract pattern models. The plaid speed is expressed in units of the component gratings' speed. The plaid speeds corresponding to the measured angles of 0, 30, 60, 90, 120, 150 deg are plotted as tick marks. The angle of 180 deg corresponds to counterphase gratings (CP) and the corresponding speed is defined as s = 0. Parameters are v_p = 1.8 (indicated by the dotted line), w_s = 0.8 and w_s = 1.5.

The abstract pattern model has 8 free parameters, listed in Table 2.

Table 2, parameters of the abstract pattern model

b	Baseline
g	Gain
m	Exponent
d_p	Preferred direction of motion
r_n	Response to nonpreferred direction
w_d	Direction tuning width
s_p	Preferred speed
w_s	Speed tuning width

Some examples of model responses to the direction-direction stimuli are shown in Figure 25. The figures show the effect of changing the response in the nonpreferred direction r_n or the preferred speed v_p. The most important difference between the predictions of the abstract component model and of the abstract pattern models lie in the symmetries of the figures. Because of the selectivity to the components, the responses of the component model are symmetric also across the vertical line $d_1 = d_p$ and the horizontal line $d_2 = d_p$. The responses of the pattern model do not have this cross-shaped response. Another difference between the models is given by the stimulus

eliciting the maximal response. For the component model this is a grating with c = 1 moving in the preferred direction, while for the pattern model it is a plaid, with d = d_p and speed v = v_p.

It will be of importance for the fits that both models predict the same response for a plaid moving in the direction d_p - Δd and for a plaid moving in the direction d_p - Δd, for an arbitrary Δd. The consequence is the symmetry across the line trough the points (360, 0) and (0, 360). We will see that many measured cells do not show this symmetry.

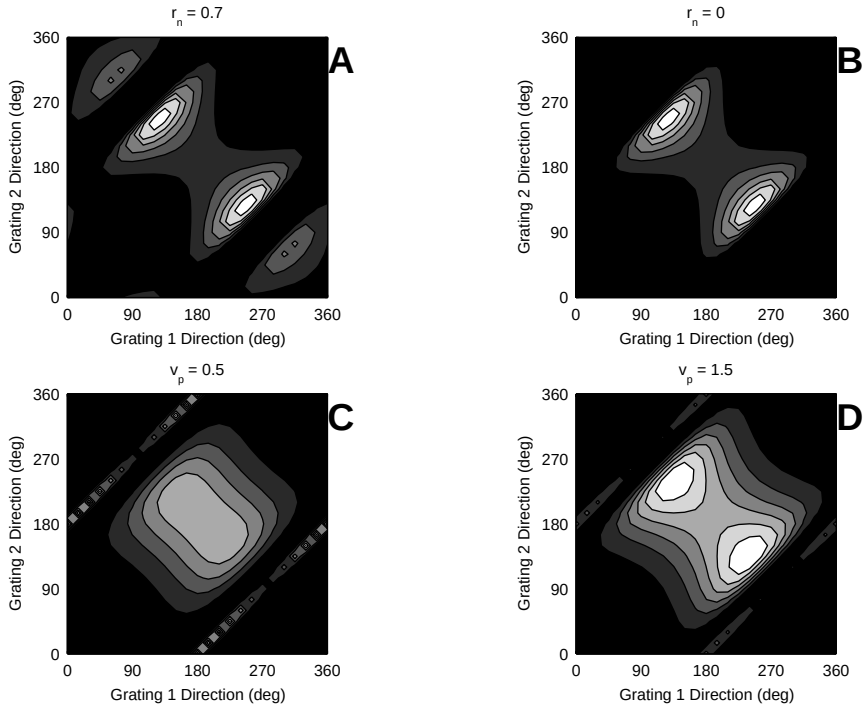

Figure 25, Examples of predictions of the abstract pattern model for direction-direction stimuli. For every horizontal pair of figures only one parameter changes between the two figures. See text for details.

We have defined speed and direction of the plaid using the intersection of constraints method. Unfortunately, the intersection of constraints has no solution for two gratings moving in opposite directions. In this case the stimulus consists of a flickering stationary grating oriented perpendicularly to the direction of motion of the component gratings. We define the speed of such a flickering grating as s = 0 and the direction d as perpendicular to the orientation two the gratings. Of the two possible directions d and d+180 we chose the one that is closer to the preferred direction d_p . With this definition and for fixed d_p and v_p the response of the cell to flickering gratings is controlled by the speed tuning width w_s : the response increases for increasing w_s (Figure 24). In the predictions in Figure 25C and D the responses to the optimally oriented counterphase gratings correspond to the response in the points (0, 180) and (180, 360).

The direction-contrast responses predicted by the abstract pattern model are in many aspects different from the predictions of the abstract component model. Some examples are plotted in Figure 26.

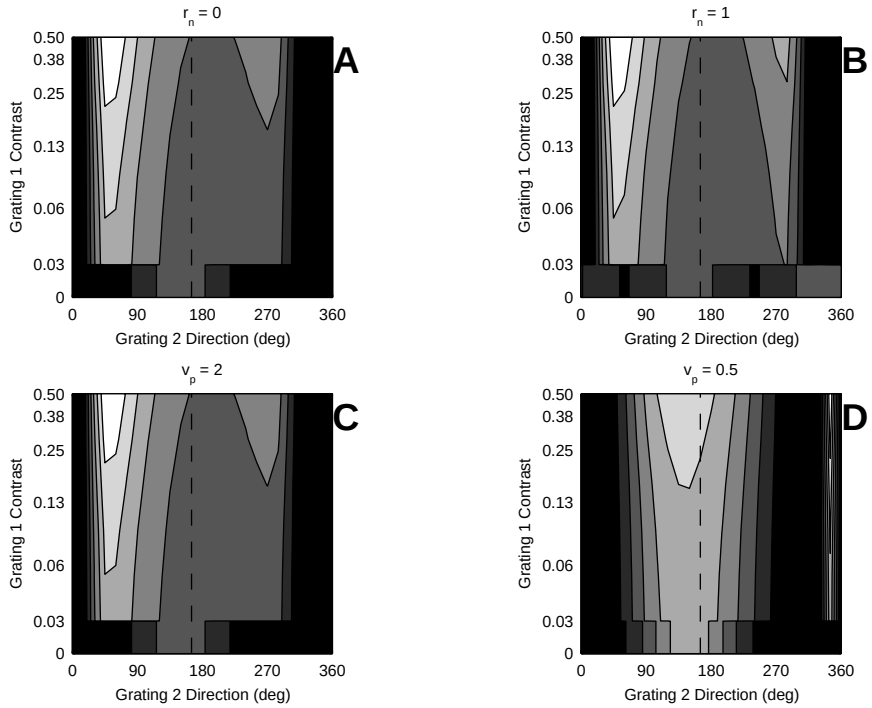

Figure 26, Examples of predictions of the abstract pattern model for direction-contrast stimuli. For every horizontal pair of figures only one parameter changes between the two figures. See text for details.

The direction-contrast responses are discontinuous in many points of the plane. A new discontinuity is introduced by the abrupt transition from a grating to a plaid when a second grating of low contrast is added to the first. The pattern model doesn't make any distinction between a plaid composed of gratings of equal contrast and a plaid composed of gratings with different contrasts. As a result, for a fixed direction d_2, the direction of motion "seen" by the abstract pattern model jumps to $(d_1 + d_2)/2$ when adding grating 1, moving in direction d_1 and with contrast $c_1 = 0.03$ (the lowest positive contrast in the stimuli). The same happens to the speed s of the stimulus, that jumps form s = 1 (i.e. the speed of the gratings) to s > 1 when adding a second grating with $d_1 \neq d_2$.

Another difference with the predictions of the abstract component model is that the direction-contrast responses predicted by the abstract pattern model are not symmetric across the line $d_2 = d_p$. This asymmetry is caused by the direction tuning G. The different contributes to the response of the abstract pattern model are shown in. The top row in Figure 27 shows the different terms in the model, namely the speed tuning G(s), the contrasts $c_1 + c_2$ and the direction tuning L(d). The bottom row shows the products

$G^*(c_1 + c_2)$ and G*L, and the product of all the three terms (corresponding to the model response for b = 0, g = 1 and m = 1).

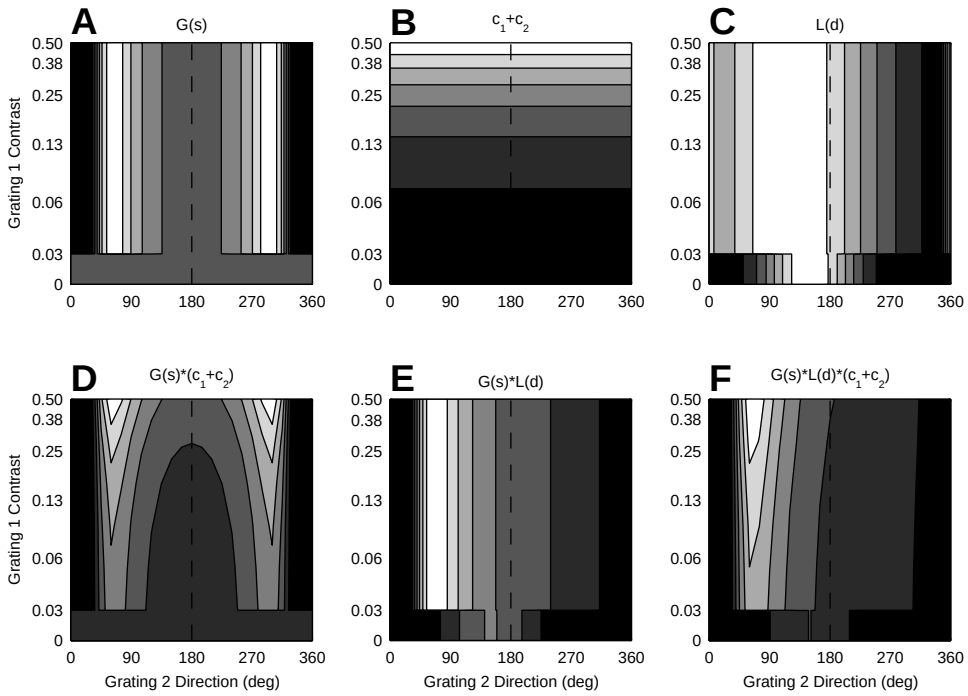

Figure 27, Different contributes to direction-contrast responses predicted by the abstract pattern model. A: speed tuning function G(s). B: contrast dependence: $c_1 + c_2$. C: direction tuning L(d). D: product $G^*(c_1 + c_2)$. E: product G*L. H: product $G^*L^*(c_1 + c_2)$.

5.2 Normalization

The second class of models is obtained by extending the abstract models defined in the previous section with a normalization stage. Here we will first discuss some arguments in favor of a normalization stage. Then we will derive an expression for the normalization signal that can be used both for gratings and plaids.

Saturation of contrast responses

Normalization plays a role for both sets of stimuli that we are analyzing. Clearly we have to consider normalization in the direction-contrast measurements, where the contrast of the individual gratings varies in an important range. But also in the direction-direction measurements we can compare two direction tunings for gratings at different contrasts, c = 0.5 and c = 1. Many of the recorded cells clearly show saturation in the response to those stimuli, i.e. the response to the c = 1 grating is much lower than two times the response to the c = 0.5 grating, which could be explained by

normalization. Moreover, as we will see in this section, normalization could play an important role even for the remaining stimuli in the direction-direction experiment.

Sclar et al. (1990) have measured contrast responses in MT and have shown that they can be approximated with the same function as for V1 cells:

$$R = R_{\max} \frac{c^n}{{c_{50}}^n + c^n} + M \qquad (14)$$

In Figure 28 we show examples of saturation in both direction-direction and direction-contrast measurements.

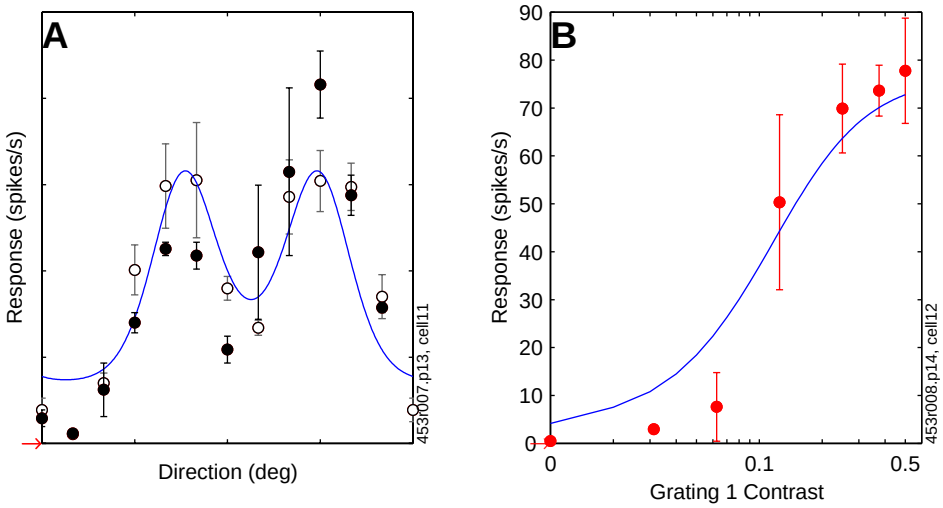

Figure 28, Saturation of cell responses for high contrasts. A: bimodal direction tuning for a grating with c = 0.5 (white markers) and c = 1.0 (black markers). The cell shows clearly saturation in the response. The dashed line is the fit of the SH-pattern model, and is almost the same for c = 0.5 and c = 1. B: example of a measured contrast response curve and fit with SH-pattern model.

The normalization signal

To derive a formulation of the normalization signal for our sets of stimuli we assume that the normalization pool is composed of phase independent, direction selective cells, with gaussian direction tuning. The linear response of one such cell to a plaid is:

$$L_d(d_1, d_2) = k\left[c_1 e^{(d-d_1)^2/2\sigma^2} + c_2 e^{(d-d_2)^2/2\sigma^2}\right]$$

where d is the preferred direction of the cell, k is an arbitrary constant, and σ is the tuning width of the cell, which we assume to be constant over the normalization pool. The directions d, d_1 and d_2 are defined in degrees modulo 360, i.e. the directions d = 0 and d = 360 correspond to the same stimulus.

If the rectified responses of the cells in the normalization pool are summed with constant weights, then the response of the pool is given by:

$$\Sigma_{NP}(d_1,d_2) = k\int d\delta \lfloor L_\delta(d_1,d_2)\rfloor^n = k\int d\delta \left\lfloor c_1 e^{(\delta-d_1)^2/2\sigma^2} + c_2 e^{(\delta-d_2)^2/2\sigma^2}\right\rfloor^n$$

(15)

where n is the exponent of the rectification, and the response of the normalization pool is a function of d_1 and d_2, or more precisely of $|d_1-d_2|$. For an appropriately chosen value of k we obtain:

$$|d_1-d_2| \approx 0 \Rightarrow \Sigma_{NP} \approx (c_1+c_2)^n$$

$$|d_1-d_2| >> \sigma \Rightarrow \Sigma_{NP} \approx \left(c_1{}^n + c_2{}^n\right)$$

(16)

Because of the nonlinearity introduced by the rectification stage the response of the normalization pool depends not only on the contrasts of the gratings but also on the difference between the directions of the two gratings. For constant grating contrasts the response of the normalization pool is maximal when the two gratings are moving in the same direction, i.e. the resulting stimulus is a grating with twice the contrast of the individual gratings. When the difference in the directions of the two gratings increases, progressively fewer cells are stimulated by both gratings, so that the normalization signal decreases. This signal reaches the minimum when the populations of cells responding to the different gratings overlap the least.

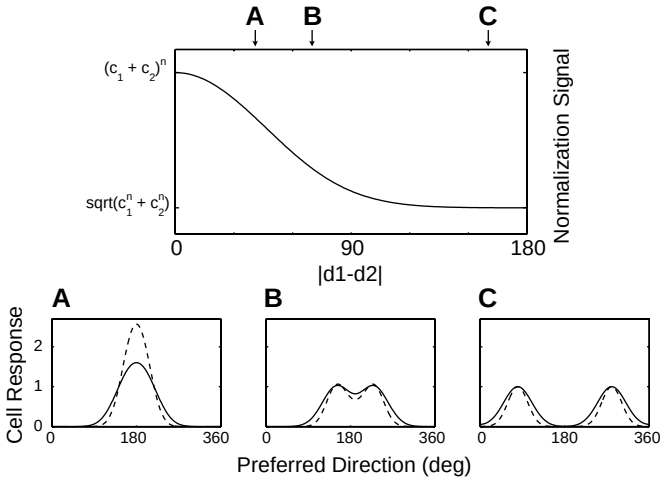

Figure 29, Normalization signal vs. responses in the normalization pool. Top: normalization signal for a plaid as a function of the angle between the gratings for a tuning width of σ = 30 deg. The corresponding response patterns in the population of cells with different preferred directions are shown for three cases: the directions of the gratings in A, B and C are respectively (160, 150, 80) for grating 1 and (200, 230, 280) for grating 2. The dashed lines correspond to the case n = 1 (no rectification) and n = 2 (half squaring).

Figure 29 shows the variation of the normalization signal with changing plaid angle and the corresponding response distribution in the normalization pool. Compare also the two limits of equation (16) with equations (10) and (11), where the normalization signal has a very similar form for gratings and plaids.

The contrast of a plaid

To obtain a contrast dependence like the one in equation (14), where in the denominator we have the power of a contrast, we can now define the contrast of a plaid as:

$$C_\sigma(d_1,d_2) = k\sqrt{\int \delta d \left[c_1 e^{(d-d_1)^2/2\sigma^2} + c_2 e^{(d-d_2)^2/2\sigma^2} \right]^2} \qquad (17)$$

With this definition, we can approximate the expression of the normalization signal as it is given in equation (15) by:

$$\Sigma_{NP}(d_1,d_2) = {C_\sigma}^n(d_1,d_2)$$

and we obtain an expression like in equation (14):

$$R \propto \frac{Num}{{c_{50}}^n + {C_\sigma}^n}$$

where *Num* stays for the numerator of the response, and will depend on the considered model. We have seen that the plaid contrast depends on the plaid angle, and therefore the model responses will depend on the plaid angle through the normalization stage.

This definition of the contrast of a plaid can be motivated also from another point of view. In the special case of a grating, the energy of the image is proportional to c^2, where c is the well defined contrast of the grating. As a result, the contrast is given by the square root of the energy in the image. In analogy we can define the contrast of a plaid as the square root of the energy of the plaid. The energy of the plaid is given by the square of the sum over the amplitudes of all frequency- and orientation-components in the image. If these amplitudes are computed by mechanisms with a direction tuning width σ, in analogy to the contrast of a grating we will obtain again equation (17) for the contrast of plaid. This definition of the contrast of a plaid simply considers the fact that for two superimposed gratings the energy of the image abruptly changes when the gratings have exactly the same orientation. Because we are dealing with a biological system, the “effective energy” measured by the system will change smoothly, without the discontinuity of the physical energy.

5.3 Abstract Models with Normalization

Having defined a normalization signal to account for contrast gain control, now we want to extend the two abstract models with a normalization stage. The pattern model is the extension of the abstract pattern model, while the component model is the extension of the abstract component model.

5.3.1 Component Model

The response of the component model to a drifting grating or plaid is:

$$R = \frac{\lfloor b + g\left(c_1 L(d_1) + c_2 L(d_2)\right)\rfloor^m}{{c_{50}}^m + {C_\sigma}^m} \qquad (18)$$

where c_{50} is the semisaturation contrast and C_σ is the normalization signal that depends on the contrast and orientation of the two gratings. We have defined and discussed the meaning of C_σ in 5.2. This form of normalization doesn't make any formal distinction between normalization in V1 and a possible normalization in MT, even if its precise formulation is motivated by our knowledge of V1 physiology.

The component model has 8 parameters, the 6 of the abstract component model (Table 1) plus the semisaturation contrast c_{50} and the tuning width σ underlying the normalization signal.

The normalization stage adds new important properties to the model responses to both the direction-direction and direction-contrast stimuli. We can consider the response of the component model as the product of two terms, i.e. the rectified linear stage and the normalization stage. The first term of the product is the same as the response of the abstract component model, while the second term is given by:

$$\frac{1}{{c_{50}}^m + {C_\sigma}^m} \qquad (19)$$

For small values of c_{50} the maximal response of the component model in the direction-direction responses is obtained for a plaid, and not anymore for a grating with contrast c = 1 moving in the preferred direction. This is shown in Figure 30. The response to gratings with c = 1 is suppressed by the large normalization signal. For large values of c_{50} the normalization signal is almost constant over all plaid angles, so that this effect is not visible.

The normalization signal depends only on the plaid angle and not on the plaid direction. As a result, normalization does not affect the shape of the direction tunings for plaids,

but does only scale the direction tunings with a factor that depends on the plaid angle. For the same values of the common parameters a plaid that produces a bimodal direction tuning in the abstract component model produces also a bimodal direction tuning in the component model.

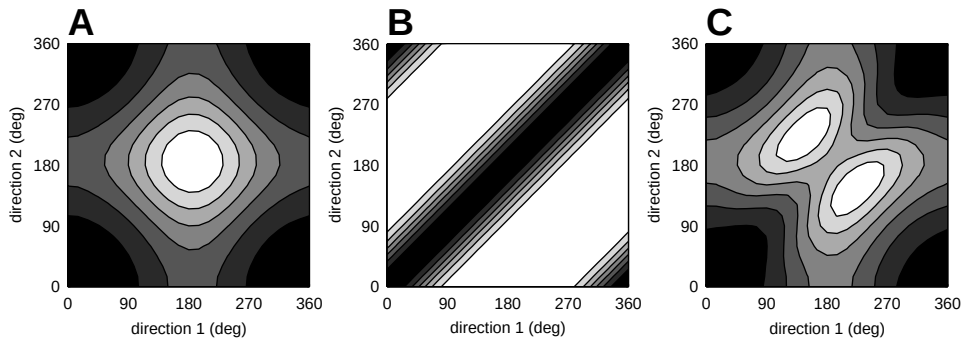

Figure 30, Effect of normalization on the direction-direction responses for the component model. A: response without normalization, corresponding to the abstract component model. B: normalization signal, given by equation (19). C: response of the component model, given by the product of A and B. In B and C: $\sigma = 25$ deg.

An example of the influence of the normalization stage on the direction-contrast responses for the component model is shown in Figure 31. Again we can consider the response of the model as the product of two terms, the rectified linear stage and the normalization signal. The linear stage is symmetric with respect to the preferred direction d_p, while the normalization signal is symmetric with respect to the direction of grating 1. As a result the product of the two is not anymore symmetric when $d_1 \neq d_p$. Moreover, the response of the model saturates or even over-saturates for large contrasts, as expected because of normalization.

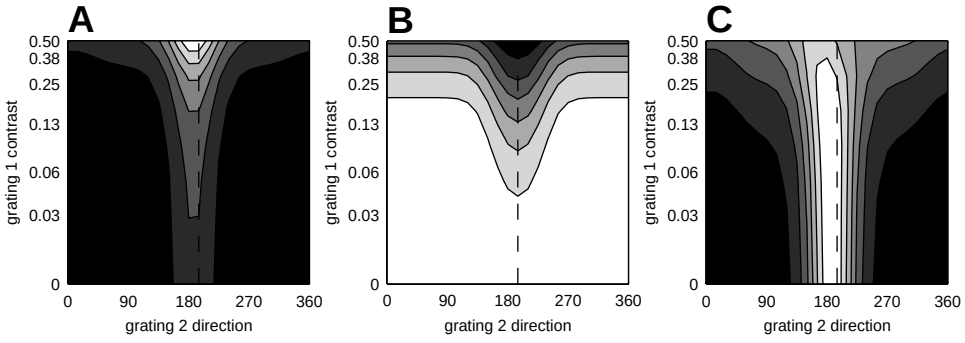

Figure 31, Effect of normalization on the direction-contrast responses for the component model. A: response of the abstract component model. B: normalization signal. C: response of the component model, corresponding to the product of A and B. $d_1 = 195$, $d_p = 187$, $\sigma = 20$ (deg).

5.3.2 Pattern Model

The response of the pattern model to a grating or plaid is:

$$R = \frac{\lfloor b + gC_\sigma F(s)L(d) \rfloor^m}{{c_{50}}^m + {C_\sigma}^m}$$

(20)

This is just the abstract pattern model followed by normalization, in analogy to the definition of the component model. The pattern model has 10 parameters, the 8 parameters of the abstract pattern model plus the semisaturation contrast c_{50} and the tuning width σ underlying the normalization signal.

Similar considerations as in the discussion on the effect of normalization on the responses of the component model hold also for the pattern model. A particularity of the abstract model is that the normalization signal changes the speed dependence of the model. Indeed, C_σ is a function of $|d_1-d_2|$, an thus of the speed of the plaid, defined through intersection of constraints. Thus the speed dependence of the abstract pattern model is the result of the combined effect of the speed tuning function G(s) and the normalization signal C_σ. These is shown in Figure 32.

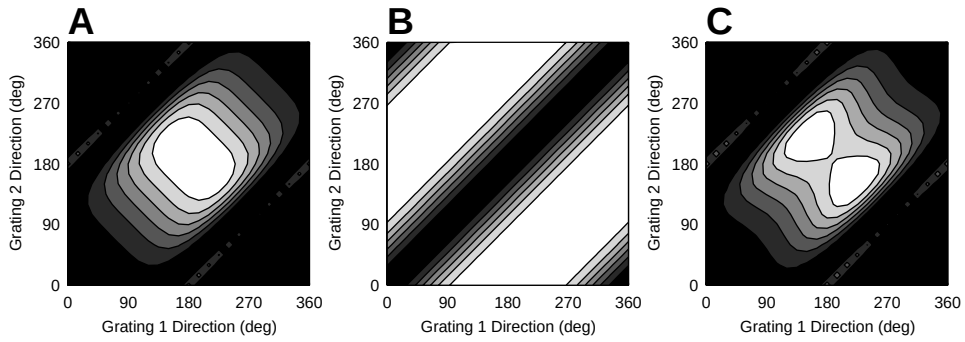

Figure 32, Effect of normalization on the speed dependence in the pattern model. A: response of the abstract pattern model. B: the normalization signal C_σ. C: response of the pattern model. The preferred speed is $v_p = 1$, while $\sigma = 30$ deg.

The main effect of normalization on the direction-contrast responses of the pattern model is the saturation of cell responses for high contrasts. This is shown in Figure 33.

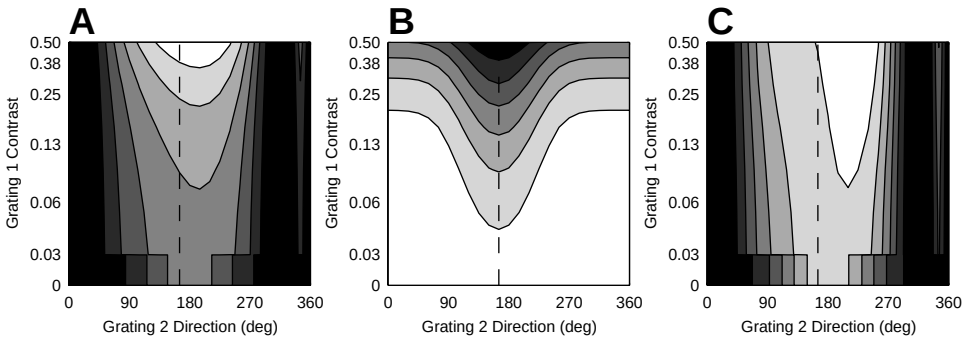

Figure 33, Effect of normalization on the direction-contrast data for the pattern model. A: response of the abstract pattern model. B: the normalization signal C_σ. C: response of the pattern model. The preferred speed is $v_p = 1$, while $\sigma = 30$ deg.

5.4 Simoncelli-Heeger Models

The third kind of models we discuss are implementations of the models for pattern and component cells proposed by Simoncelli and Heeger (1998). We have discussed the original models in section 3.3. Here we derive simplified versions of these models that are tailored to the particular set of stimuli we are analyzing. The simplifications allow us to formulate the model responses in a form that can be better fitted to the data.

We have made two important simplifications to the full models. First, we don't implement explicitly a normalization stage at the level of MT. Second, in the full models a component cell receives excitatory input from V1 cells lying on a line in frequency space, while a pattern cell receives excitatory input from cells lying on a plane. All the stimuli in a set for the direction-direction or direction-contrast measurements are composed of gratings with the same temporal and spatial frequencies. Therefor, in our implementation of the models we consider only the V1 afferents to MT with preferred spatial frequency equal to the spatial frequency of the gratings in the stimuli. As a result, a component cell receives input from one V1 complex cell while a pattern cell receives input from V1 complex cells lying on an ellipse.

5.4.1 SH-Component Model

The response of the SH-component model to a grating or plaid is given by:

$$R = \lfloor b + gV(S) \rfloor^n \tag{21}$$

where b is the baseline, g is the gain, n is the exponent of rectification in MT and V(S) is the response of a normalized V1 complex cell tuned to the spatial frequency of the stimulus S:

$$V = \frac{\lfloor c_1 H(S_1) + c_2 H(S_2) \rfloor^m}{{c_{50}}^m + {C_\sigma}^m}$$

where H(S) is the response of the underlying linear (phase-independent) stage to a grating with unit contrast, m is the exponent of rectification in V1, and the other parameters have the same meaning as for the previous models. We have assumed that the sponstaneous firing rate of a V1 cell is zero. A grating is defined through the spatial frequency and direction (i.e. the wave vector) and the temporal frequency:

$$S = (\vec{k}_s, \omega_s)$$

H(S) is linear but phase-independent and is determined by the receptive field of the complex cell. H(S) is obtained by integrating over frequency space the product of the stimulus energy with the amplitude response function of the receptive field. The ampliture response function for a direction selective cell consists of two blobs in symmetric positions with respect to the origin of the frequnecy space, while the energy of the stimulus consists of the sum of two delta functions. For a grating this means:

$$H(S) = \int d^2k d\omega \left[\delta(\vec{k} - \vec{k}_s)\delta(\omega - \omega_s) + \delta(\vec{k} + \vec{k}_s)\delta(\omega + \omega_s)\right] \cdot \left[h^+(\vec{k}, \omega) + h^-(\vec{k}, \omega)\right]$$

where h^+ and h^- are the two lobes of the amplitude response. We consider a V1 complex cell that has gaussian temporal frequency tuning, gaussian direction tunings and logarithmic-gaussian tuning for spatial frequency. In this case we can compute the integral and we obtain:

$$H(S) = H^+(S) + H^-(S), \text{ with}$$

$$H^\pm(S) = \exp\left[-\frac{(d-\theta)^2}{2{w_d}^2} - \frac{(\omega \mp \phi)^2}{2{w_t}^2}\right] \cdot \exp\left[-\left(\ln_2 \frac{k}{\kappa}\right)\frac{1}{2{w_k}^2}\right]$$

where (θ, ϕ, κ) are the preferred direction, temporal- and spatial-frequency of the complex cell and w_d, w_t, w_k are the width of the corresponding tuning functions. The preferred spatial frequency is $\kappa = k_s$. The preferred speed v_p and preferred direction of motion d_p of the MT component cell are simply $v_p = \phi/\kappa$ and $d_p = \theta$.

The SH-component model has 11 parameters:

Table 3, parameters of the SH-component model

b	Baseline
g	Gain
C_{50}	Semisaturation contrast
n	Exponent in MT
m	Exponent in V1
σ	Tuning width underlying C_σ

d_p	Preferred direction of motion
v_p	Preferred speed
w_k	Spatial frequency tuning width
w_t	Temporal frequency tuning width
w_d	Direction tuning width

In this simplified form the SH-model for component cells is very similar to the component model discussed in 5.3.1. The larger number of parameters is misleading because, as we will see in the next chapter, 3 of the 11 parameters are fixed for the fits, namely w_k, v_p and m. This parameters are not constrained by the considered stimuli. As a result, only 8 parameters are free in the fits, as in the component model.

The considerations on the direction-direction and direction-contrast responses that we made in the discussion of the previous component models hold also for the SH-component model. However, in this formulation of the response the mechanisms leading to the response characteristics of a particular cell are explicit. For example, the response in the nonpreferred direction, controlled through r_n in the component model, is now controlled through the combination of v_p and w_t. By decreasing the preferred speed v_p or by increasing the temporal frequency tuning width w_t the linear output H(S) is different from zero also for a stimulus moving in the nonpreferred direction. This effect is controlled by the term in the integral given by the product of stimulus-energy in the positive temporal-frequency-space and the amplitude response in the negative temporal-frequency-space, and vice versa.

5.4.2 SH-Pattern Model

The response of the SH-pattern model to a grating or plaid is:

$$R = \left\lfloor b + \frac{g}{N} \sum_{\theta} V^{\theta}(S) \right\rfloor^{n} \qquad (22)$$

as in the SH-component model, with the difference that now we sum over N V1 complex cells lying on an ellipse in frequency space, with preferred directions θ uniformly distributed between 0 and 360 deg. The ellipse is defined by:

$$\phi = v_x \kappa \cos(\theta) + v_y \kappa \sin(\theta) \quad \text{and} \quad \kappa = k_s$$

where $v_p = (v_x, v_y)$ is the preferred velocity of the cell.

The SH-pattern model has 12 parameters, the same 11 as the SH-component model plus N, i.e. the number of cells on the ellipse. We have fixed N to a large value, so that the resulting frequency space “receptive field” of the MT pattern cell has smooth contours

even for small tuning width of the underlying V1 cells. Similarly to the SH-component model, some parameters will be fixed for the fits.

Direction-direction responses

The SH-pattern model predicts a bimodal direction tuning for gratings moving slower than the preferred speed of the cell. This is shown in Figure 34C. The mechanisms underlying the response of the SH-pattern model are best understood by considering only the sum over rectified linear V1 responses:

$$P(S) = \sum_{\theta} \left\lfloor c_1 H^{\theta}(S_1) + c_2 H^{\theta}(S_2) \right\rfloor^m$$

The response of P for m = 1 is shown in Figure 34A. It consists of the sum of the individual response to the two gratings. We have seen in Figure 14 that for $v_p > v_{grating}$ the energy of every grating crosses the plane containing the underlying V1 receptive fields in two points lying in symmetric positions around the preferred direction d_p. The maxima of the response for grating 1 lie on two vertical lines, while for grating 2 they lie on two horizontal lines. This is equivalent to the component models, with the difference that the response to a grating is bimodal instead of unimodal. The resulting response of P to plaids has four local maxima.

For m = 2 the situation is similar, with the difference that two of the four maxima are more pronounced, as shown in Figure 34B. The two pronounced maxima correspond to the situation where the energy of the two gratings lie in the plane in the same point, i.e. the energy of one grating with c = 1 lies in the plane. On the other hand, the two reduced peaks correspond to the situation where the energy of the two gratings lies in the plane in different points, i.e. a plaid moves in the preferred direction of the cell with preferred speed.

The particular form of the normalization signal for direction-direction responses (see for example Figure 30B) increases again the response to plaids compared to the response to c = 1 gratings, as shown in Figure 34C.

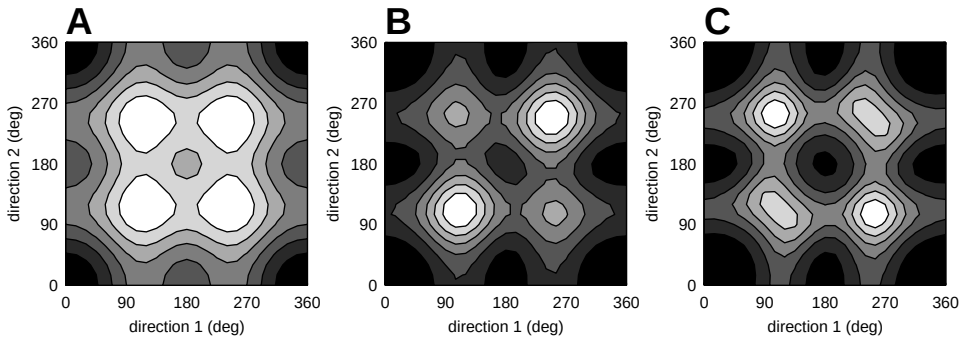

Figure 34, SH-pattern model response for $v_p > v_{grating}$. In all the figures $v_p = 2$. A: the response of the rectified linear V1 stage P for m = 1. B: the response of the rectified linear V1 stage P for m = 2. C: response of the SH-pattern model for m = 2, $\sigma = 30$. See text for details.

For $v_p < v_{grating}$ the SH-pattern predicts the same direction-direction responses as a component selective cell, as discussed in Figure 14. This is illustrated in Figure 35.

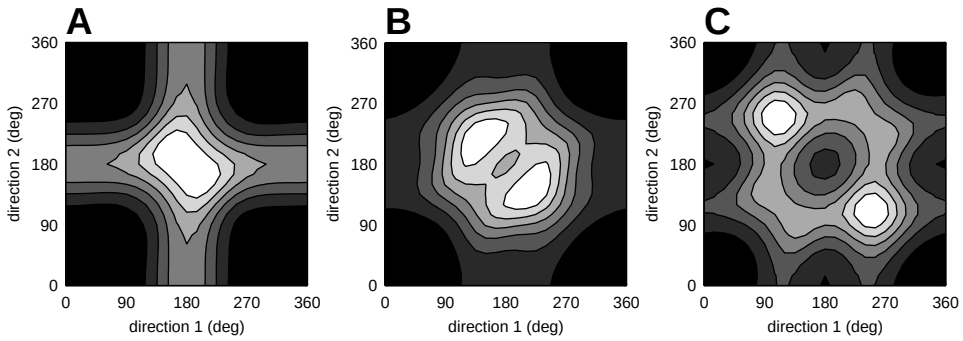

Figure 35, Predicted response of the SH-pattern model for different preferred speeds. A: $v_p = 1.0$; B: $v_p = 1.6$; C: $v_p = 2.7$. All the speeds in units of the grating speed.

Direction-contrast responses

Similar considerations as for the direction-direction responses predicted by the SH-pattern model hold also for the direction-contrast responses. Both the combined effect of the underlying linear part of the cell, the exponent m of rectification in V1 and normalization and the effect of changing the preferred speed of the cell are shown in Figure 36.

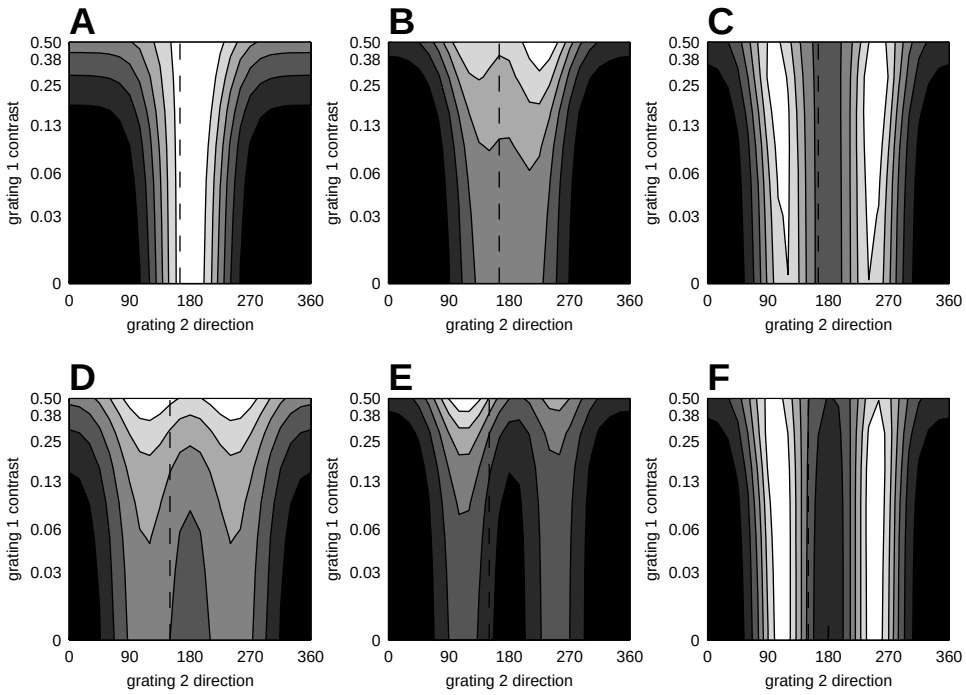

Figure 36, Direction-contrast response predicted by the SH-pattern model. A-C: predicted response for different preferred speeds. A: $v_p = 1.0$; B: $v_p = 1.6$; C: $v_p = 2.7$. All the speeds in units of the grating speed. D: the response of the rectified linear V1 stage P for m = 1. E: the response of the rectified linear V1 stage P for m = 2. F: response of the SH-pattern model for m = 2, $\sigma = 30$.

Differences with the full model

Some of the differences between the SH-pattern model and the full model proposed by Simoncelli and Heeger (1998) play a role even for the set of stimuli used in this study. In the SH-model we consider only V1 afferents with preferred spatial frequency equal to the spatial frequency of the stimulus, i.e. $\kappa = k_s$, see 5.4.1. This is a reasonable approximation for the case of stimuli with constant spatial frequency. However this simplification has some important effects on the response of the model.

First, the preferred directions δ of the V1 afferents lying on the ellipse in frequency space are homogeneously distributed between 0 and 360 deg. The consequence is that for $v_p \neq 0$ the centers of the corresponding receptive field are not homogeneously distributed in frequency space. More precisely this choice produces a higher density of cells is the regions lying far away form the spatial frequency plane (i.e. in the preferred or nonpreferred direction) compared to regions close to the spatial frequency plane (i.e. directions perpendicular to the preferred direction).

Second, in the full model the cells on the plane in frequency space that respond maximally when a grating is moving in the preferred or nonpreferred direction are approximately the cells that are closest to point in frequency space where the energy of

the grating is different from zero. For $v_p \neq 0$ these are cells with $\kappa < k_s$, and thus do not lie on the ellipse considered in the SH-pattern model. For a grating moving in the preferred or nonpreferred direction the maximal response over the cells lying on the ellipse is smaller than the maximal response over the cells on the plane. Because of that the SH-model underestimates the response of gratings moving in the preferred and nonpreferred directions. However, the underestimation of the responses is larger when the energy of the stimulus lies far away form the receptive field plane. As a consequence, the response to gratings moving in the nonpreferred direction is more underestimated than the response to gratings moving in the preferred direction. This problem arises not only for the SH-pattern model, but also for the SH-component model.

Third, we have not considered subtractive off-plane inhibition. As pointed out by Simoncelli and Heeger (1998) off-plane inhibition is fundamental for example for the explanation of speed tunings for gratings.

These differences between the full model and the SH-model have different effects on the predicted responses, and up to a certain degree they tend to compensate each other. We will discuss these issues in detail in section 8.1 and 8.2. In particular, we will see that these simplifications cause an underestimation of the responses of the SH-pattern model to gratings moving in the nonpreferred direction, and thus also to counterphase gratings. On the other hand, the SH-component model can compensate the underestimation by appropriately changing the value of w_t.

6 Methods

In the previous chapters we have seen some examples of measured cell responses and many examples of model predictions. These examples allowed us to understand the range of possible model responses and the ability of the various models to reproduce at least qualitatively the characteristics of measured responses. To get a more quantitative measure of this ability we will now try to fit the models to the data. We do that by minimizing the Euclidean distance between model prediction and measurements.

We can consider the measurements as an array r_{rs}, where the subscript r indicates the repeat and s indicates the stimulus. For each stimulus s we consider the model prediction m_s, and we define the (mean square) distance between data and predictions as:

$$d(r_{rs}, m_s) = \frac{1}{N_s N_r} \sum_{r,s} (r_{rs} - m_s)^2$$

where N_r is the number of repeats and N_s is the number of stimuli.

With this choice for the distance to minimize, we can use the percentage of variance as an intuitive measure of fit quality. The percentage of variance explained by a model is:

$$\%\text{variance} = 100 * \left[1 - d(r_{rs}, m_s) / d(r_{rs}, \bar{r})\right] \qquad (23)$$

where $\bar{r}$ is the response mean across stimuli and repeats, and $d(r_{rs}, \bar{r})$ is the variance across stimuli and repeats of the cell responses.

For each data set, we fitted the predictions of the 6 models described in the previous chapter. For reference, the abstract component and abstract pattern models are defined through equations (12) and (13), the component and pattern model are defined in equation (18) and (20), and the SH-component and the SH-pattern model are defined in equations (21) and (22). The fits for the direction-direction data (19 cells) and the direction-contrast data (12 cells) where computed separately.

The parameters of the models were allowed to vary inside some predefined boundaries. These boundaries are listed in Table 4. To reduce the number of free parameters, in some cases the minimum and maximum allowed are the same, indicating that a parameter was pegged at that value. We will consider in more detail the reasons for our choice of the parameter boundaries in section 8.2.

Table 4, Parameter boundaries for the fits.

	Abstract Models		SH-Models	
Parameter	min	max	min	max
b	0	200	0	200
g	0	4000	0	4000
c_{50}	0.01	0.8 *	0.01	0.8
n	0.5	5	0.5	5
σ	15 deg**	80 deg**	30 deg	30 deg
m	-	-	2	2
d_p	140 deg	220 deg	140 deg	220 deg
r_n	-1	1	-	-
s_p	0.1	5	0.1	5
w_s	0.1	3	-	-
w_k	-	-	1 octave	1 octave
w_d	15 deg	120 deg	15 deg	80 deg
w_t	-	-	0.2	2
N	-	-	32***	32***

* 100 for the pattern model
** 30 for the pattern model
*** 1 for the SH-component model

7 Results

The small population of 19 cells that we considered exhibits a wide variety of response characteristics. It is however possible to roughly divide at least a subset of the cells in three different classes, on the basis of the qualitative analysis of their responses to the direction-direction stimuli. The first class consists of cells that are in essence pattern-direction selective following the definition introduced by Movshon et al. (1983). For these cells the shape of the direction tuning for plaids is approximately invariant for different plaid angles, and the absolute maximum of the cell response is obtained for a plaid with an angle greater than zero (i.e. not for a grating with c = 1). The second class consists of cells that are clearly selective for the components of the plaid, and show the typical cross-shaped response profile in direction-direction experiments. We have seen examples of cells in these two categories in Figure 18. The third class consists of cells that show a bimodal direction tuning for gratings, and are thus candidate for being pattern-direction selective as defined in the model of Simoncelli and Heeger (1998).

In this chapter we will start by considering the responses of one cell for each of these three classes to direction-direction experiments. We will then consider the best fits of the four models with normalization to see whether our qualitative cell categorization corresponds to different performances of the pattern and component models. We will then look at fits of the direction-contrast data and finally we will compare the performance of the models for the two data sets, for individual cells and over the entire cell population.

7.1 Direction-direction experiments

A putative patter-direction selective cell

In Figure 18B we have seen an example of a cell that is roughly consistent with the definition of pattern direction selectivity given by Movshon et al. (1983). The shape of the direction tuning for this cell remains constant over a wide range of plaid angles, and the response is maximal for a plaid with an angle of 60-90 degrees, corresponding to a plaid speed between 1.2 and 1.4 times the speed of the components. The partial correlations for the cell are R_c = 0.49, R_p = 0.73 for a plaid angle of 120 deg, so this cell would be classified as “pattern” according to Movshon et al. (1983).

The best fits of this cell for the four models with normalization and the corresponding percentages of variance are shown in Figure 37. Surprisingly, all the models provide very similar and almost equally good fits. In particular, both the pattern and the component models are able to reproduce a salient characteristic of the responses, namely that the response is maximal for plaids and not for gratings. We have seen in chapter 5 that this ability of the component models is a consequence of normalization.

For this cell and for many others, the most important differences between the models are given by the predicted responses for large plaid angles.

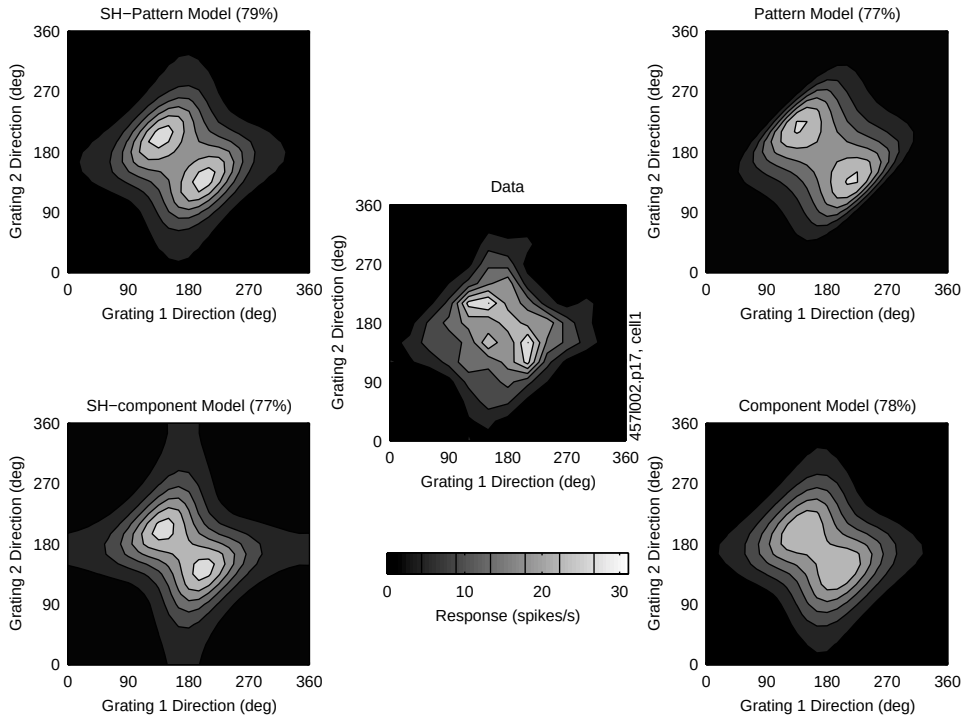

Figure 37, Fits of the direction-direction response for a putative pattern-direction-selective cell. Only the predictions of the four models with normalization are shown. The percentage of variance explained by the models is indicated in parentheses.

A putative component-direction selective cell

In Figure 18A we have seen an example of a cell that would be classified as component-direction selective following the definition of Movshon et al. The cell has the cross-shaped response that we would expect from a mechanism that responds to the components of the plaid. Indeed, the partial correlations are $R_c = 0.89$ and $R_p = 0.28$.

The fits of this cell's responses are shown in Figure 38. Here, the only model that is clearly unable to fit the responses is the Pattern Model, which explains only 67% of the variance. Surprisingly, the SH-Pattern model, instead, performs almost as well (77% of the variance) as the two Component models (79% and 80% of the variance). What is happening? We have already seen in the discussion of the Simoncelli-Heeger models that the SH-pattern model behaves like a component cell when the preferred speed of the cell is lower than the speed of the gratings. By contrast, the Pattern model is not able to produce a similar response, and its fit displays important failures, especially at

large plaid angles. We will discuss these failures of the pattern model in more detail in the Discussion.

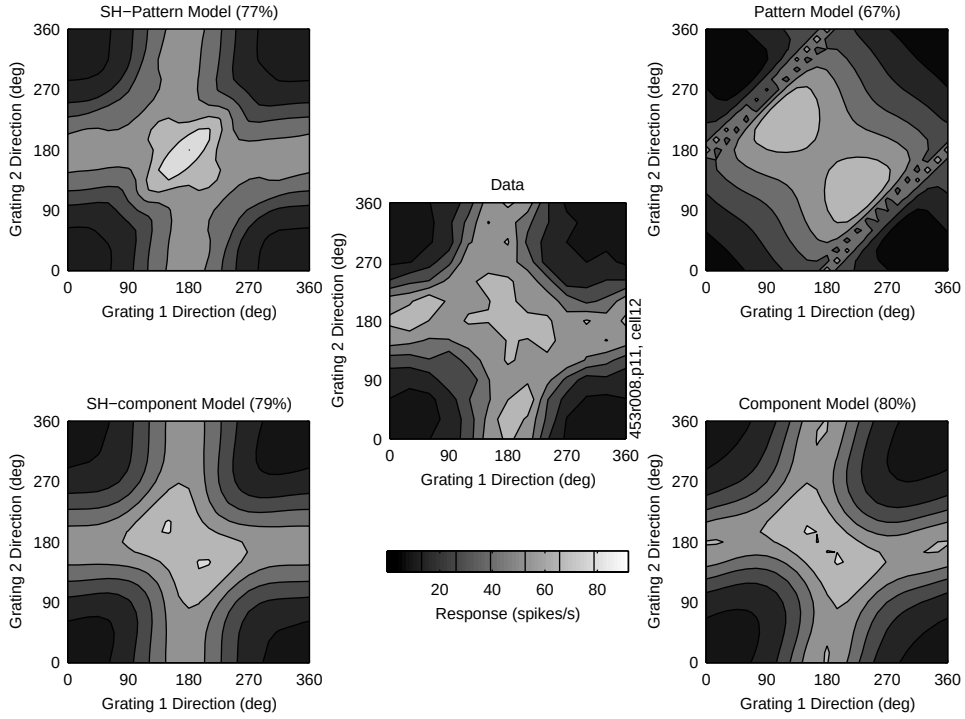

Figure 38, Fits of the direction-direction responses for a putative component-direction-selective cell.

A putative Simoncelli-Heeger pattern-direction selective cell

Earlier we have discussed a way to characterize pattern and component cells based on the speed dependence of the direction tuning for gratings. Indeed, we expect a pattern cell performing some sort of intersection of constraints to have a bimodal direction tuning for slow moving gratings.

An example of such a cell and the fits of the models are shown in Figure 39. The predictions and quality of the fits are very different across the models. The only model that explains a reasonable percentage of the variance in the data (63%) is the SH-Pattern model. This is the only model that predicts the observed bimodal direction tuning is the SH-pattern model. While the component model can produce a larger response to plaids than to gratings (because of normalization), it cannot predict a bimodal response to gratings.

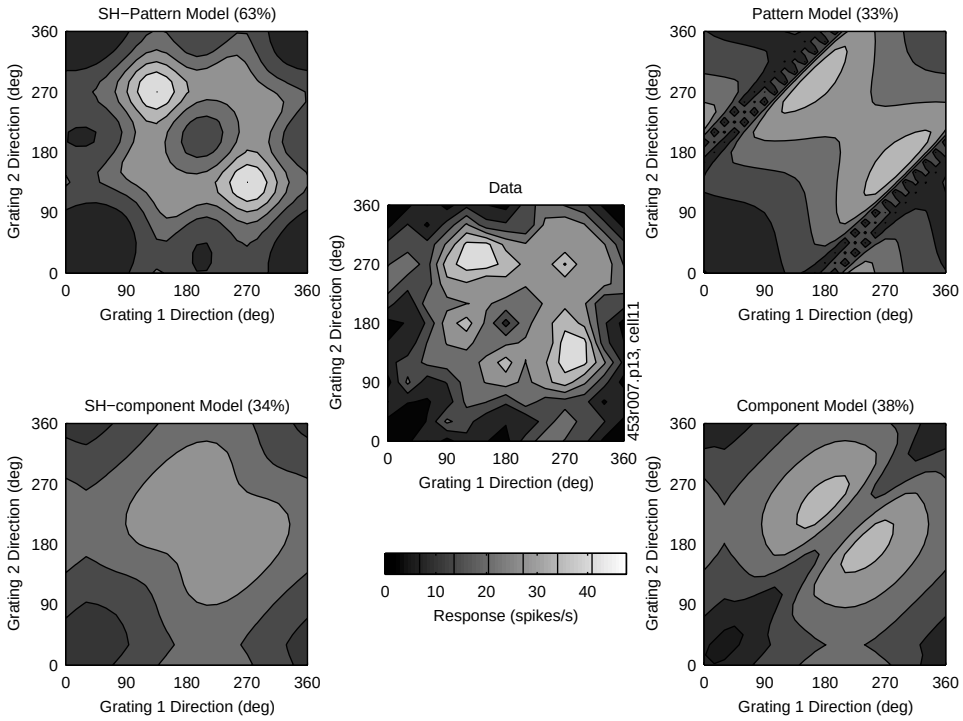

Figure 39, Fits of the direction-direction responses for a cell with bimodal direction tuning for gratings, a candidate for being truly pattern-direction-selective.

7.2 Direction-contrast experiments

We now consider the responses in direction-contrast experiments of two of the three cells examined above (the data were not collected for the cell in Figure 39)

The fits of the direction-contrast data for the putative pattern-direction selective cell illustrated in Figure 38 are shown in Figure 40. With this data set it is possible to exclude one of the four models, the Pattern model.. The remaining models - the SH models and the component models - all provide good fits, explaining a much higher percentage of the variance (78%) than the pattern model (50%).

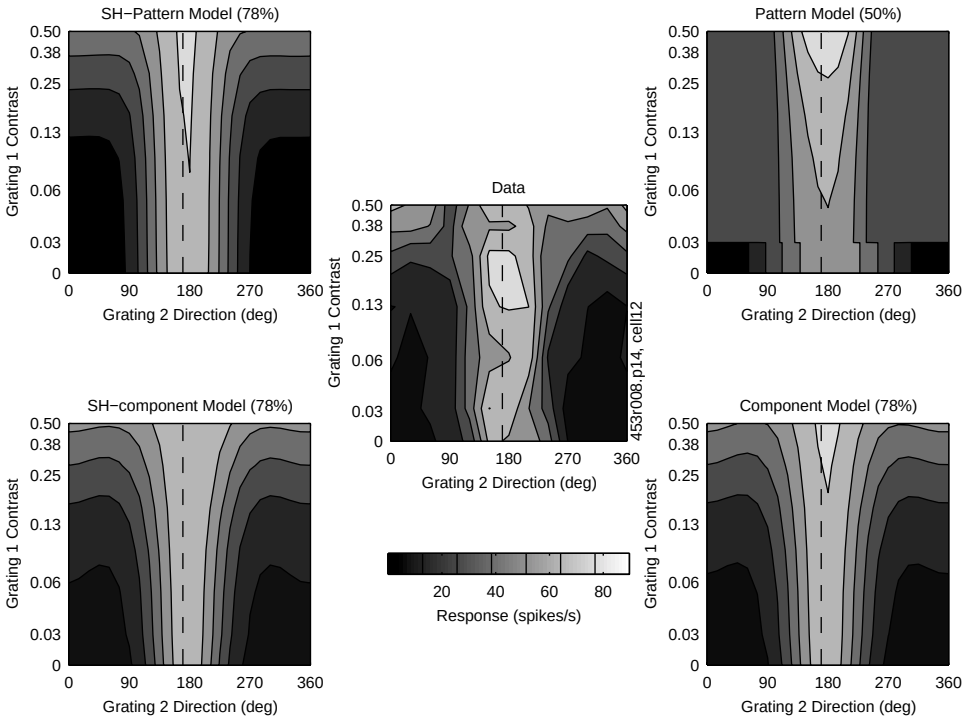

Figure 40, Example of fits for the direction-contrast data. The SH models and the component model are equally good, while the pattern model explains less variance in the data. The direction-direction data for the same cell are shown in Figure 38.

The cell in Figure 40 has a direction-direction response that is typical for a cell selective to the components of the plaid, and was thus indicated as a putative component-direction selective cell. An apparently completely different cell is shown in Figure 41. This cell has a bimodal direction tuning for grating 2 independently of the contrast of grating 1, in particular when $c_1 = 0$. The only model that can predict a bimodal direction tuning for a grating alone is the SH-pattern model. When we add the second grating (i.e. $c_1 > 0$) the responses are influenced also by normalization, in such a way that also the component models can produce a response that is bimodal as a function of the direction of grating 2. For this particular cell, however, the amplitude of the bimodality is captured only by the SH-pattern model and less precisely also by the pattern model for $c_1 > 0$.

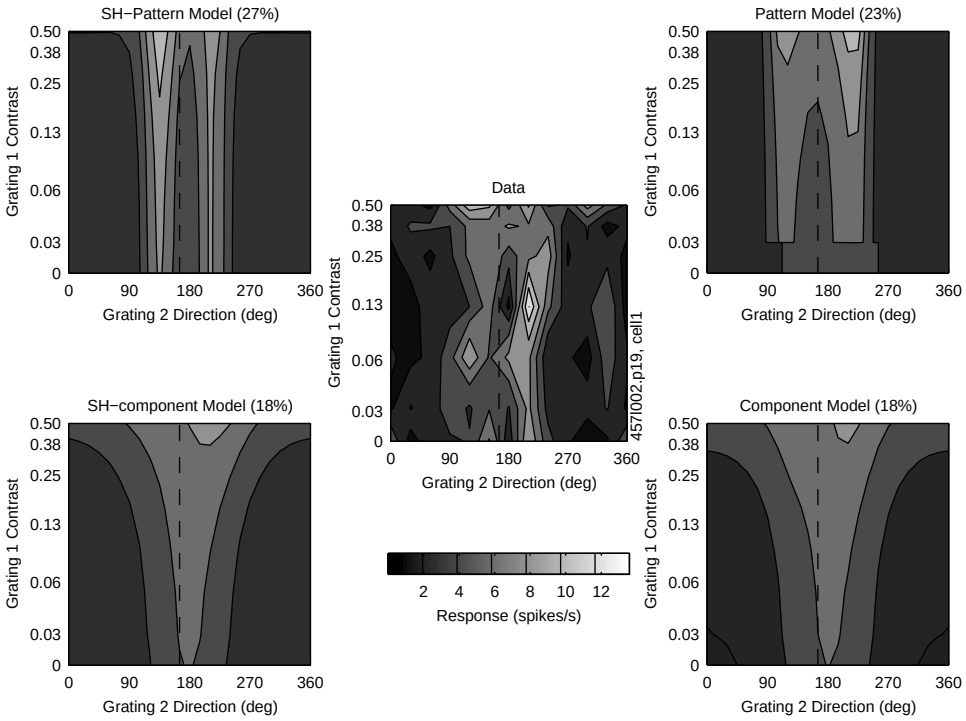

Figure 41, Fits of the direction-contrast data for a cell that shows bimodal response in the direction tuning for a grating alone. Only the SH-pattern model predicts correctly the response of the cell.

7.3 Comparison of the two data sets

To reduce the effect of cortical adaptation (Maffei et al., 1973) the stimuli inside each block or repeat were presented in a random order. However, the adaptation state could be different between the measurement of the direction-contrast and direction-direction responses, and thus affect the value of some of the parameters characterizing the cell. The values of a subset of the parameters for the best fits with the SH-pattern model are shown in Figure 42. While the estimates of preferred direction d_p and preferred speed v_p are mostly constant across experiments, The exponent of rectification in MT (n) and the semisaturation contrast in V1 (c_{50}) estimated from the two experiments are considerably different. Variations in these values are broadly consistent with known effects of cortical adaptation (Carandini and Ferster, 1997).

As an example of a cell that shows an extremely different characteristic in the direction-direction and the direction-contrast responses we consider in more detail the cell shown in Figure 37 and Figure 41. The direction tuning to gratings with contrast c = 0.5 is measured in both experiments and thus provides a good benchmark to compare the state of the cell during the experiments. Figure 43A and B show the direction tuning for gratings with c = 0.5 and c = 1.0 in the direction-direction experiment. Figure 43C

shows the direction tuning for grating 2 (c = 0.5) alone, while D is the direction tuning for grating 2 when grating 1 is superimposed with d_1 = 165 and c_1 = 0.13.

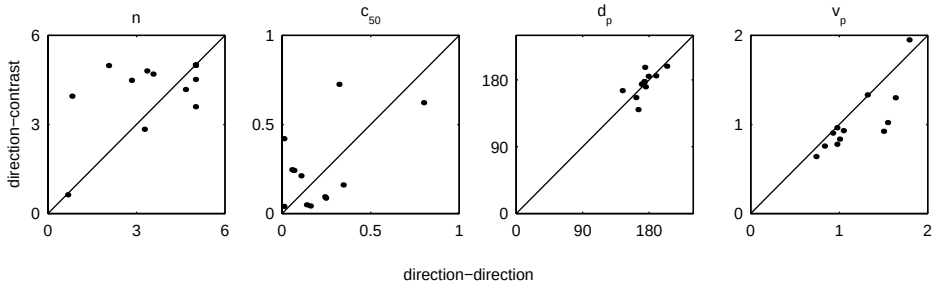

Figure 42, Parameters of the SH-pattern model obtained with direction-directoin and with direction-contrast data sets . The exponent of rectification in MT (n) and the semisaturation contrast in V1 (c_{50}) estimated from the two experiments are considerably different. By contrast, the estimates of preferred direction d_p and preferred speed v_p are mostly constant across experiments.

The direction tunings in the direction-direction response is unimodal, and is well predicted by both the SH-pattern and SH-component models. On the other hand, the direction tuning in the direction-contrast response is bimodal, and can be predicted only by the SH-pattern model. We believe that the bimodality in the direction tuning is not just an effect of the considerable noise in the direction-contrast data because it is present for almost all values of the contrast of grating 1 (see the Appendix for the full set of measurements).

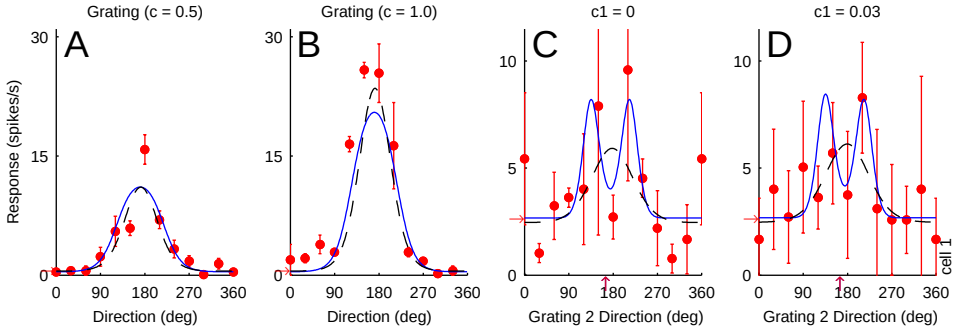

Figure 43, Comparison of the direction tuning for gratings measured in the direction-direction and direction-contrast experiments for the cell in Figure 37 and Figure 41. Both the SH-pattern (dashed) and the SH-component (solid) provide good fits of the direction-direction response. The direction tuning in the direction-contrast response is bimodal, and can be predicted only by the SH-pattern model. The vertical arrow in C and D represents the direction of grating 1. The difference in the two direction tunings could be due to contrast adaptation of the cells in V1 tuned for the direction of grating 1.

Besides the possibility that the cell is truly a Simoncelli-Heeger pattern cell and the direction of grating 1 corresponds to the preferred direction of the cell, it is also possible that the cell response is strongly influenced by contrast adaptation in V1. In fact, across an entire direction-contrast experiment, there are much more presentations

of gratings with direction d_1 than for every other direction. It is thus imaginable that V1 cells tuned for directions close to d_1 are more strongly adapted.

We have not found other cells with such large discrepancies between the direction tunings in the two different experiments. However, we cannot exclude the possibility that contrast adaptation in V1 is relevant for the response of some cells, and could thus influence the performances of the different models.

7.4 Quality of the Fits

To get a general impression about the ability of the models to fit the data we will now compare the quality of the fits for the different models. As a measure of the quality of the fits we will use the percentage of variance explained by a model defined in equation (23).

Abstract models: effect of normalization

We have seen that normalization adds new properties to the abstract pattern and component models both in the direction-direction and direction contrast responses. The effect of normalization on the quality of the fits is shown in Figure 44.

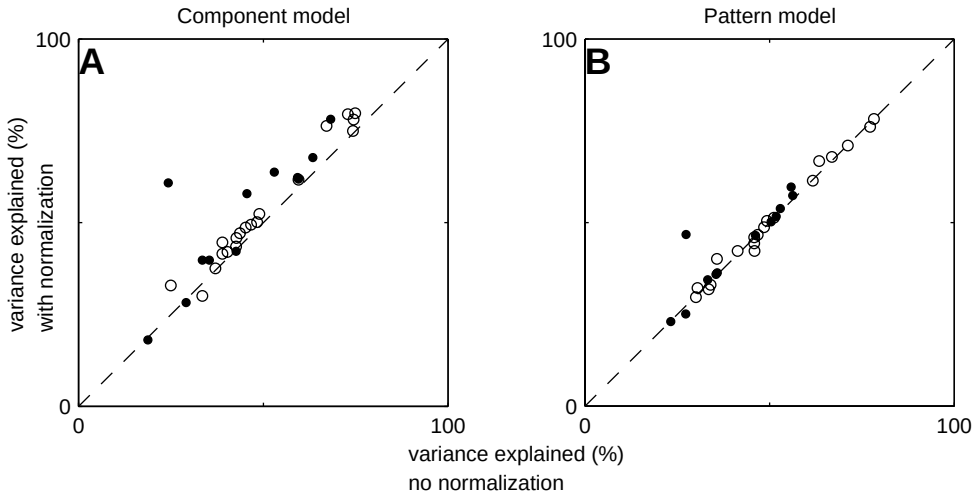

Figure 44, Quality of the fits for the abstract models with vs. without normalization, for the direction-direction data (white markers) and the direction-contrast data (black markers).

For the component model the normalization stage improves the fits of both data sets. The largest increase in the quality of the fits is obtained with the direction-contrast data. In this data set the increase of quality is maximal for cells either with strong saturation of responses or with a strong asymmetry in the response across the axes of the preferred grating direction. Both the asymmetry and the saturation in the direction-contrast data are predicted by the component model only when adding normalization.

An examples of a cell with strong saturation for high contrast gratings is shown in Figure 45. The quality of the fit with the component model is increased by almost 40%.

Normalization has two effects for the direction-direction data. First it changes the position of the maximal response in the direction-direction response. Without normalization the response is maximal for gratings moving in the preferred direction. After the division with the plaid-angle dependent normalization signal the maximal response is obtained for plaids. Second it controls the contrast response as with the direction-contrast data. This contrast response is measured with the direction-direction data with two direction tunings for gratings, one for a grating contrast c = 0.5, the other for a grating contrast c = 1. Many cells show a saturation in the response to the c = 1 gratings that can be predicted only by the models with normalization.

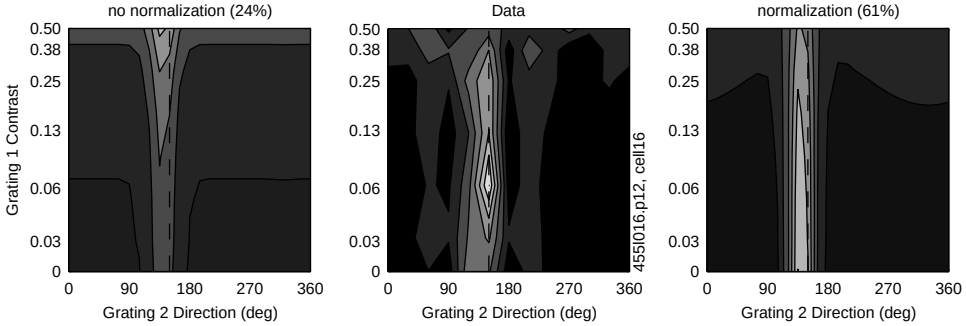

Figure 45, Effect of normalization on the abstract component model. Best fits with abstract component model (i.e. no normalization) and component model (i.e. with normalization) for a cell with strong saturation of responses for high contrast gratings.

For the pattern model the quality of the fits is generally unchanged by the normalization stage. The predicted direction-contrast responses are asymmetric already for the abstract pattern model (i.e. without normalization). The only cell that is much better fitted with normalization than without is the cell in Figure 45, a cell that shows over-saturation in the response to high contrast gratings.

Comparison of the models

The quality of the fits for the component and SH-component model are shown in Figure 46. As expected because of the very similar properties of the two models, their performance does not differ significantly. This allows us to restrict the remaining discussion to the pattern model and the two SH-models.

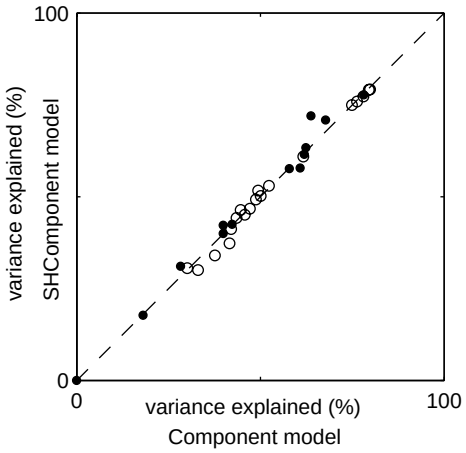

Figure 46, Comparison between the quality of the component model and the SH-component models for direction-direction data (white markers) and direction-contrast data(black markers).

The quality of the fits with the SH-pattern, SH-component and pattern models are shown in Figure 47. For the direction-direction data the quality of the fits is generally very similar for all the models. We have seen in the previous sections that for some cells all the models provide a good description of the response. It would thus not surprise if for a subset of cells the quality of the fits with the different models was very similar. However, there are several cells that, like the cell in Figure 39, show a bimodality in the direction tuning to gratings. Because this response characteristic is predicted only by the SH-pattern model, it is surprising that for these cells the quality of the fits with this model is not clearly larger than for the other models.

For the direction-contrast data the predictions of the pattern model are clearly worse than the predictions of the SH models. On the other hand, the relation between the quality of the SH-pattern and the SH-component model is the same as for the direction-direction data. Again we have to understand why the SH-pattern model is not clearly better for some cells. In the next chapter we will try to understand the reasons for this situation.

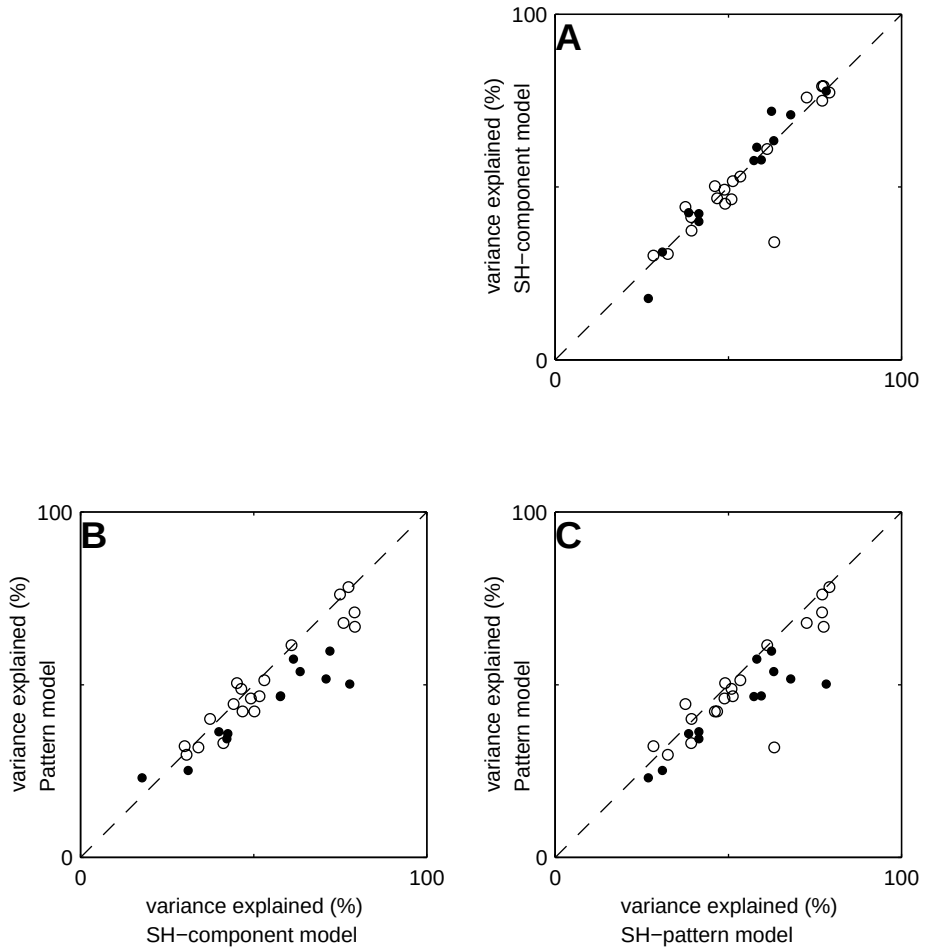

Figure 47, Comparison between the quality (% of variance explained by the model) of the SH-pattern, SH-component and pattern models for the direction-direction data (white markers) and direction-contrast data (black markers).

8 Discussion

8.1 Where the models fail

In the last chapter we have seen how well the different models perform in predicting the measurements for some representative cells. In particular we have seen that for some cells all the models are able to predict the measured response, while for other cells only a subset of the models is able to account for the essential characteristics of the response. Now we will focus on errors in the model predictions that are recurrent over a large number of cells. First, we will consider cells that show a particular asymmetry in the response. Indeed, for some cells the preferred direction of a grating is different from the preferred direction of a plaid, and even the preferred direction of a plaid may depend on the plaid angle. All the models fail in predicting such a response characteristic. Second, we will see that the pattern model is particularly bad in the prediction of the responses for large plaid angles and in the fits of the direction-contrast data. And third, we will discuss why the SH-pattern model often underestimates the response to counterphase gratings.

8.1.1 Asymmetric Direction Tuning

All the models discussed until now predict direction-direction responses that are symmetric around the preferred direction of the cell. As a result, a plaid or a grating moving in the direction $d_p - \Delta d$ evokes the same response as when it is moving in the direction $d_p + \Delta d$. The preferred direction d_p is the one that evokes the largest response to gratings. On the other hand, this symmetry is not always observed in measured responses. In particular, for some cells the direction eliciting the largest response changes with the plaid angle. The consequence is that all models fail in predicting the cell response. Figure 48 shows two examples of cells with asymmetric direction tunings.

The cell in Figure 48B has similar characteristics as a Simoncelli-Heeger pattern cell tuned for high speeds. The cell shows the same four local maxima as in Figure 34. These maxima corresponding to stimuli for which the energy of both gratings lies in the plane that determines the MT receptive field. However, the two peaks in the direction tuning for gratings are not of the same amplitude, and the response to plaids is much more pronounced for plaids moving in direction between 0 and 180 degrees. As a consequence, all models make bad predictions of the cell response. In particular, also the SH-pattern model, the only one that is able to produce a bimodal direction tuning for gratings, does not perform better than the other models.

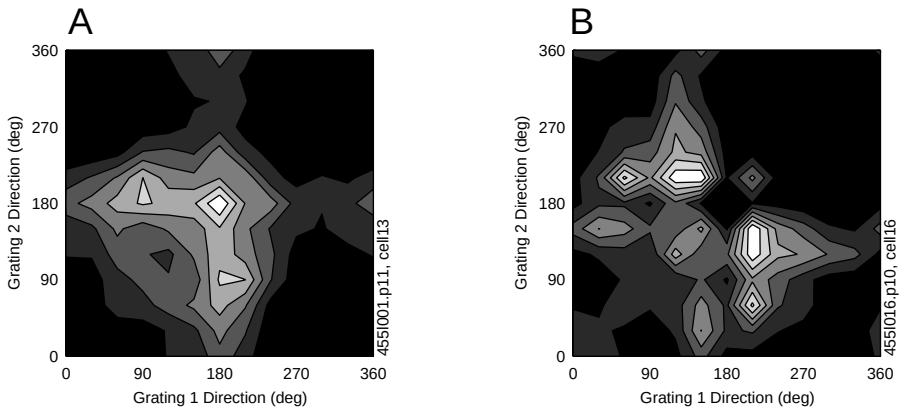

Figure 48, Two cells with asymmetric direction tuning for plaids and gratings. A grating or plaid moving in the directions d_p - Δd does not evoke the same response as when it is moving in the direction d_p + Δd. The result is an asymmetry across the line through the points (0, 360) and (360, 0).

A possibility that could explain this asymmetry in the responses is that, unlike the Simoncelli-Heeger pattern model, these cells sum the V1 outputs with non-constant weights. To test this hypothesis we have implemented an extension of the SH-pattern model where the weights λ(δ) of the V1 inputs depend on the preferred direction δ of the V1 cell. The weights are expressed by two gaussians, both centered on d_p, i.e. the preferred direction of the MT cell. Assume that d_p = 180 degrees. One gaussian determines the weights for angles smaller than d_p, the other one for angles larger than d_p:

$$\lambda_L(\delta) = e^{-(\delta - d_p)^2 / 2w_L} \quad \text{for} \quad \delta < d_p$$

$$\lambda_R(\delta) = e^{-(\delta - d_p)^2 / 2w_R} \quad \text{for} \quad \delta > d_p$$

where w_L and w_R are the tuning width of the two gaussians. The asymmetry in the direction-direction responses arises for $w_L \neq w_R$.

Figure 49 shows the best fit with this model for a cell with asymmetric direction tunings. The corresponding weights are illustrated in a polar plot. The model captures the asymmetry of the response, and the quality of the fit is 10 % higher as for the previously discussed models. The two tuning width are w_R = 50 deg and w_L = 40 deg. Even if the preferred speed for the fit is v_p = 3.3, the direction tuning for gratings is not bimodal. Interestingly, the preferred direction is d_p = 124 deg. Thus, we can interpret the response as a prediction of the SH-pattern model for high preferred speeds (Figure 34, with the difference that on of the four local maxima is missing.

This result suggests that at least some of the discrepancies between the models and the data could be explained by differences in the weights of the afferents to MT. However, a model that tries to capture a similar situation has necessarily more parameters than the SH-model already has.

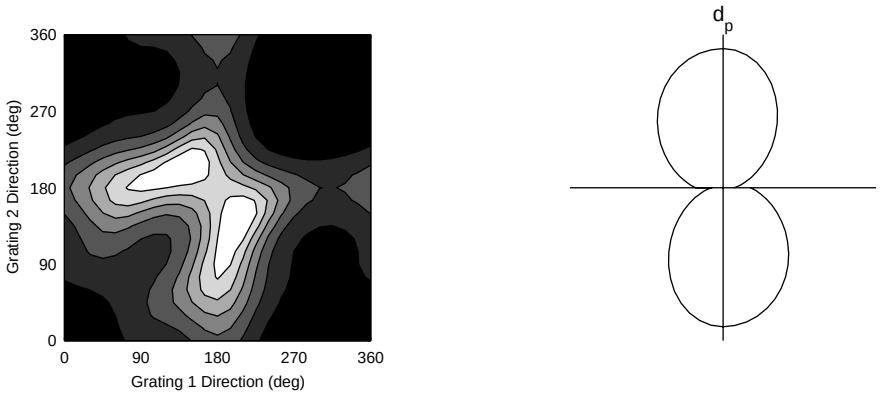

Figure 49, Best fit of an extension of the SH-pattern model to the cell in Figure 48A. The V1 afferents are summed with variable weights as a function of the preferred direction of the cells. The weights used for this prediction are shown in the polar plot on the right. See text for details.

8.1.2 Abstract Pattern Model

The abstract pattern model fails very often in the prediction of the direction tuning for fast plaids (i.e. plaids with large angle between the components). Whenever a cell has a bimodal direction tuning for fast plaids the abstract pattern model provides bad fits. We have already seen an example in Figure 38, and Figure 50 shows the measurements for three other cells together with the predictions of the pattern model and the SH-pattern model.

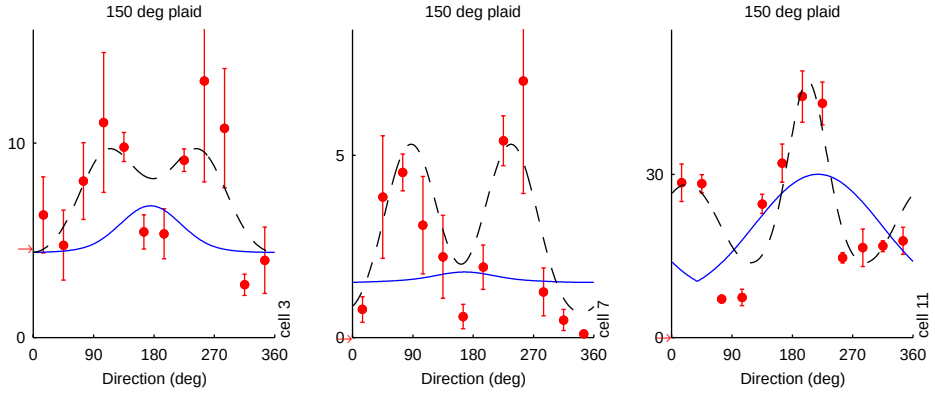

Figure 50, Prediction of the pattern and SH-pattern models for fast plaids. The dashed line represents the SH-pattern model prediction, the solid line the pattern model prediction. The fits were computed on the complete direction-direction responses.

The consequence of these errors in the predictions of the pattern model is that a “component” cell, defined following Movhon et al. (1983), cannot be accurately described by the abstract pattern model. This is not a surprise, because the abstract pattern model has been explicitly constructed to produce the same shape for the direction tuning for gratings and plaids. It is however significant, because on the other hand the SH-pattern model can predict the response of a component cell.

The quality of the predictions for the direction-contrast data is generally much lower for the pattern model as for the other models. A first reason is the discontinuity in the response when a second grating is added to the first. Whenever the second grating is added to the first, independently of the contrast of the gratings, the pattern model treats the stimulus as a plaid. The resulting discontinuity in the response arises both from the direction- and the speed-tuning functions. We have discussed these issues in detail in 5.3.2. A second reason is the inability to predict the responses of a component-selective cell, as in the direction-direction data. The direction-contrast data contains a direction tuning for grating 2 when grating 1 is superimposed to it at a fixed direction d_1. The responses to these stimuli are measured also in the direction-direction data, and, depending on the value of d_1, they can be very different for what we have called a putative pattern cell and a putative component cell. As a consequence, for both data sets the quality of the fits with the pattern model is low for a component-selective cell. And finally, there is no reason why the pattern model should correctly predict the measured contrast responses. The contrast dependence of the numerator in equation (20) is completely ad hoc, and has been chosen mainly because of its simplicity.

8.1.3 SH-Models

A minor but recurrent imprecision in the fits with the SH-pattern model is an underestimation of the maximal response to counterphase gratings. This underestimation does not affect the quality of the fits in a dramatic way. However, it gives some insights into the function of the parameters in the different models.

It is convenient to compare the fits of the SH-pattern and the SH-component models for a cell that is classified as a “component” cell following Movshon et al. (1983). In the discussion of the SH-pattern model (5.4.2) we have seen that this model can predict responses that are very similar to the predictions of the SH-component model. However, for some “component” cells the predictions of the fits with the two models differ for counterphase gratings, as shown in figure Figure 51. The SH-pattern model generally underestimates the amplitude of the orientation tuning for counterphase gratings.

This underestimation is a consequence on the simplifications underlying the SH-pattern model. While the full pattern model proposed by Simoncelli and Heeger (1998) considers cell on a plane, the SH-pattern model considers only cells lying on an ellipse. This has effects mostly on the response to gratings moving in the nonpreferred direction. A similar approximation underlies also the SH-component model, which considers only one input cell, instead of many cells lying on a line. However, the responses of the model are not affected by this approximation.

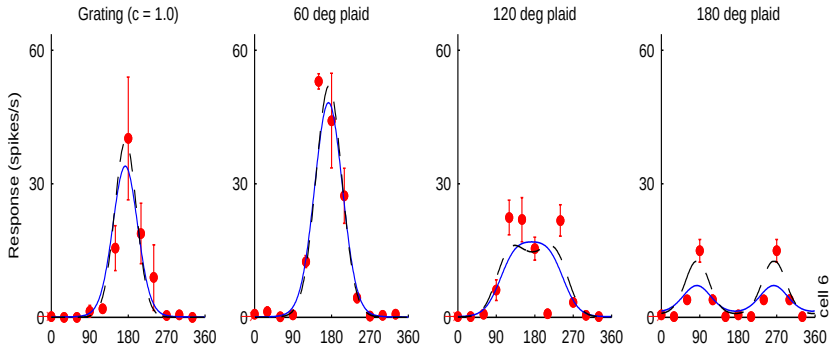

Figure 51, Example of underestimation of the response to counterphase gratings by the SH-pattern model. The figure shows the data for a "component" cell and the best fits for the SH-pattern model (solid) and the SH-component model (dashed). The most important difference between the model predictions is given by the predicted response to counterphase gratings.

It is helpful to consider the frequency domain description of the SH-models to understand why the same approximation has different consequences on the two models. Both the SH-component and the SH-pattern models consider only V1 afferents with preferred spatial frequency κ equal to the spatial frequency k_s of the stimulus. However, in the full models the cell responding maximally to a grating is the one that in frequency space lies closest to the point where the energy of the grating is different from zero. The response of the cell with $\kappa = k_s$ is always equal or smaller than the response of the cell closest to the energy of the stimulus. This underestimation of the response in the SH-models is important when the stimulus energy is far away from the plane or the line determining the receptive field of the MT cell. In particular the response of a grating moving in the preferred direction is less underestimated than the response of a grating moving in the nonpreferred direction.

This underestimation of the responses for counterphase gratings is thus common to both SH-models. Moreover, for both models the underestimation can be compensated by an increase of the temporal frequency tuning width w_t. This is illustrated in Figure 52.

There is however an important difference between the effect of an increase of w_t in the two models. For the SH-component model the direction tuning for gratings is affected only for directions close to the nonpreferred one. In the limit of very large values of w_t the direction tuning has two maxima lying on the preferred and the nonpreferred directions, while the minimum of the response depends on the direction tuning width w_d. On the other hand, for the SH-pattern model the direction tuning is affected for all directions. In the limit of very large values of w_t the response to a grating is independent of its direction. As a consequence, only the SH-component model can generally compensate the underestimation to counterphase gratings.

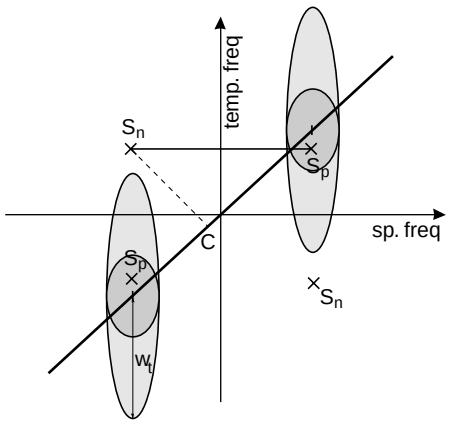

Figure 52, Receptive field of SH-model-cells in the frequency domain. The figure shows the receptive field of the V1 complex cell afferent to MT with the same preferred direction as the MT cell for two different temporal frequency tuning width w_t. The crosses indicate the energy of a grating moving in the preferred direction (S_p) and in nonpreferred direction (S_n). In the full Simoncelli and Heeger model there are other V1 cells lying on the plotted line trough the origin. The point C indicates the position of the cell with maximal response for gratings moving in nonpreferred direction.

In Figure 51 we have already seen an example of a cell for which the fits with the two SH-models show these differences. This cell is a "component" cell, and therefore the preferred velocity of the SH-pattern cell is lower than 1 (v_p = 0.92). The direction tuning width for the two models are very similar (w_d = 58 deg for the SH-pattern model, w_d = 59 deg for the SH-component model), while the values of w_t differ significantly: w_t = 0.2 for the SH-pattern model, wt = 1.0 for the SH-component model. This difference explains the larger response of the SH-component model for the counterphase gratings, compared to the response of the SH-pattern model.

One of the undesired effects of an increase of w_t on the response of the SH-pattern model is the reduction of the bimodality in the direction tuning for slow moving gratings. For a large w_t the direction tuning is unimodal even for $v_p > 1$. An example is shown in Figure 53. The figure shows the fits of the SH-pattern model for the cell already shown in Figure 48B. Even for v_p = 1.5 the direction tuning is almost unimodal, because of the large value the temporal frequency tuning width (w_t = 1.3).

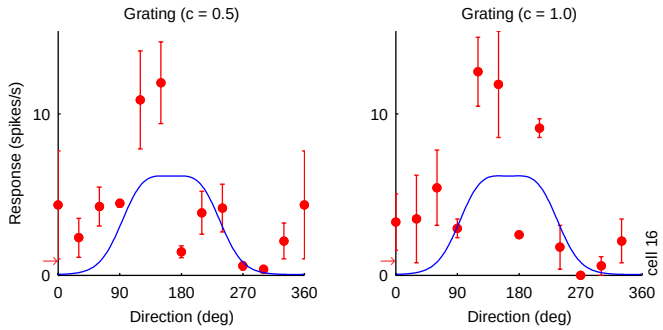

Figure 53, The bimodality in the direction tuning for gratings predicted by the SH-pattern model is not visible for large values of w_t. The line is the best fit for the SH-pattern model. The data is the same as in Figure 48B.

We have seen a similar example in Figure 43, where we have compared the direction tunings for gratings measured in the direction-direction and in the direction-contrast measurements. In the fits of the first experiment the direction tuning predicted by the SH-pattern model is unimodal, while it is clearly bimodal for the fits of the second experiment. The relevant parameters are $v_p = 1.3$, $w_t = 0.34$, $w_d = 51$ deg for the direction-direction data and $v_p = 1.3$, $w_t = 0.20$, $w_d = 23$ for the direction-contrast data. In this case the bimodality is not visible for the direction-direction response because of the combined effect of the increase of w_t and w_d.

Therefore, we can conclude that the approximation of summing only over a subset of the V1 afferents considered in the full model has very different effects on the SH-pattern and the SH-component models. The SH-component model is a good approximation of the full model for the purposes of this study. On the other hand, the predictions of the SH-pattern model are probably different from the predictions of the full model on a subset of the considered stimuli. However, to compare the predictions of the SH-pattern model with the predictions of the full model, we have to consider also the other simplifications underlying the SH-model. Most importantly we have not implemented the off-plane inhibition of the full model. This off-plane inhibition is maximal for stimuli with energy lying far away from the plane of the MT cell. The SH-pattern model underestimates the response for these same stimuli. Therefore, the SH-pattern model possibly predicts similar responses as the full model with off-plane inhibition.

8.2 The number of free parameters

We have already defined the boundaries for the parameters of the models in Table 4. The precise choice of these boundaries was not arbitrary, but is imposed by the properties of the stimuli and the models used in this study. In this section we will discuss in detail why some of the parameters cannot be constrained by the data and thus were fixated in the fits.

The SH-component and SH-pattern models have the same number of parameters. However, the SH-component model has one less free parameter in the fits. More precisely, the preferred speed for the SH-component model is fixed to $v_p = 1$. The reason is best understood in frequency space. In the considered experiments the frequency space is explored only in a plane parallel to the spatial frequency plane. As a consequence, the differences between the response of a cell tuned to $v_p \neq 1$ and a cell with $v_p = 1$ can be completely compensated by changing the temporal frequency tuning width w_t of the only V1 complex cell underlying the receptive field of the MT cell (Figure 52). The consequence is that only one of the two parameters v_p and w_t is effectively constrained by the data, and thus only one was free in the fits.

For similar reasons the value of other parameters is fixed in the fits. First, the spatial frequency tuning width w_k in the SH models is not constrained by the data and is thus fixed to the arbitrary value of 1 octave. Second, the exponent of rectification in V1 in the SH models is fixed to m = 2. Even if a change in m has an effect on the predictions of the SH-pattern model, as we have seen in the discussion of the model, these effects are small enough to be neglected. And finally, to reduce the number of parameters and thus facilitate the fitting procedure, the direction tuning width underlying the normalization stage is fixed to σ = 30 degrees for the SH-models and the pattern model.

These choices also point to a difference between the full models proposed by Simoncelli and Heeger and our simplified implementations. In the full models the parameters have a direct biological meaning. This meaning is lost for most of the parameters in our implementations. For example, the underestimation of the predictions of the SH-pattern to gratings moving in nonpreferred direction can be compensated by an increase of the temporal frequency tuning width w_t. Therefore, the value of w_t reached in a fit is influenced both by the real temporal tuning width of the underlying V1 cells, and by the compensation of the underestimation of the responses to counterphase gratings. And similarly, the SH-models do not consider the MT normalization stage that has been implemented in the full models. The possible combined effect of normalization in V1 and MT is approximated by a normalization stage that formally takes place in V1. Thus the parameters controlling the normalization stage in our implementation, namely c_{50} and σ, model both the normalization in V1 and the normalization in MT.

8.3 Summary and Conclusions

The aim of this study was to get a better understanding about the mechanisms underlying motion processing in macaque area MT. Previous authors have identified two different classes of cells in MT, namely component- and pattern-selective cells. Movshon et al. (1983) were able to distinguish these two cell classes by comparing the direction tunings for gratings and plaids. In this study we have analyzed large data sets exploring the cell responses to a wider range of stimuli, all based on the superposition of two gratings.

To analyze these large data sets we have implemented different models for pattern and component cells and we have fitted them to the measurements. We have used two completely different approaches in the derivation of the model responses. First, we have implemented abstract component and pattern models that are thought to be extensions of the original models proposed by Movshon et al. that allow quantitative predictions of the responses to the larger data sets used in this study. We have implemented these abstract models in two ways: once without normalization (abstract component and

abstract pattern models) and once with normalization (component and pattern models). Second, we have used simplified implementations of the two stage models for component and pattern cells proposed by Simoncelli and Heeger (1998). These models, unlike the abstract models, make precise assumptions about the detailed neuronal mechanism underlying the cell responses. The resulting number of free parameters is too large to fit the models to the data. To reduce the number of parameters, we had to implement simplified versions of the models (SH-component and SH-pattern model). An undesired effect of our simplifications is that the SH-pattern model underestimates the responses of the original pattern model to gratings moving in the nonpreferred direction. Moreover, some of the parameters in our simplified implementation have lost the direct biological meaning that they have in the full model.

We have implemented a normalization stage for the abstract models and the SH models in a common form. In our implementation the normalization signal is a function of the plaid angle, reflecting the fact that for two superimposed gratings the energy of the image changes for different angles between the gratings. The normalization stage ads new important features to the abstract models. It generally increases significantly the quality of the fits with the component model, while the quality remains generally unchanged for the pattern model.

The formulations of the component model and of the SH-component model are in many aspects equivalent. Thus, it is not surprising that their predictions are almost undistinguishable. The SH-pattern model predicts responses that are very similar to the predictions of the component models whenever the preferred speed of the pattern cell is higher than the speed of the gratings in the stimulus. As a consequence, for the right choice of the model parameters, these three models make very similar predictions. Indeed, for many cells the quality of the fits for these three models is almost equal.

This difficulty in the discrimination of the SH-pattern and SH-component models is due to the particular set of stimuli used in this study. We have seen that earlier authors have used a subset of these stimuli to distinguish pattern and component cells (3.2.1). In many cases the speed of the gratings used for the classification was chosen to elicit the largest response in the considered cell. Thus, if the speed of the gratings alone and of the gratings in the plaid is the same, we expect a putative SH-pattern cell to be classified as a component cell. Therefore, this method could underestimate the fraction of pattern cells in MT.

In section 3.3 we have seen that the models can be better distinguished by using stimuli with variable speeds of the components. In the case of gratings, the shape of the direction tunings predicted by the SH-component model remains the same independently of the gratings' speed, while for the SH-pattern model the direction tuning is unimodal for fast gratings and bimodal for slow gratings. Similar differences in the direction tunings arise also for other stimuli, and are best explained by comparing

the energy distribution of the stimulus and the shape of the “linear receptive field” underlying the model cell (i.e. a plane for a pattern cell, a line for a component cell).

For our set of stimuli, important differences between the predictions of the SH-models arise only when the preferred speed of the SH-pattern model is larger than the speed of the gratings, and thus the resulting direction tuning for gratings is bimodal. Some cells show such a response characteristic that can be predicted only by the SH-pattern model. However, only in few cases the quality of the fits with the SH-pattern model is larger than for the fits with the component models. We have discussed two reasons for this situation. First, for many cells the direction eliciting the largest response changes with the plaid angle. None of the models can predict a similar response characteristic, and the resulting quality of the fits is low for all the models. Second, the underestimation of the responses to gratings by the SH-pattern model is partially compensated by an increase of the temporal frequency tuning width of the underlying V1 complex cells, with the undesired effect of reducing the bimodality in the direction tuning for slow moving gratings. This hides the most important feature of the SH-pattern model, and thus reduces the differences between the performance of the SH-pattern and the SH-component models.

The underestimation of the responses to counterphase gratings and the resulting increase of w_t can be avoided by considering all the V1 afferents considered in the full Simoncelli-Heeger models, i.e. cells lying on a line for the SH-component model, cells lying on a plane for the SH-pattern model. This would increase the computational time needed for the fits, but would not necessarily change the number of parameters in the model. However, the off-plane inhibition considered in the full model has similar effects on the predicted responses as the discussed approximation. This peaks against important differences in the predictions of the full model and the SH-pattern model. The problems arising for cells that show a preferred direction that depends on the plaid angle are harder to solve. In section 8.1 we have discussed the possibility that such cells perform a weighted sum of V1 complex cells with weights that vary across the input cells.

The quality of the fits with the pattern model is never significantly higher than for the fits with the other models. In many cases, especially for data with variable contrast of the gratings, it is even much lower. The pattern model has been constructed to respond only to the variables of a plaid as a whole, remaining completely blind to the motion of the individual components. Direction and speed of a plaid are mysteriously computed with intersection of constraints, independently of the contrast of the gratings. This computation causes several abrupt changes in the responses. The first discontinuity arises in the transition from a counterphase grating to a plaid. It is a consequence of the fact that intersection of constraints has no solution for counterphase gratings, and could thus be corrected only by changing the mechanism underlying the computation of speed

and direction. The second discontinuity arises in the transition from a plaid to a grating when a low contrast grating is added to a high contrast grating. To eliminate this discontinuity it would be necessary to consider the contrast of the gratings in a much more elaborated way as we did in the pattern model.

The SH-pattern and SH-component models allow to predict, at least qualitatively, a large set of the measured responses and for some cells they even provide very good fits of the data. We have seen that for other cells the quality of the fits can be possibly increased with an extension of the SH-pattern model that considers a weighted sum of V1 inputs, with non-constant weights. But even on large data sets like the one analyzed in this study, the number of parameters may become too large. A better solution seems to be a different choice of stimuli, in particular stimuli that differ in the speed of the components. By exploring more directions in frequency space other then the spatial frequency directions, it would be possible to clearly distinguish the predictions of the SH-component and the SH-pattern models.

9 References

Adelson, E. H. and Bergen, J. R. (1985). Spatiotemporal energy models for the perception of motion. *J Opt Soc Am [A]*, **2**(2): 284-99.

Adelson, E. H. and Bergen, J. R. (1986). Perceptual dimensions of spatio-temporal vision. *Investigative Opthalmology and Visual Science Supplement (ARVO)*, : 27:141.

Albright, T. D. (1984). Direction and orientation selectivity of neurons in visual area MT of the macaque. *J Neurophysiol*, **52**(6): 1106-30.

Britten, K. H., Shadlen, M. N., Newsome, W. T. and Movshon, J. A. (1992). The analysis of visual motion: a comparison of neuronal and psychophysical performance. *J Neurosci*, **12**(12): 4745-65.

Carandini, M. and Ferster, D. (1997). A tonic hyperpolarization underlying contrast adaptation in cat visual cortex. *Science*, **276**: 949-952.

Carandini, M., Heeger, D. J. and and Movshon, J. A. (1997). Linearity and normalization in simple cells of the macaque primary visual cortex. *J Neurosci*, **17**(21): 8621-44.

Carandini, M., Heeger, D. J. and and Movshon, J. A. (1999). Linearity and Gain Control in V1 Simple Cells. *Cerebral Cortex*, **13**: 401-443.

De Valois, R. L. and De Valois, K. (1988). *Spatial Vision*. Oxford: Oxford University Press.

Heeger, D. J. (1987). Model for the extraction of image flow. *J. Opt. Soc. Am. A*, **4**: 1455--1471.

Heeger, D. J. (1992a). Half-squaring in responses of cat striate cells. *Vis Neurosci*, **9**(5): 427-43.

Heeger, D. J. (1992b). Normalization of cell responses in cat striate cortex. *Vis Neurosci*, **9**(2): 181-97.

Hubel, D. and Wiesel, T. (1962). Receptive fields, binocular interaction, and functional architecture in the cat's visual cortex. *Journal of Physiology (London)*, **160**: 106-154.

Maffei, L., Fiorentini, A. and Bisti, S. (1973). Neural correlate of perceptual adaptation to gratings. *Science*, **182**(116): 1036-8.

Majaj, N., Carandini, M. and Movshon, J. A. (1999). Local integration of features for the computation of pattern direction by neurons in macaque area MT. *ECVP Abstract*, .

Movshon, J. A., Adelson, E. H., Gizzi, M. S. and and Newsome, W. T. (1983). The analysis of moving visual patterns. , .

Movshon, J. A., Thompson, I. D. and Tolhurst, D. J. (1978). Nonlinear spatial summation in the receptive fields of complex cells in the cat striate cortex. *J. Physiol. (London)*, **283**: 78-100.

Newsome, W. T. and Pare, E. B. (1988). A selective impairment of motion perception following lesions of the middle temporal visual area (MT). *J Neurosci*, **8**(6): 2201-11.

Okamoto, H., Kawakami, S., Saito, H., Hida, E., Odajima, K., Tamanoi, D. and Ohno, H. (1999). MT neurons in the macaque exhibited two types of bimodal direction tuning as predicted by a model for visual motion detection. *Vision Res*, **39**(20): 3465-79.

Rodman, H. R. and Albright, T. D. (1989). Single-unit analysis of pattern-motion selective properties in the middle temporal area (MT). *Exp Brain Res*, **75**: 53-64.

Salzman, C. D., Murasugi, C. M., Britten, K. H. and Newsome, W. T. (1992). Microstimulation in visual area MT: effects on direction discrimination performance. *J Neurosci*, **12**(6): 2331-55.

Sclar, G., Maunsell, J. H. and and Lennie, P. (1990). Coding of image contrast in central visual pathways of the macaque monkey. *Vision Res*, **30**(1): 1-10.

Simoncelli, E. P. (1993). Distributed representation and analysis of visual motion, PhD Thesis. , .

Simoncelli, E. P. and Heeger, D. J. (1998). A model of neuronal responses in visual area MT. *Vision Res*, **38**(5): 743-61.

van Santen, J. P. and Sperling, G. (1985). Elaborated Reichardt detectors. *J Opt Soc Am [A]*, **2**(2): 300-21.

Wandell, B. (1995). *Foundations of Vision*. Sunderland, Massachussets: Sinauer.

Watson, A. b. and amd Ahumada, A. J. (1983). A look at motion in the frequency domain. *NASA Tech. Memo. TM-84352*, .

10 Appendix

Here we give all the parameters of the best fits for the component model (Table 5), the pattern model (Table 6), the SH-pattern model (Table 7) and the SH-component model (Table 8). Moreover we show the plots of all the measured data and the predictions of the best fits with these four models.

Both the data and the fits are plotted two times. First, we show the entire direction-direction data (on the top of the page) and the direction-contrast data (on the bottom of the page, if measured). Second, we plot profiles through the responses. The two first columns in a page represent profiles through the direction-direction response, the third and the fourth column represent profiles through the direction-contrast responses (if measured). Each column shows the data and the predictions of two models. In the first column the component model (solid) and the SH-component model (dashed). In the second column the pattern model (solid) and the SH-pattern model (dashed). In the third column the same models as in the first, in the fourth column the same models as in the second. The percentage of variance explained by the models is given in brackets (plots of responses) or is given at the bottom of the page (profiles).

In the plots of the profiles of direction-contrast responses the fixed direction of grating 1 is indicated by an arrow below the d_2-axes. For all the profiles the spontaneous firing rate of the cell is indicated by an horizontal arrow on the left of the vertical axes.

Table 5, Parameters of the component model

cell	b	g	C_{50}	n	σ (deg)	d_p (deg)	r_n	w_d (deg)
				Direction-Direction Data				
1	0.0	3.5	0.55	2.7	27	171	-0.26	67
2	0.9	1.0	0.80	4.6	27	200	-0.36	90
3	1.3	1.8	0.80	2.9	18	180	-0.01	52
4	0.8	1.3	0.80	3.7	18	189	-0.20	65
5	1.0	1.2	0.80	5.0	33	171	-0.13	48
6	0.1	2.0	0.50	4.8	26	174	0.12	56
7	0.0	4.9	0.30	1.5	21	163	0.24	44
8	0.0	15.5	0.01	1.0	46	192	0.12	48
9	0.0	2.2	0.47	3.1	36	220	-0.10	79
10	0.2	1.1	0.15	3.7	15	185	0.00	75
11	1.3	3.6	0.35	2.0	15	210	-0.01	115
12	1.3	1.2	0.78	5.0	57	175	0.24	64
13	0.9	2.0	0.77	3.8	56	160	-0.13	73
14	0.5	4.1	0.80	2.0	15	173	0.00	76
15	0.9	1.3	0.80	3.3	32	175	0.01	65
16	0.2	1.5	0.41	4.7	45	149	-0.21	120
17	0.0	1.9	0.34	4.6	80	176	0.00	114
18	0.0	5.5	0.22	2.0	22	165	0.00	73
19	3.3	41.1	0.06	0.9	53	183	-0.03	67
				Direction-Contrast Data				
1	1.5	3.7	0.80	1.5	15	180	0.00	59
2	0.0	1.6	0.05	5.0	37	182	-0.02	108
3	1.3	2.8	0.56	2.1	20	186	-0.27	32
4	0.7	1.4	0.55	3.4	21	187	-0.19	33
5	1.6	16.8	0.31	1.3	15	176	-0.37	30
6	0.0	1.9	0.45	4.7	29	173	-0.05	86
7	0.2	25.0	0.80	1.0	19	154	-0.02	29
12	0.0	31.8	0.11	1.3	46	177	0.12	50
13	0.0	1.9	0.12	5.0	48	170	0.15	81
14	0.6	1.5	0.80	3.6	28	195	0.09	70
15	0.9	1.1	0.80	3.9	19	172	-0.13	53
16	0.7	2.5	0.32	2.5	72	140	0.00	19

Table 6, Parameters of the pattern model

cell	b	g	C_{50}	n	σ (deg)	d_p (deg)	r_n	w_d (deg)	v_p	w_s
					Direction-Direction Data					
1	118.1	379	73.0	1.7	30	171	-0.26	44	1.3	0.9
2	93.3	37.9	69.6	5.0	30	205	-0.54	44	1.6	0.8
3	54.7	349.5	2.9	0.7	30	175	-0.08	38	1.6	1.4
4	3.0	3.5	1.8	2.2	30	190	-0.46	43	1.2	1.1
5	5.7	11.9	1.3	1.6	30	168	-1.00	37	1.1	1.3
6	1.7	2.2	1.1	3.3	30	171	-1.00	42	1.1	1.0
7	1.4	0.6	1.2	5.0	30	171	-1.00	38	0.7	1.6
8	8.6	25.7	1.8	1.0	30	188	-0.21	65	2.2	3.0
9	2.0	1.1	1.9	5.0	30	220	-0.02	56	1.5	1.3
10	0.7	3.4	0.4	1.4	30	186	-0.03	54	1.2	1.0
11	6.1	3.9	2.0	2.3	30	218	-0.02	83	2.5	3.0
12	927.3	7506.2	0.1	0.5	30	172	-0.15	48	2.0	3.0
13	842.3	7168.2	100.0	0.8	30	154	-0.10	41	1.9	2.0
14	73.4	39.6	48.7	3.3	30	175	-0.49	81	1.2	0.9
15	36.2	309.2	4.3	0.6	30	174	-0.10	43	2.0	2.0
16	0.8	4.9	0.0	1.3	30	149	0.00	53	2.7	3.0
17	11.0	36.9	1.2	1.0	30	178	-0.28	49	1.4	0.9
18	23.7	82.3	4.5	1.3	30	165	-0.75	120	1.7	1.9
19	62.3	1004.4	0.1	0.5	30	184	-0.04	63	2.4	2.8
					Direction-Contrast Data					
1	32.7	80.2	11.7	1.1	30	183	-0.37	60	1.1	0.2
2	2.1	1.2	1.8	5.0	30	194	-0.53	70	1.7	2.1
3	6.1	22.3	1.1	1.1	30	188	0.00	24	0.1	3.0
4	1.8	6.1	0.7	1.7	30	187	-0.11	24	0.3	1.3
5	1.3	3.8	1.0	5.0	30	177	-0.09	34	4.0	2.6
6	0.2	2.3	0.6	4.3	30	187	0.00	49	2.3	3.0
7	1.0	1.4	1.1	5.0	30	153	0.00	48	2.8	3.0
12	249.2	620.1	8.9	1.0	30	183	-1.00	57	0.9	0.2
13	2.6	121.2	1.0	1.4	30	178	0.15	28	5.0	3.0
14	1.6	2.3	1.5	3.3	30	220	0.02	113	0.1	2.2
15	1.1	1.6	1.0	5.0	30	168	-0.01	38	3.6	3.0
16	0.9	2.1	0.4	2.5	30	147	-0.02	15	1.4	1.0

Table 7, Parameters of the SH-pattern model

	b	g	n	C_{50}	m	σ (deg)	d_p (deg)	v_p	w_k	w_d (deg)	w_t	N
						Direction-Direction Data						
1	0.8	3.9	4.7	0.32	2	30	171	1.32	0.42	51	0.34	32
2	0.9	2.4	5.0	0.11	2	30	204	1.79	0.42	48	0.82	32
3	1.5	3.3	3.3	0.14	2	30	179	0.97	0.42	58	0.20	32
4	0.9	2.1	5.0	0.25	2	30	189	0.83	0.42	44	0.78	32
5	1.3	4.4	3.6	0.16	2	30	170	1.00	0.42	55	0.20	32
6	0.4	12.7	2.8	0.05	2	30	173	0.92	0.42	58	0.20	32
7	0.5	53.4	0.8	0.01	2	30	162	0.97	0.42	40	0.20	32
8	1.7	20.6	2.1	0.26	2	30	194	0.85	0.42	15	0.61	32
9	0.7	4.2	3.1	0.29	2	30	195	1.57	0.42	43	0.87	32
10	0.8	2.3	4.9	0.01	2	30	187	1.46	0.42	49	0.41	32
11	1.7	3.6	3.8	0.01	2	30	203	2.70	0.42	46	1.08	32
12	31.5	7682.9	0.7	0.34	2	30	174	0.74	0.42	15	0.67	32
13	1.0	3.4	5.0	0.24	2	30	143	1.63	0.42	37	0.95	32
14	1.1	3.2	5.0	0.80	2	30	174	1.55	0.42	53	0.51	32
15	1.2	4.5	2.1	0.07	2	30	175	1.05	0.42	69	0.21	32
16	0.3	3.7	3.3	0.01	2	30	165	1.50	0.42	42	1.31	32
17	1.0	5.3	2.3	0.01	2	30	177	1.27	0.42	52	0.76	32
18	1.3	4	3.5	0.01	2	30	164	1.53	0.42	56	0.52	32
19	1.6	2.3	3.8	0.01	2	30	183	1.07	0.42	34	1.03	32
						Direction-Direction Data						
1	1.3	10.4	4.2	0.73	2	30	174	1.33	0.42	23	0.20	32
2	0.8	2.8	5.0	0.21	2	30	198	1.95	0.42	45	1.08	32
3	1.5	16.6	2.8	0.05	2	30	185	0.78	0.42	46	0.20	32
4	1.2	8.5	5.0	0.09	2	30	186	0.76	0.42	42	0.22	32
5	1.2	6.6	4.7	0.04	2	30	174	0.84	0.42	67	0.20	32
6	1.0	4.9	4.5	0.25	2	30	178	0.90	0.42	77	0.20	32
7	1.1	3.2	4.0	0.42	2	30	156	0.96	0.42	72	0.20	32
12	0.0	8000	0.6	0.16	2	30	177	0.64	0.42	24	0.50	32
13	1.4	4.2	3.6	0.09	2	30	166	1.30	0.42	49	0.30	32
14	1.1	2.4	4.5	0.62	2	30	197	1.02	0.42	74	0.20	32
15	1.1	2.4	5.0	0.24	2	30	171	0.93	0.42	66	0.20	32
16	1.1	5.6	4.8	0.04	2	30	140	0.92	0.42	15	0.20	32

Table 8, Parameters of the SH-component model

	b	g	n	C_{50}	m	σ (deg)	d_p (deg)	v_p	w_k	w_d (deg)	w_t	N
						Direction-Direction Data						
1	0.8	2.6	2.9	0.42	2	30	172	1	0.42	65	0.26	1
2	1.1	0.6	5.0	0.01	2	30	202	1	0.42	81	0.37	1
3	2.0	3.5	1.8	0.19	2	30	179	1	0.42	59	0.27	1
4	1.1	1.4	3.1	0.33	2	30	189	1	0.42	65	0.24	1
5	1.2	6.3	1.8	0.21	2	30	170	1	0.42	56	0.90	1
6	0.0	4.1	2.7	0.27	2	30	174	1	0.42	59	1.07	1
7	0.0	8.3	1.1	0.38	2	30	163	1	0.42	50	1.35	1
8	1.3	72.7	0.6	0.19	2	30	192	1	0.42	51	1.02	1
9	0.8	2.6	2.3	0.51	2	30	220	1	0.42	68	0.20	1
10	0.9	0.5	5.0	0.01	2	30	184	1	0.42	67	0.32	1
11	50.7	834.9	0.5	0.80	2	30	211	1	0.42	97	0.53	1
12	0.0	5814.8	0.5	0.06	2	30	175	1	0.42	55	0.94	1
13	1.6	19.3	1.2	0.37	2	30	164	1	0.42	62	0.40	1
14	1.7	7.3	1.5	0.80	2	30	174	1	0.42	69	0.20	1
15	1.3	3.8	1.4	0.22	2	30	175	1	0.42	70	0.20	1
16	0.9	0.6	4.5	0.01	2	30	152	1	0.42	95	0.20	1
17	1.3	5	1.6	0.01	2	30	178	1	0.42	73	0.21	1
18	1.7	14	1.3	0.28	2	30	164	1	0.42	72	0.24	1
19	4.3	5.9	1.4	0.01	2	30	185	1	0.42	83	0.20	1
						Direction-Direction Data						
1	1.4	0.7	3.0	0.38	2	30	178	1	0.42	66	0.20	1
2	0.9	0.6	5.0	0.03	2	30	185	1	0.42	100	0.40	1
3	1.3	0.4	5.0	0.05	2	30	186	1	0.42	51	0.26	1
4	1.1	0.5	5.0	0.08	2	30	186	1	0.42	48	0.86	1
5	1.0	0.9	5.0	0.04	2	30	175	1	0.42	65	1.18	1
6	0.0	2	3.9	0.01	2	30	181	1	0.42	75	1.13	1
7	0.3	1.7	3.1	0.02	2	30	155	1	0.42	66	1.41	1
12	8.0	562.6	0.7	0.14	2	30	176	1	0.42	48	1.00	1
13	1.4	1.8	2.9	0.09	2	30	172	1	0.42	64	0.25	1
14	1.2	1.2	3.7	0.65	2	30	197	1	0.42	78	0.20	1
15	1.1	0.6	5.0	0.23	2	30	171	1	0.42	68	0.80	1
16	1.4	3.3	2.0	0.04	2	30	140	1	0.42	20	0.50	1

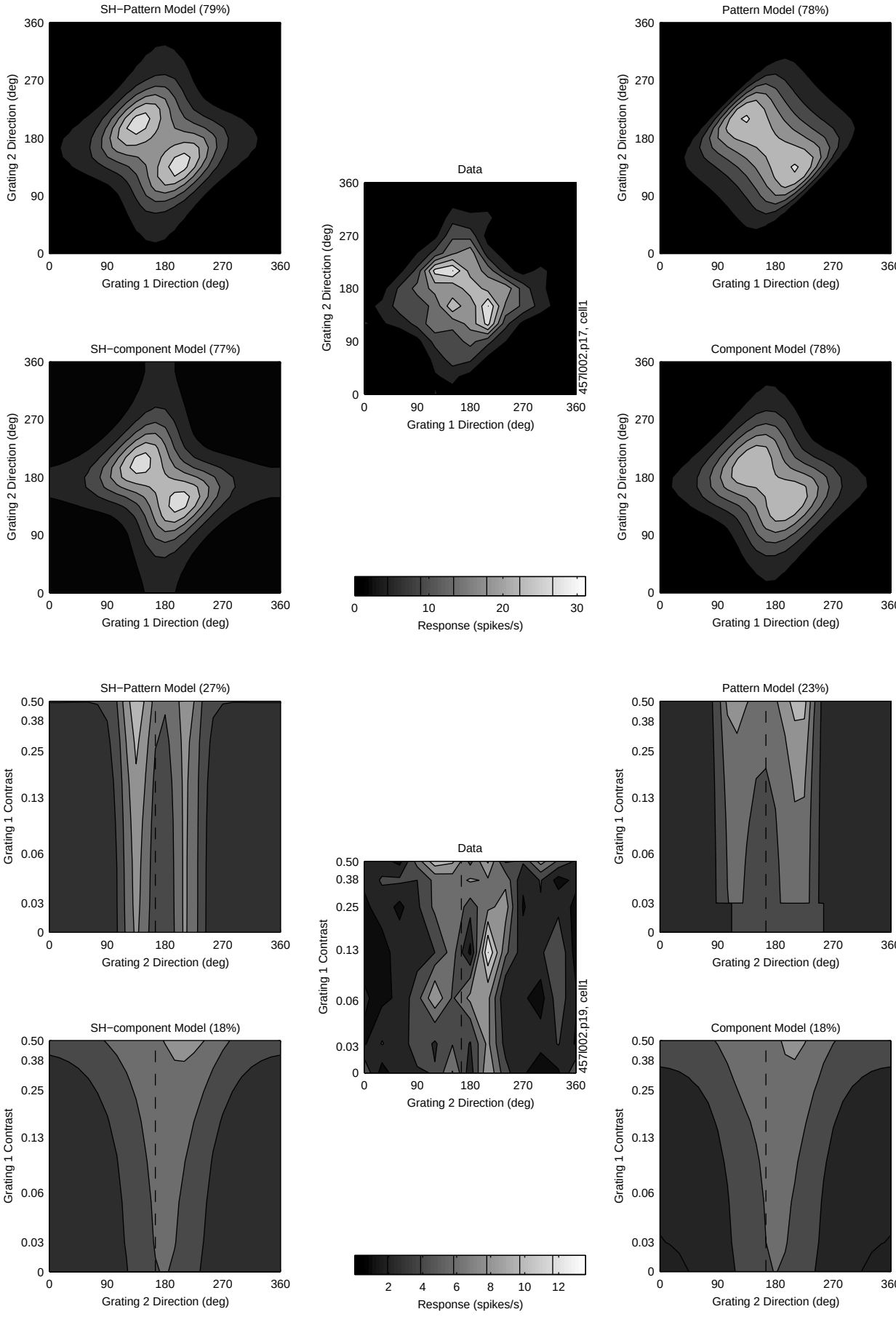
SH−Pattern Model (79%)
Pattern Model (78%)
Data
SH−component Model (77%)
Component Model (78%)
Grating 2 Direction (deg)
Grating 1 Direction (deg)
0
90
180
270
360
457l002.p17, cell1
Response (spikes/s)
0
10
20
30
SH−Pattern Model (27%)
Pattern Model (23%)
Data
SH−component Model (18%)
Component Model (18%)
Grating 1 Contrast
Grating 2 Direction (deg)
0.50
0.38
0.25
0.13
0.06
0.03
0
457l002.p19, cell1
2
4
6
8
10
12

Cell1

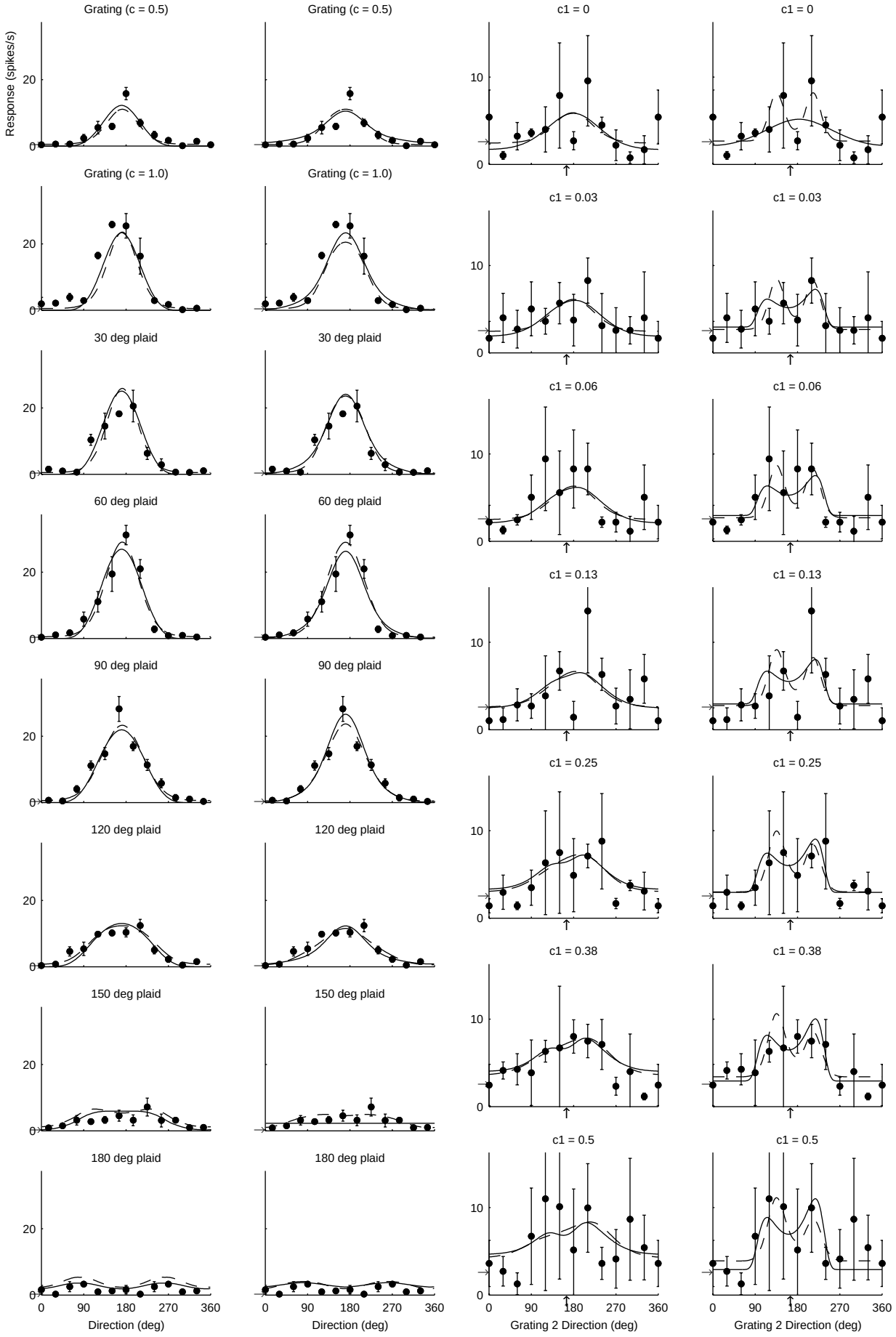

Component Model : 78%

SH−Component Model : 77%

Pattern Model : 78%

SH−Pattern Model : 79%

Component Model : 18%

SH−Component Model : 18%

Pattern Model : 23%

SH−Pattern Model : 27%

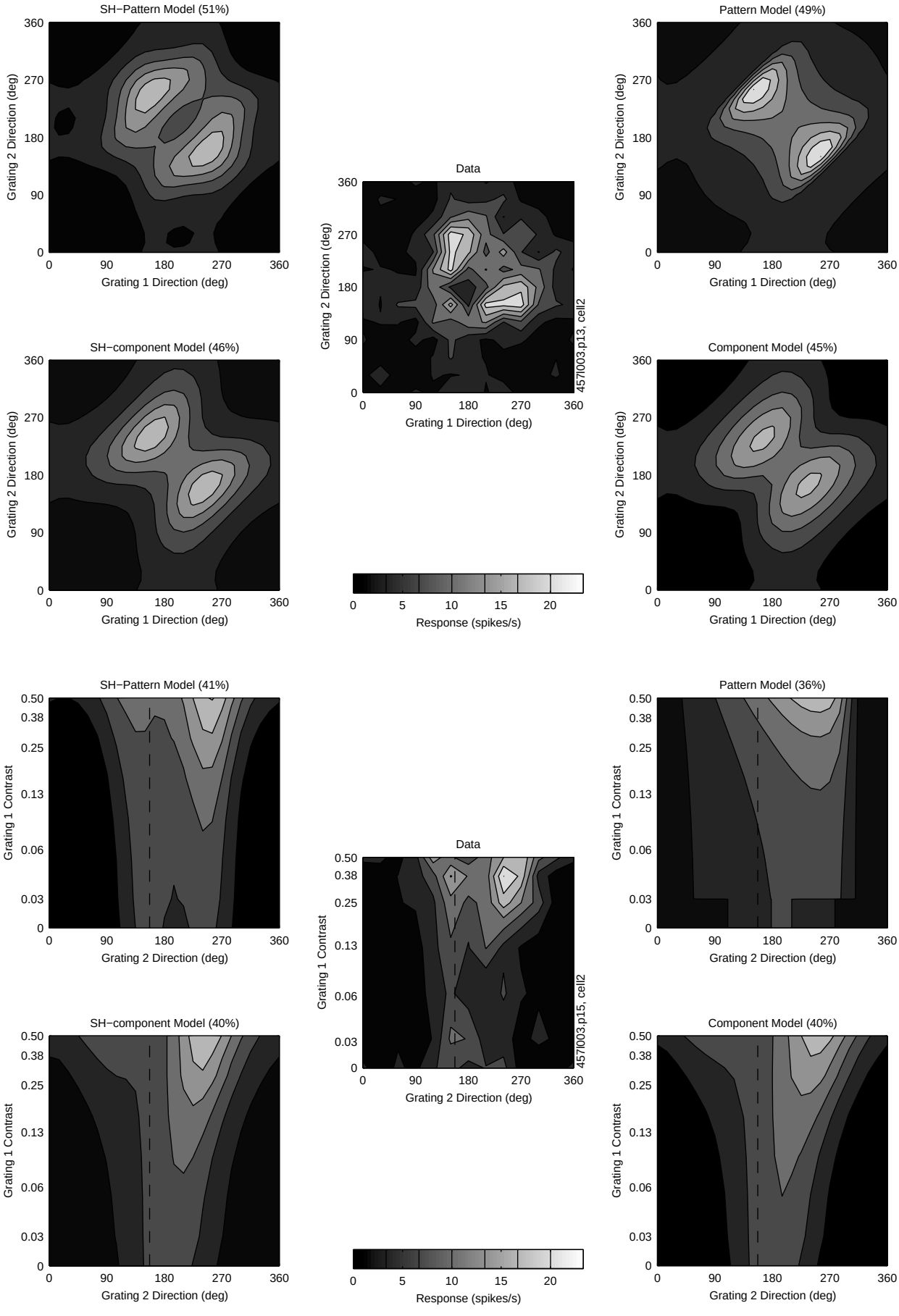
SH−Pattern Model (51%)
Pattern Model (49%)
Data
SH−component Model (46%)
Component Model (45%)
Grating 2 Direction (deg)
Grating 1 Direction (deg)
0
90
180
270
360
457l003.p13, cell2
Response (spikes/s)
0
5
10
15
20
SH−Pattern Model (41%)
Pattern Model (36%)
Data
SH−component Model (40%)
Component Model (40%)
Grating 1 Contrast
Grating 2 Direction (deg)
0.50
0.38
0.25
0.13
0.06
0.03
0
457l003.p15, cell2

Cell2

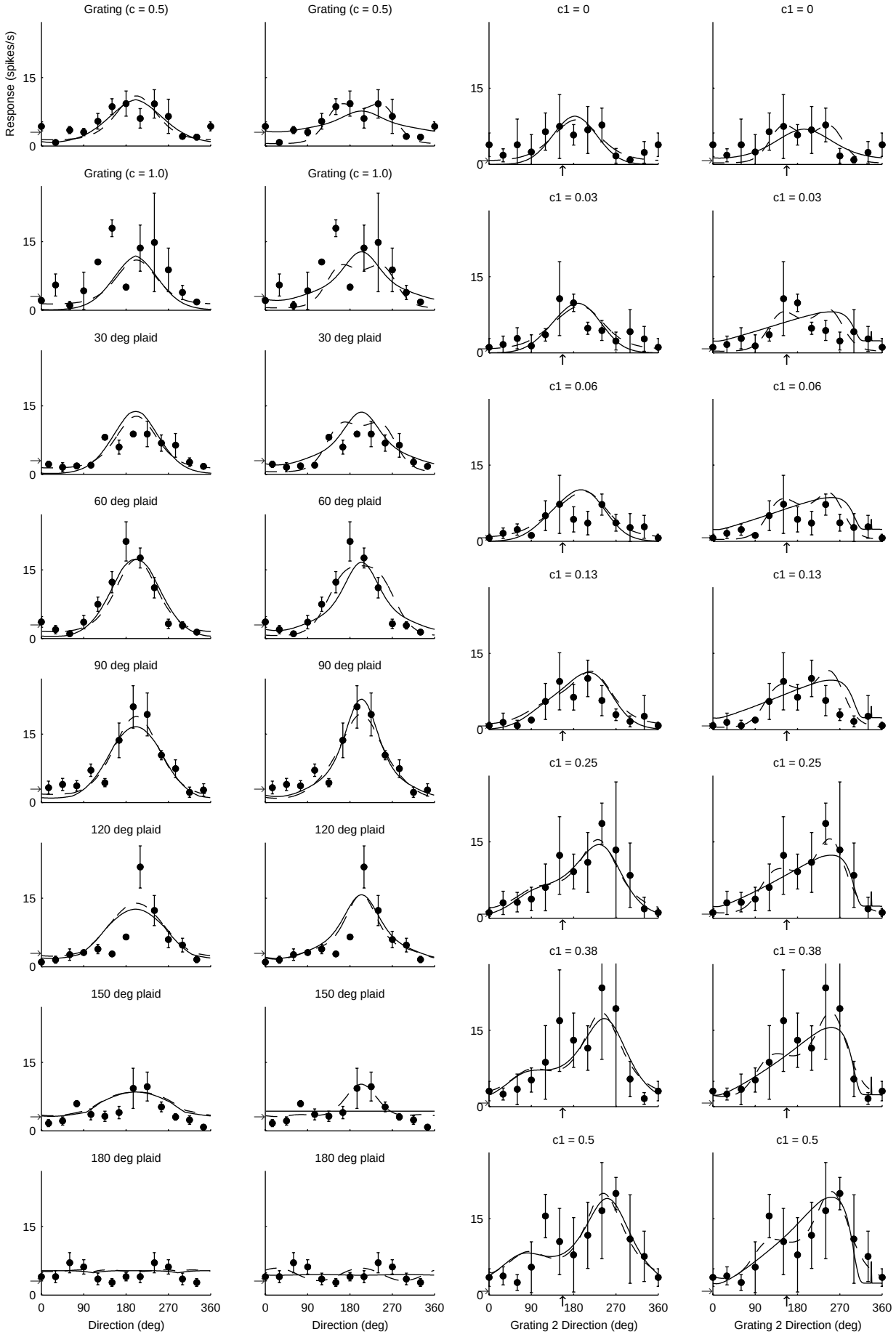

Component Model : 45%
SH−Component Model : 46%

Pattern Model : 49%
SH−Pattern Model : 51%

Component Model : 40%
SH−Component Model : 40%

Pattern Model : 36%
SH−Pattern Model : 41%

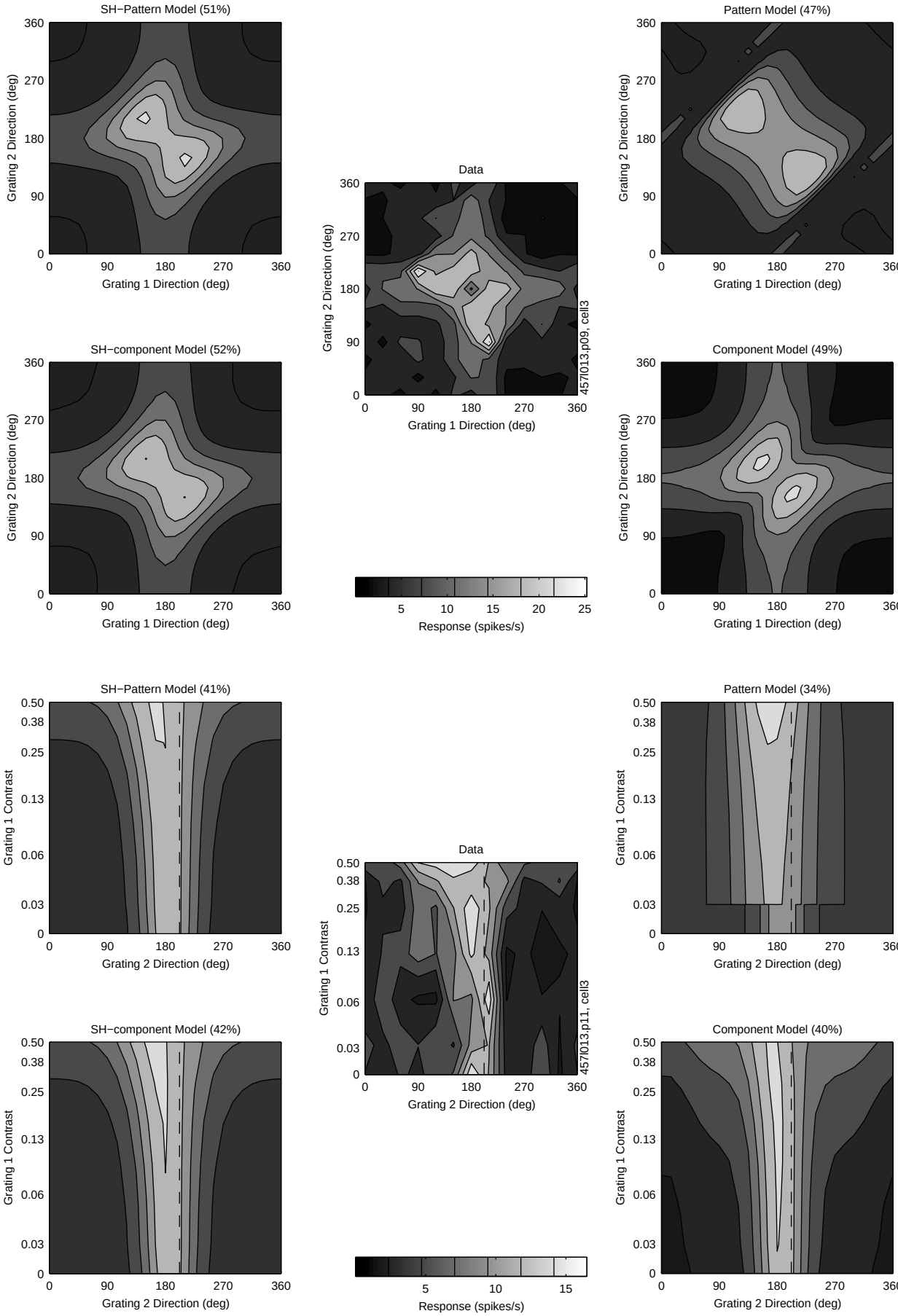
SH−Pattern Model (51%)
Pattern Model (47%)
Data
SH−component Model (52%)
Component Model (49%)
Grating 2 Direction (deg)
Grating 1 Direction (deg)
457l013.p09, cell3
Response (spikes/s)
SH−Pattern Model (41%)
Pattern Model (34%)
Data
SH−component Model (42%)
Component Model (40%)
Grating 1 Contrast
Grating 2 Direction (deg)
457l013.p11, cell3
Response (spikes/s)

Cell3

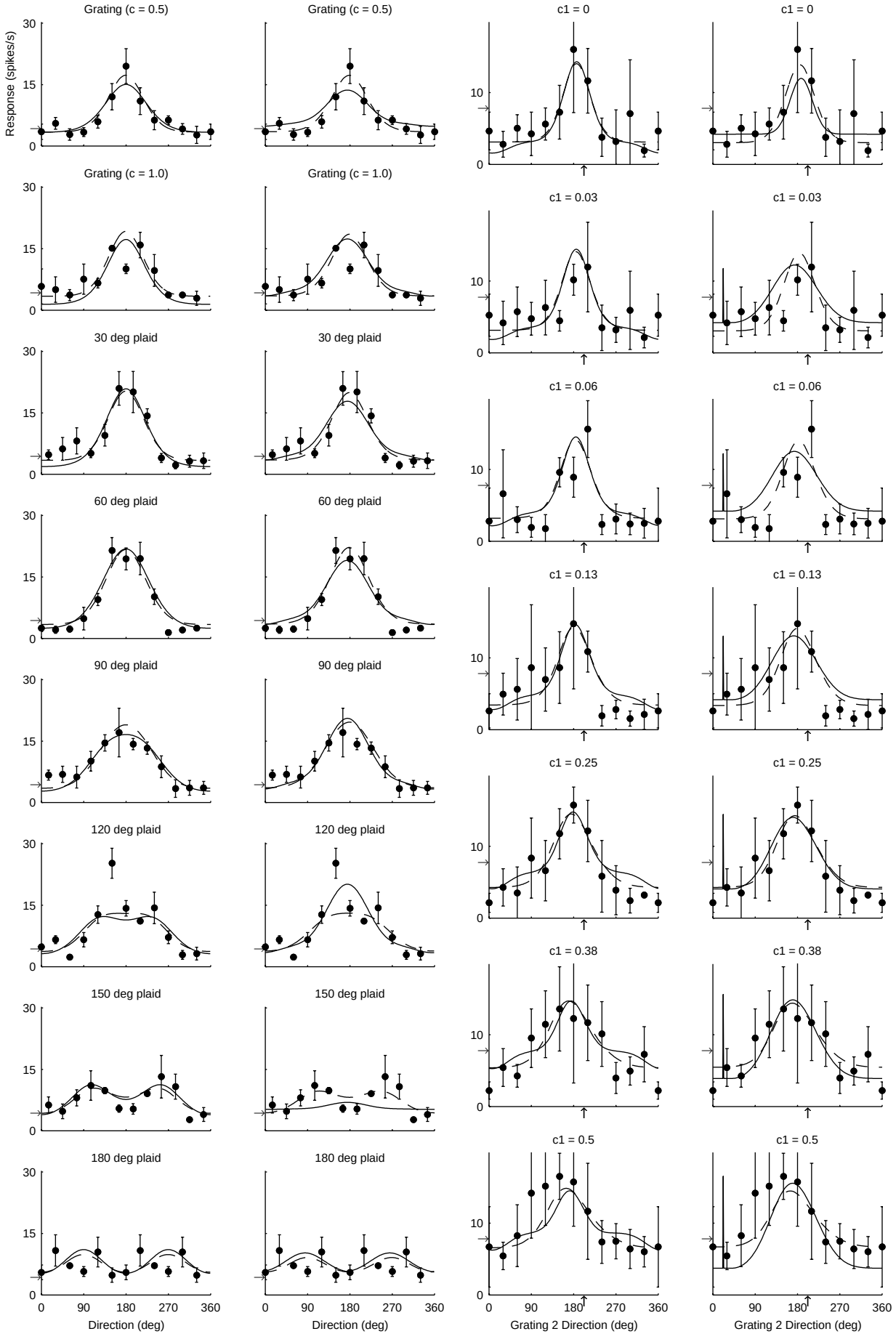

Component Model : 49%
SH−Component Model : 52%

Pattern Model : 47%
SH−Pattern Model : 51%

Component Model : 40%
SH−Component Model : 42%

Pattern Model : 34%
SH−Pattern Model : 41%

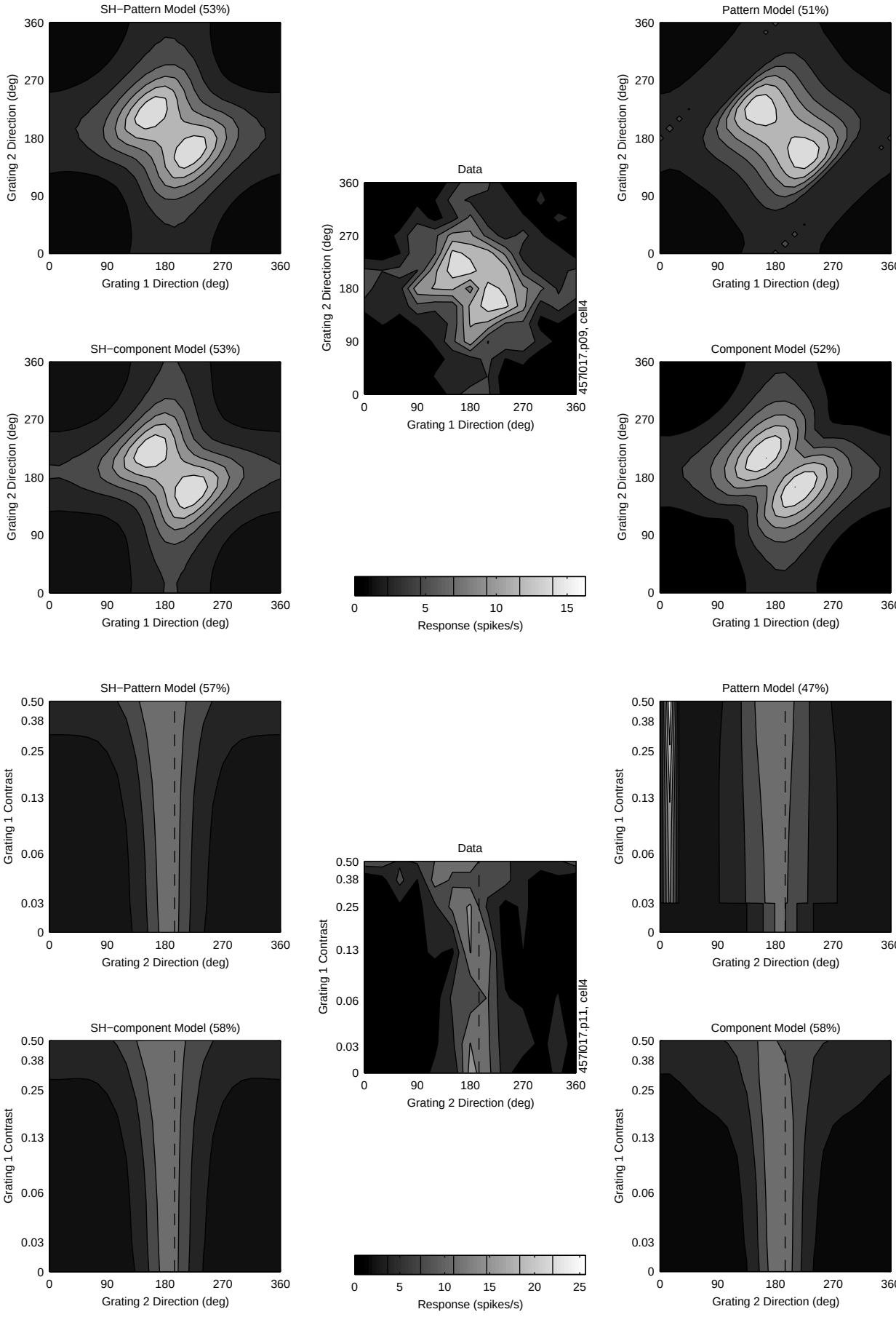
SH−Pattern Model (53%)
Pattern Model (51%)
Data
SH−component Model (53%)
Component Model (52%)
Grating 2 Direction (deg)
Grating 1 Direction (deg)
0
90
180
270
360
457l017.p09, cell4
0
5
10
15
Response (spikes/s)
SH−Pattern Model (57%)
Pattern Model (47%)
Data
SH−component Model (58%)
Component Model (58%)
Grating 1 Contrast
Grating 2 Direction (deg)
0.50
0.38
0.25
0.13
0.06
0.03
0
457l017.p11, cell4
0
5
10
15
20
25
Response (spikes/s)

Cell4

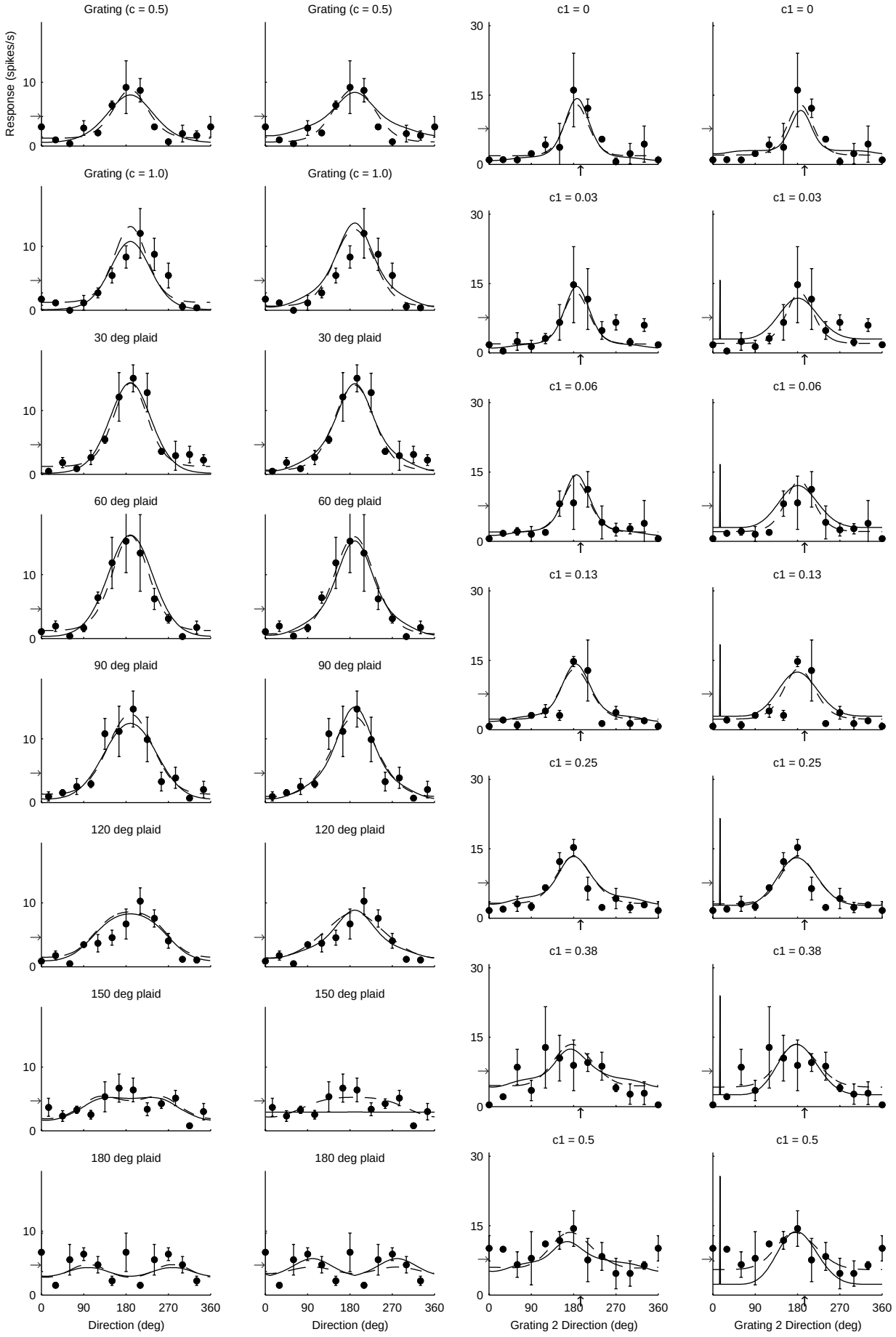

Component Model : 52%

SH−Component Model : 53%

Pattern Model : 51%

SH−Pattern Model : 53%

Component Model : 58%

SH−Component Model : 58%

Pattern Model : 47%

SH−Pattern Model : 57%

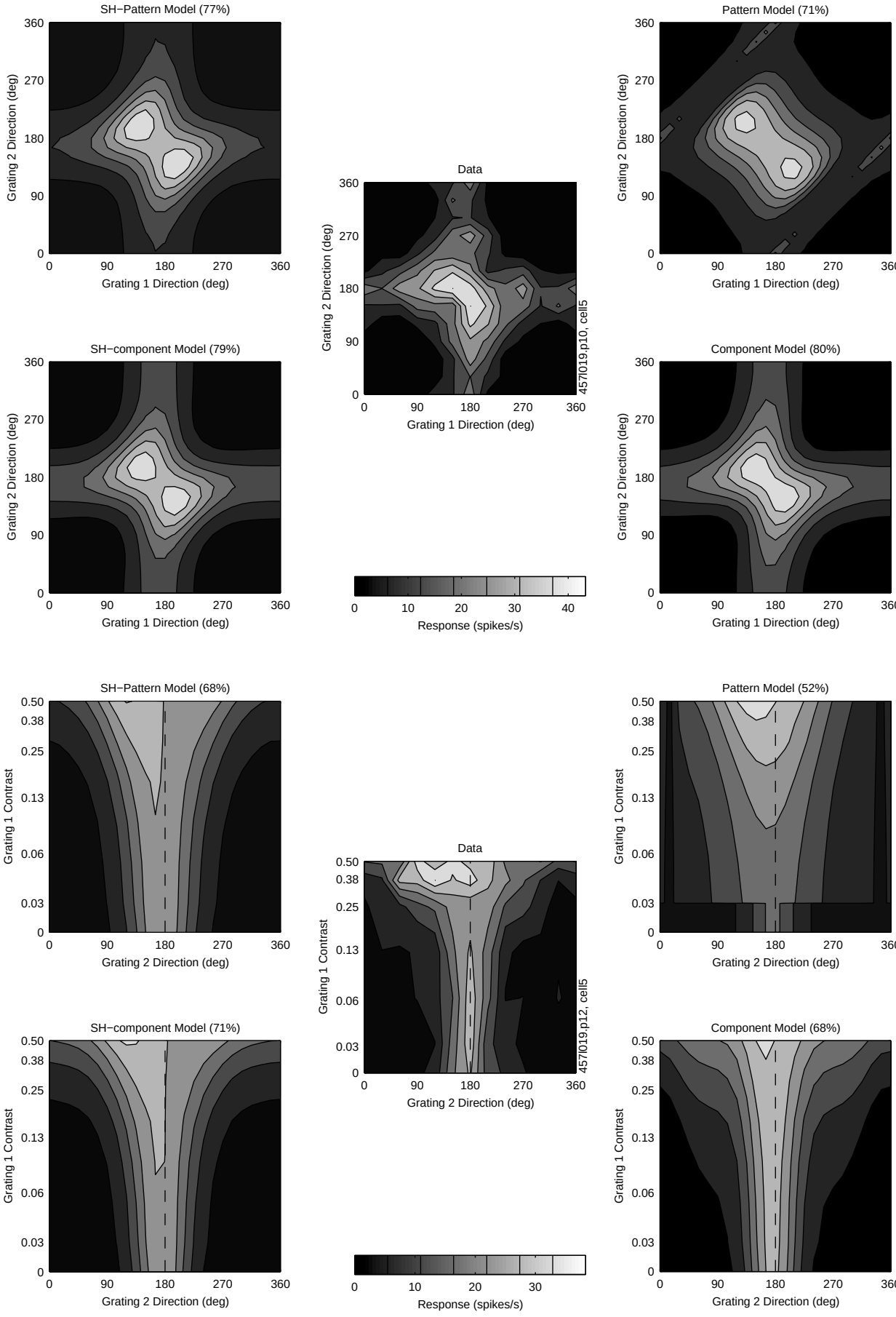
SH−Pattern Model (77%)
Pattern Model (71%)
Data
SH−component Model (79%)
Component Model (80%)
Grating 2 Direction (deg)
Grating 1 Direction (deg)
0
90
180
270
360
457l019.p10, cell5
0
10
20
30
40
Response (spikes/s)
SH−Pattern Model (68%)
Pattern Model (52%)
Data
SH−component Model (71%)
Component Model (68%)
Grating 1 Contrast
Grating 2 Direction (deg)
0.50
0.38
0.25
0.13
0.06
0.03
0
457l019.p12, cell5
0
10
20
30
Response (spikes/s)

Cell5

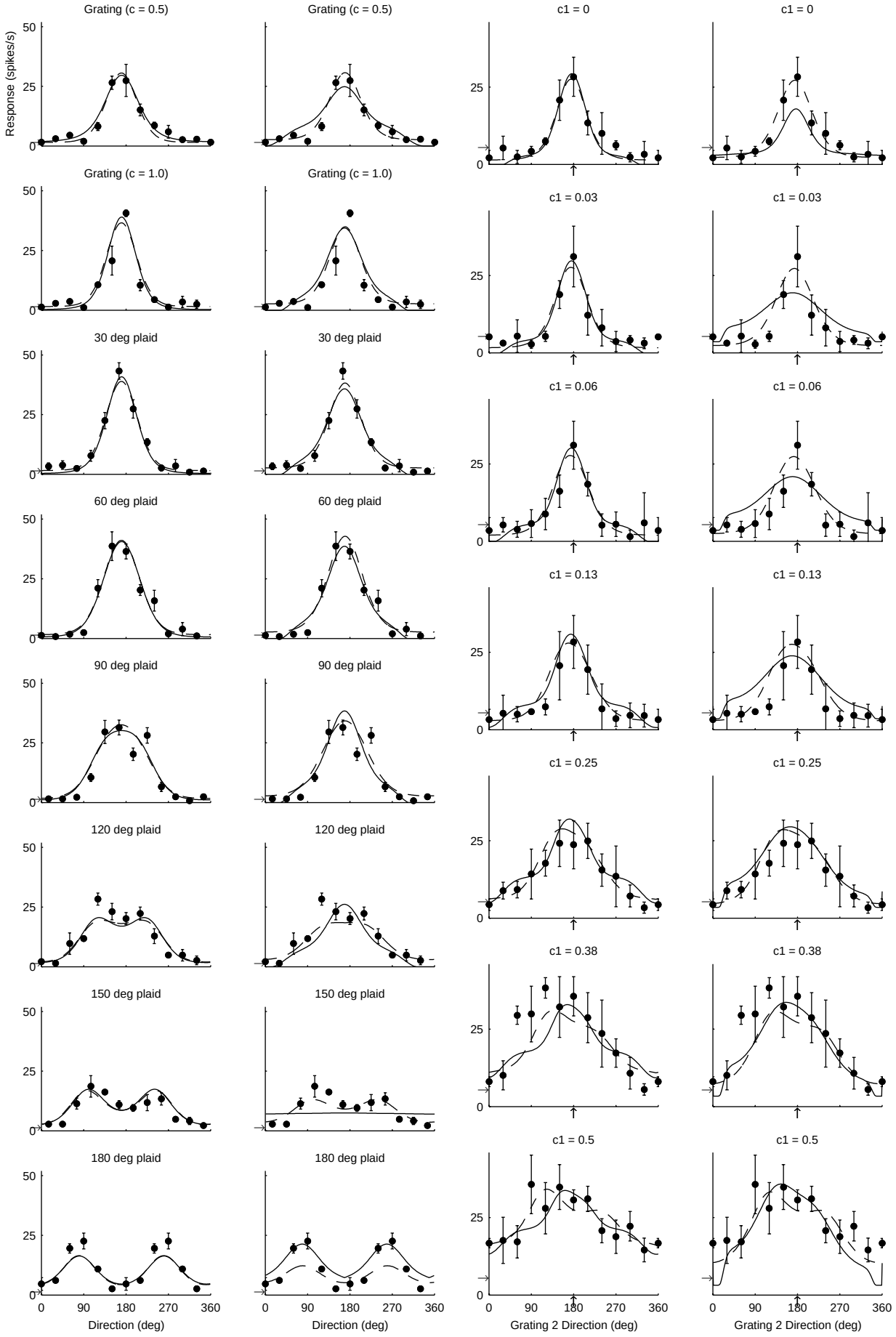

Component Model : 80%
SH−Component Model : 79%

Pattern Model : 71%
SH−Pattern Model : 77%

Component Model : 68%
SH−Component Model : 71%

Pattern Model : 52%
SH−Pattern Model : 68%

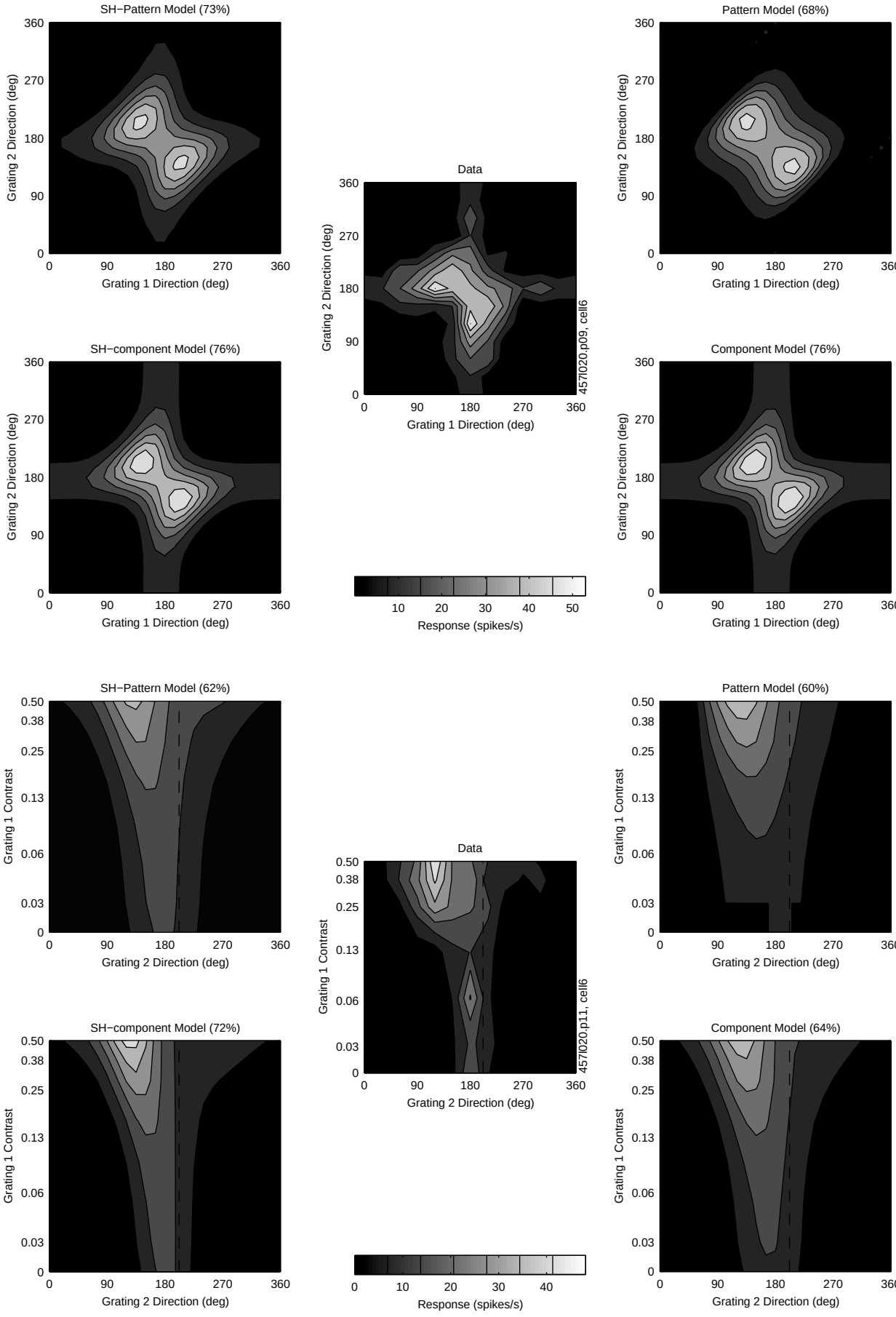
SH−Pattern Model (73%)
Pattern Model (68%)
Data
SH−component Model (76%)
Component Model (76%)
Grating 2 Direction (deg)
Grating 1 Direction (deg)
0
90
180
270
360
457l020.p09, cell6
10
20
30
40
50
Response (spikes/s)
SH−Pattern Model (62%)
Pattern Model (60%)
Data
SH−component Model (72%)
Component Model (64%)
Grating 1 Contrast
Grating 2 Direction (deg)
0.50
0.38
0.25
0.13
0.06
0.03
457l020.p11, cell6
0
10
20
30
40
Response (spikes/s)

Cell6

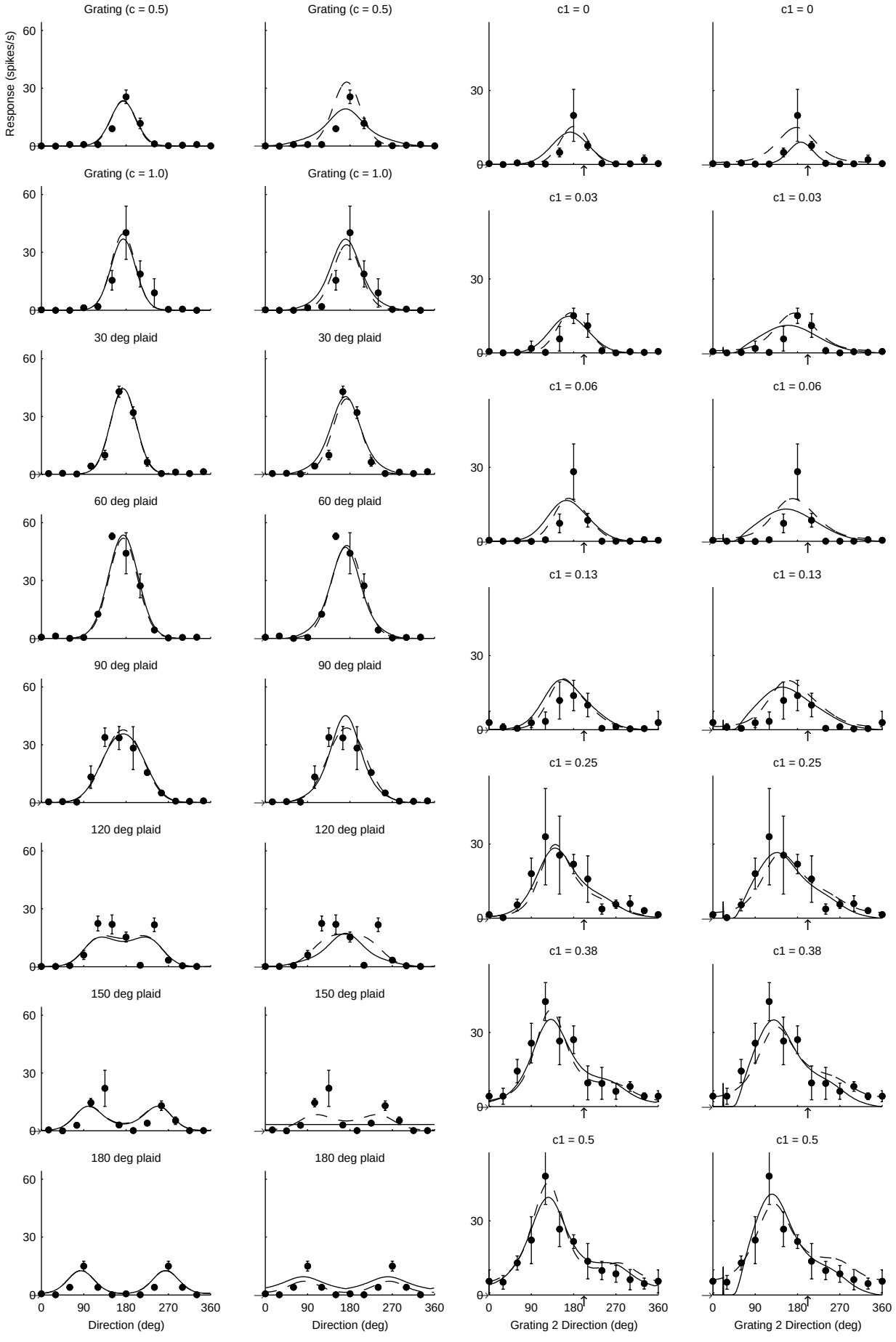

Component Model : 76%

SH−Component Model : 76%

Pattern Model : 68%

SH−Pattern Model : 73%

Component Model : 64%

SH−Component Model : 72%

Pattern Model : 60%

SH−Pattern Model : 62%

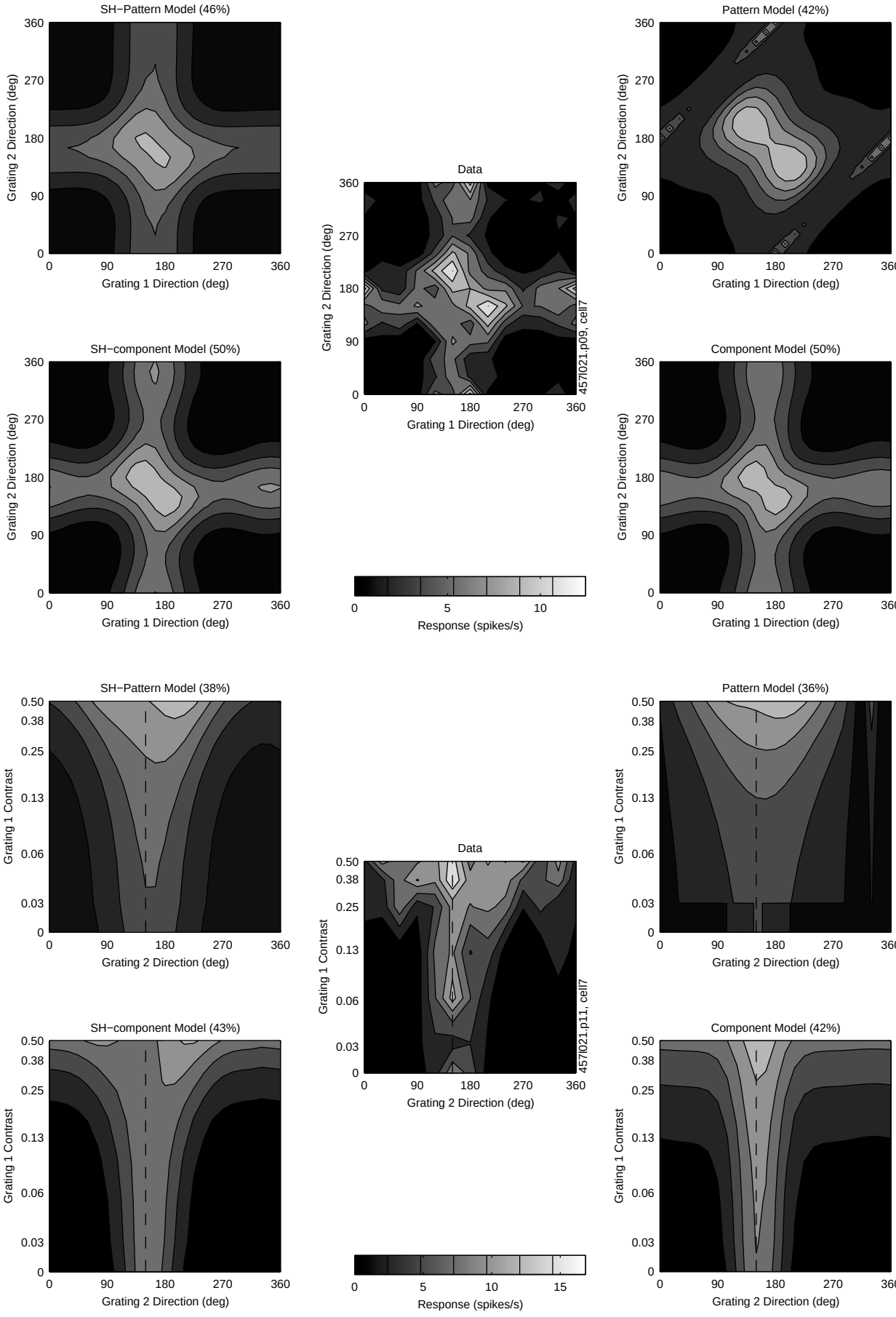
SH−Pattern Model (46%)
Data
Pattern Model (42%)
SH−component Model (50%)
Component Model (50%)
Grating 2 Direction (deg)
Grating 1 Direction (deg)
0
90
180
270
360
457l021.p09, cell7
0
5
10
Response (spikes/s)
SH−Pattern Model (38%)
Data
Pattern Model (36%)
SH−component Model (43%)
Component Model (42%)
Grating 1 Contrast
Grating 2 Direction (deg)
0.50
0.38
0.25
0.13
0.06
0.03
457l021.p11, cell7
0
5
10
15
Response (spikes/s)

Cell7

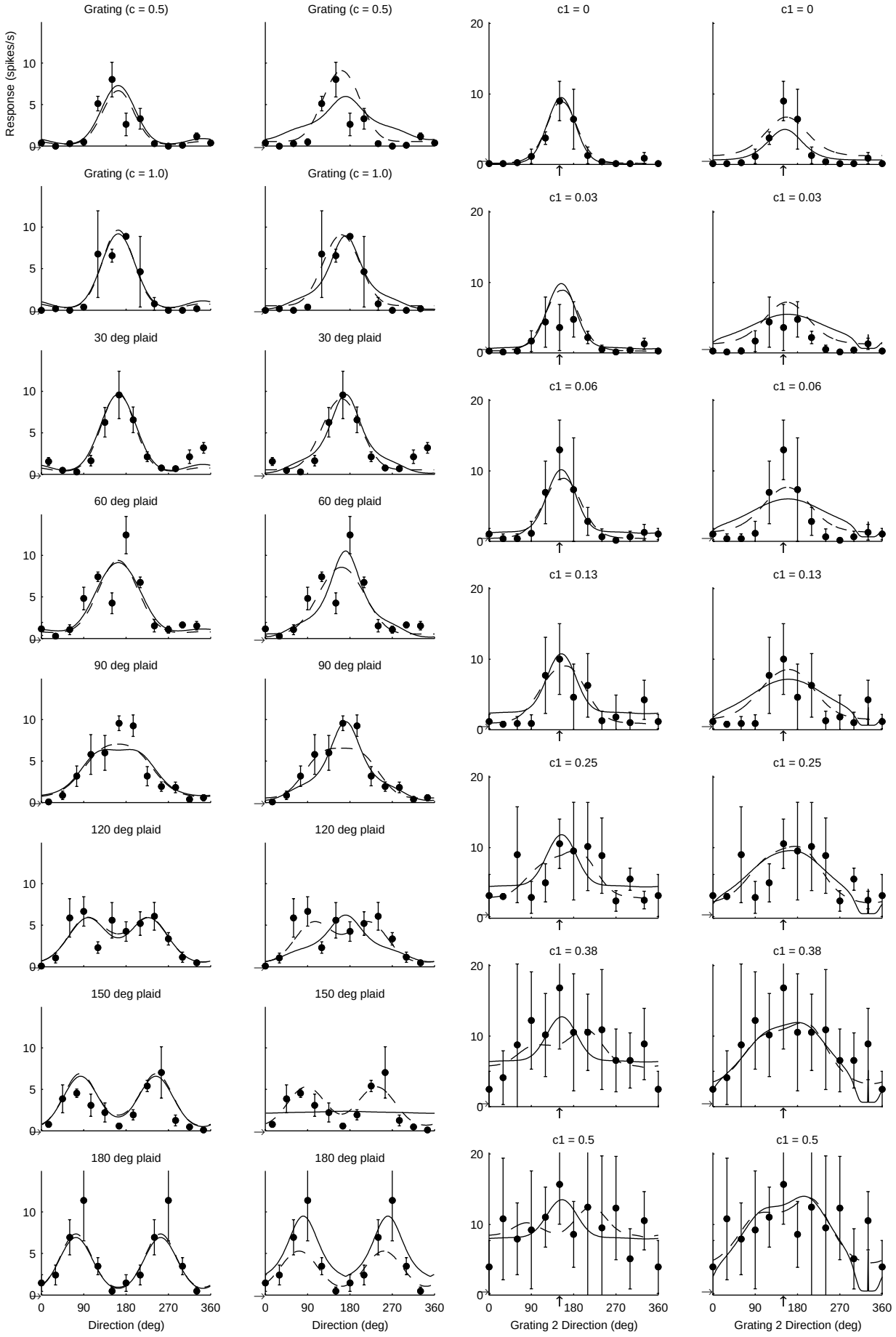

Component Model : 50%

SH−Component Model : 50%

Pattern Model : 42%

SH−Pattern Model : 46%

Component Model : 42%

SH−Component Model : 43%

Pattern Model : 36%

SH−Pattern Model : 38%

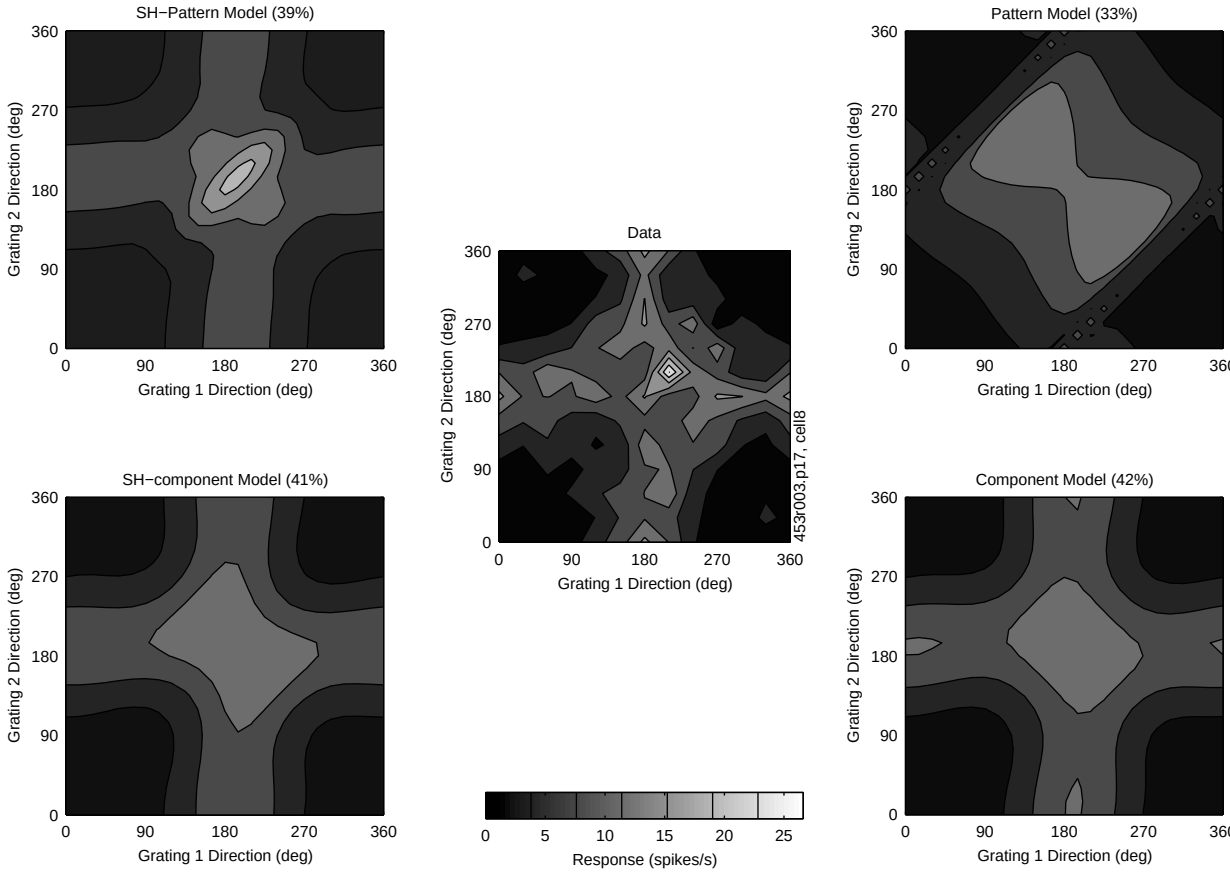
SH−Pattern Model (39%)
Pattern Model (33%)
Data
SH−component Model (41%)
Component Model (42%)
Grating 2 Direction (deg)
Grating 1 Direction (deg)
0
90
180
270
360
453r003.p17, cell8
0
5
10
15
20
25
Response (spikes/s)

Cell8

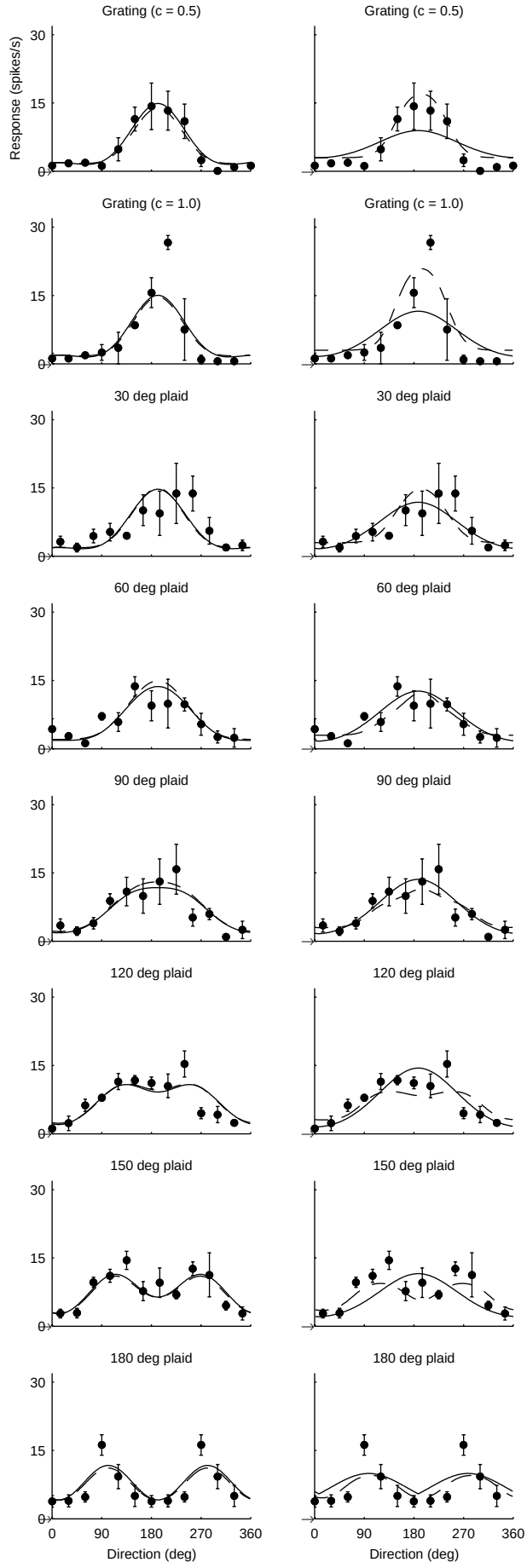

Component Model : 42%

SH−Component Model : 41%

Pattern Model : 33%

SH−Pattern Model : 39%

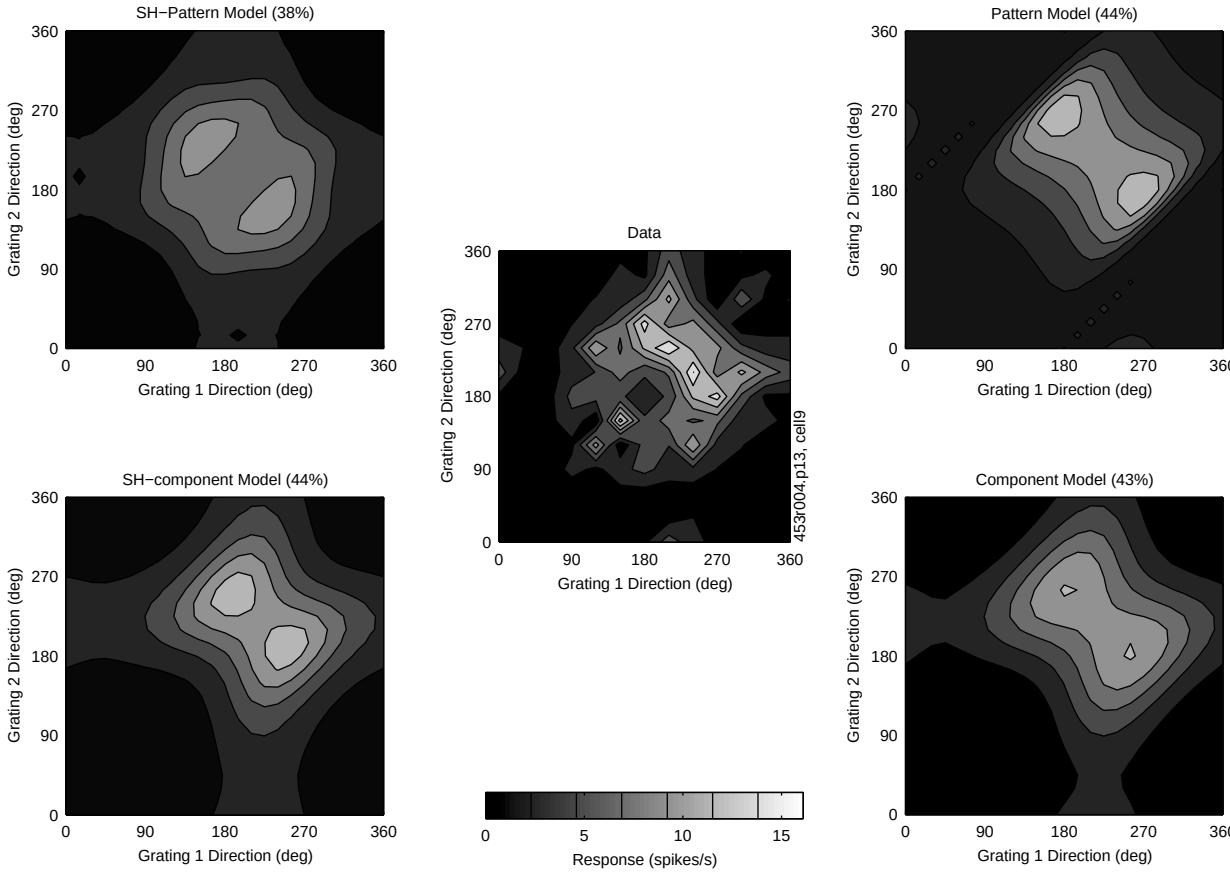
SH−Pattern Model (38%)
Data
Pattern Model (44%)
SH−component Model (44%)
Component Model (43%)
Grating 2 Direction (deg)
Grating 1 Direction (deg)
0
90
180
270
360
453r004.p13, cell9
0
5
10
15
Response (spikes/s)

Cell9

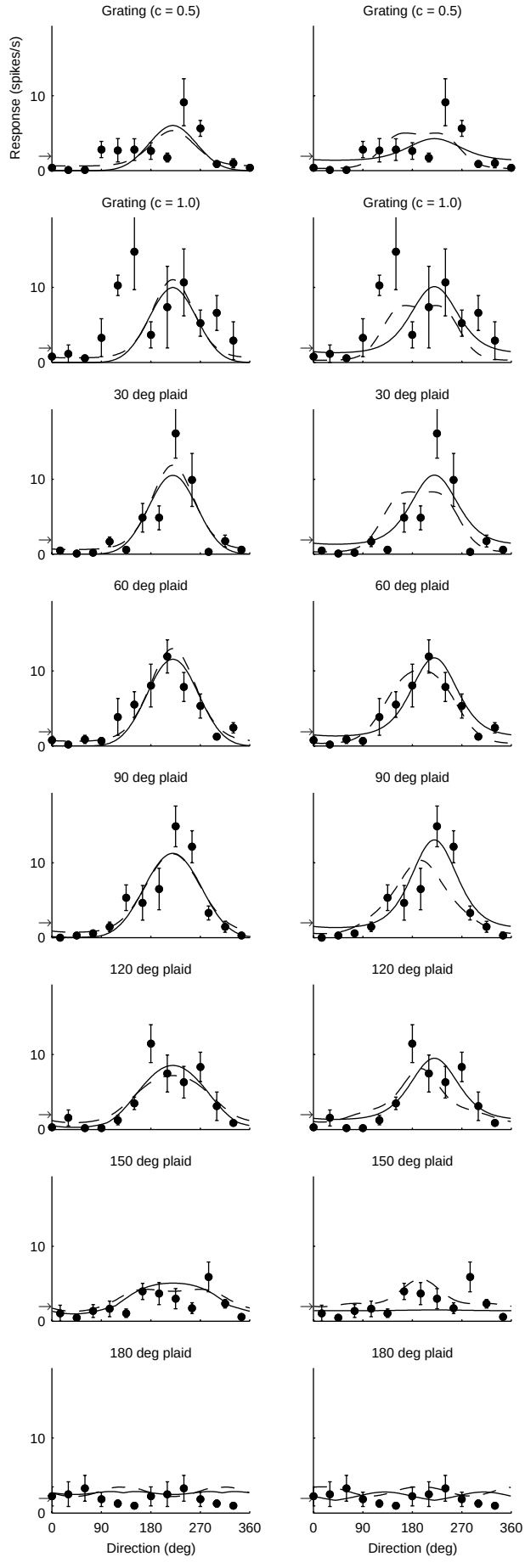

Component Model : 43%

SH−Component Model : 44%

Pattern Model : 44%

SH−Pattern Model : 38%

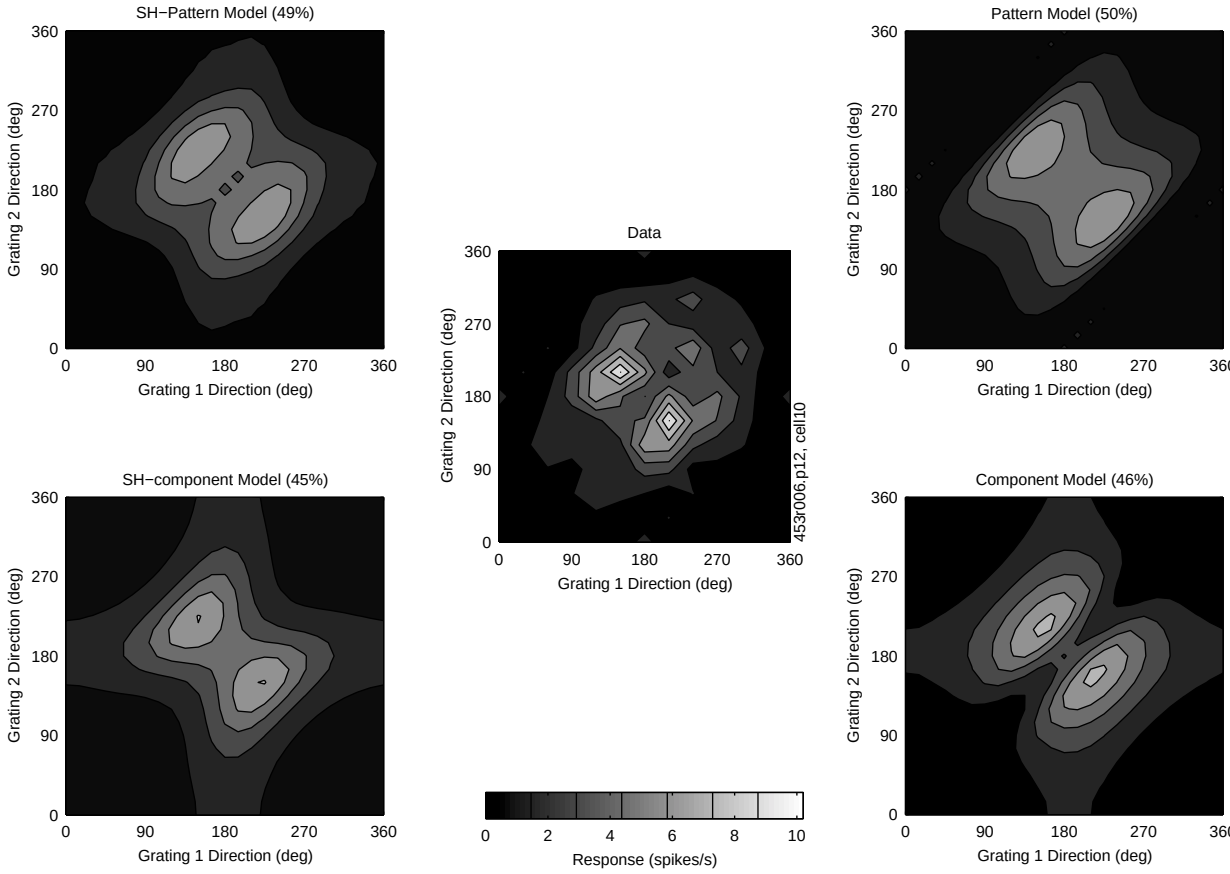
SH−Pattern Model (49%)
Pattern Model (50%)
Data
SH−component Model (45%)
Component Model (46%)
Grating 2 Direction (deg)
Grating 1 Direction (deg)
0
90
180
270
360
453r006.p12, cell10
0
2
4
6
8
10
Response (spikes/s)

Cell10

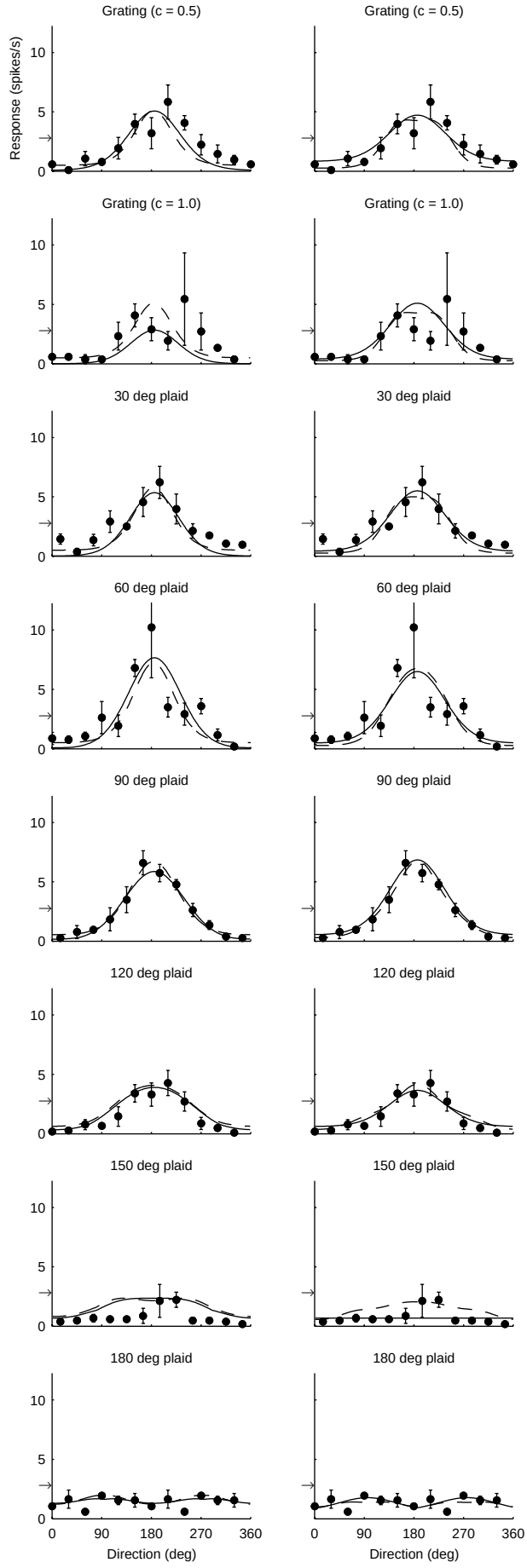

Component Model : 46%

SH−Component Model : 45%

Pattern Model : 50%

SH−Pattern Model : 49%

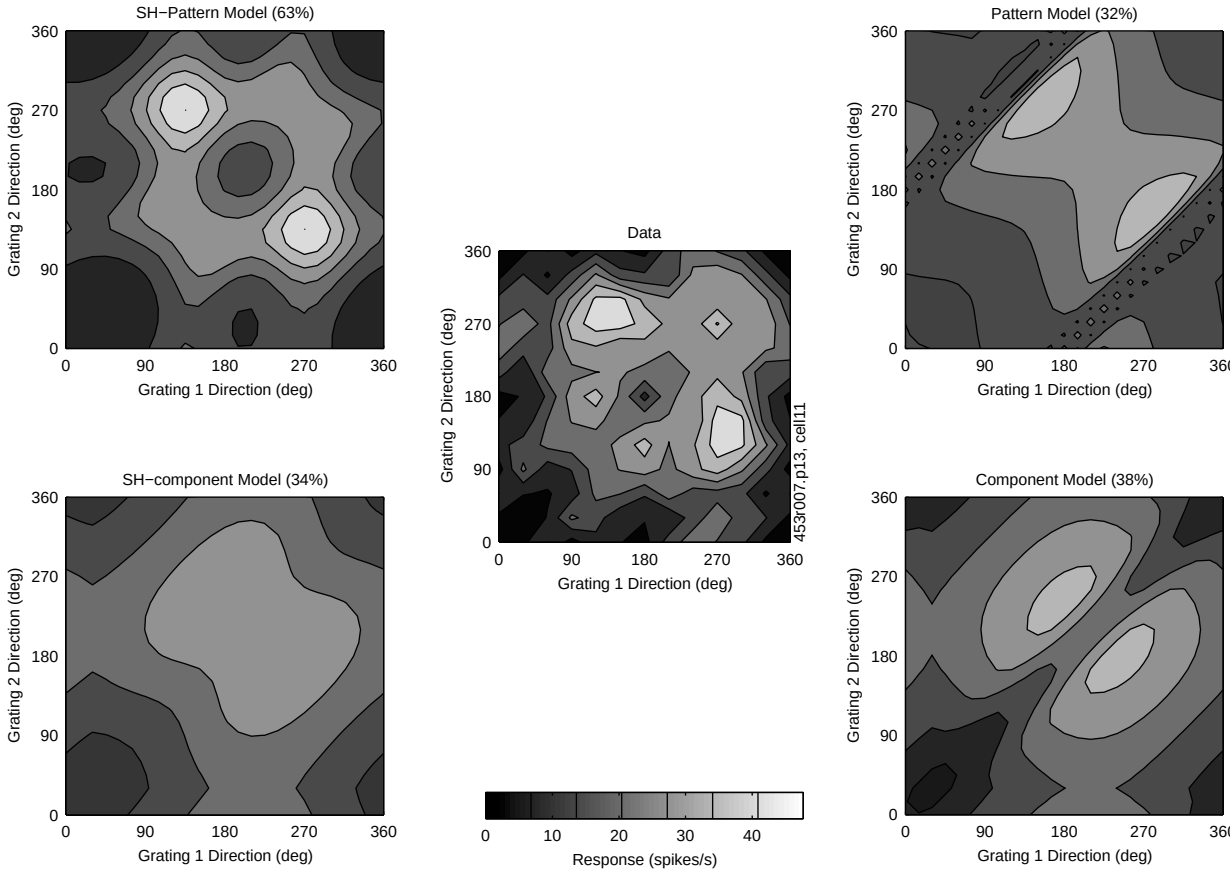
SH−Pattern Model (63%)
Pattern Model (32%)
Data
SH−component Model (34%)
Component Model (38%)
Grating 2 Direction (deg)
Grating 1 Direction (deg)
0
90
180
270
360
453r007.p13, cell11
0
10
20
30
40
Response (spikes/s)

Cell11

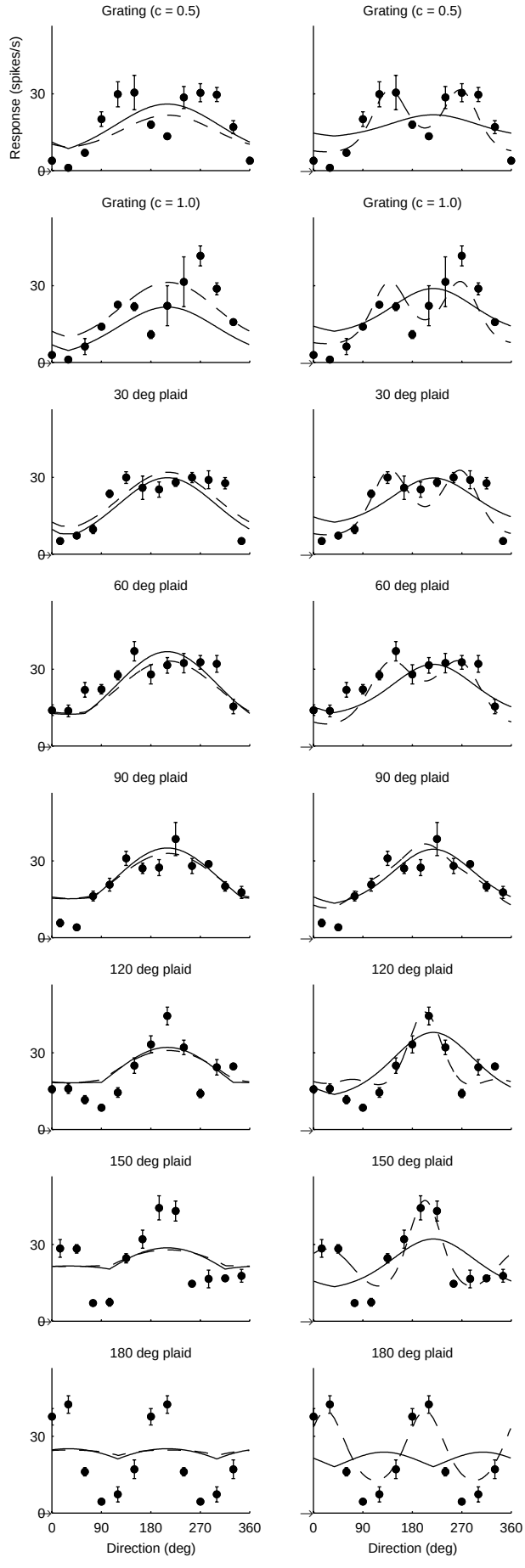

Component Model : 38%

SH−Component Model : 34%

Pattern Model : 32%

SH−Pattern Model : 63%

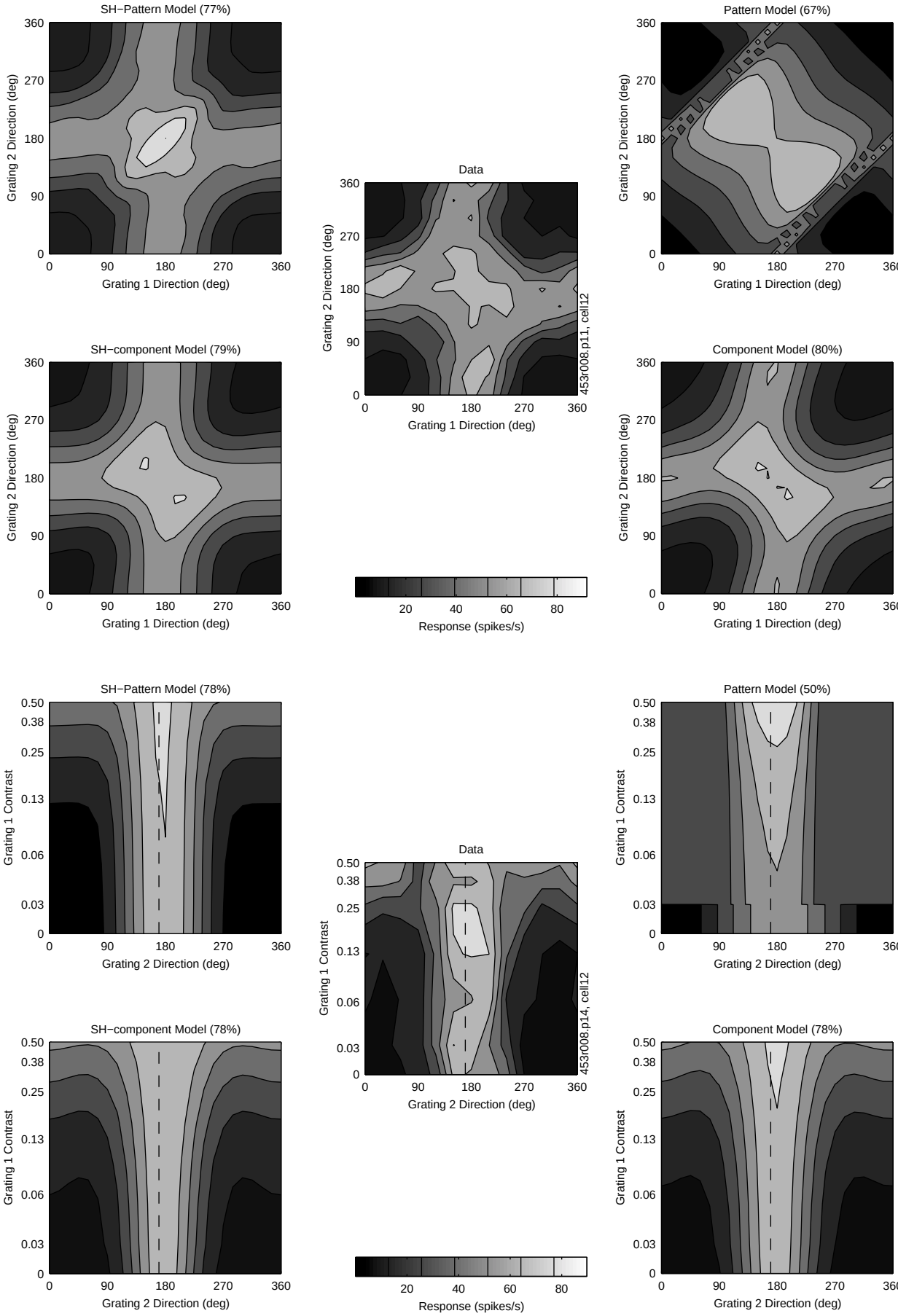
SH−Pattern Model (77%)
Data
Pattern Model (67%)
SH−component Model (79%)
Component Model (80%)
Grating 2 Direction (deg)
Grating 1 Direction (deg)
0
90
180
270
360
453r008.p11, cell12
20
40
60
80
Response (spikes/s)
SH−Pattern Model (78%)
Pattern Model (50%)
SH−component Model (78%)
Component Model (78%)
Grating 1 Contrast
0.50
0.38
0.25
0.13
0.06
0.03
453r008.p14, cell12

Cell12

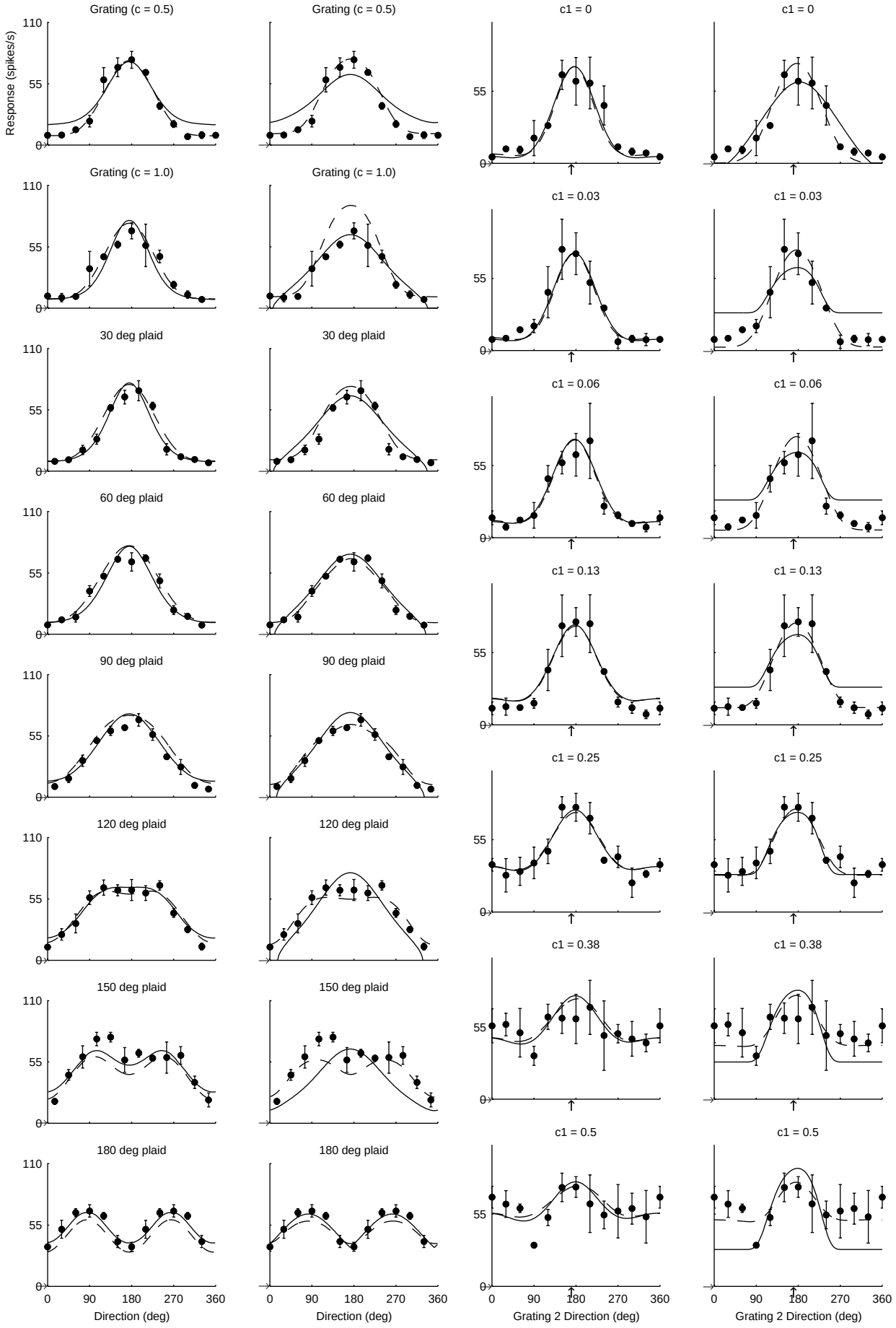

Component Model : 80%
SH−Component Model : 79%

Pattern Model : 67%
SH−Pattern Model : 77%

Component Model : 78%
SH−Component Model : 78%

Pattern Model : 50%
SH−Pattern Model : 78%

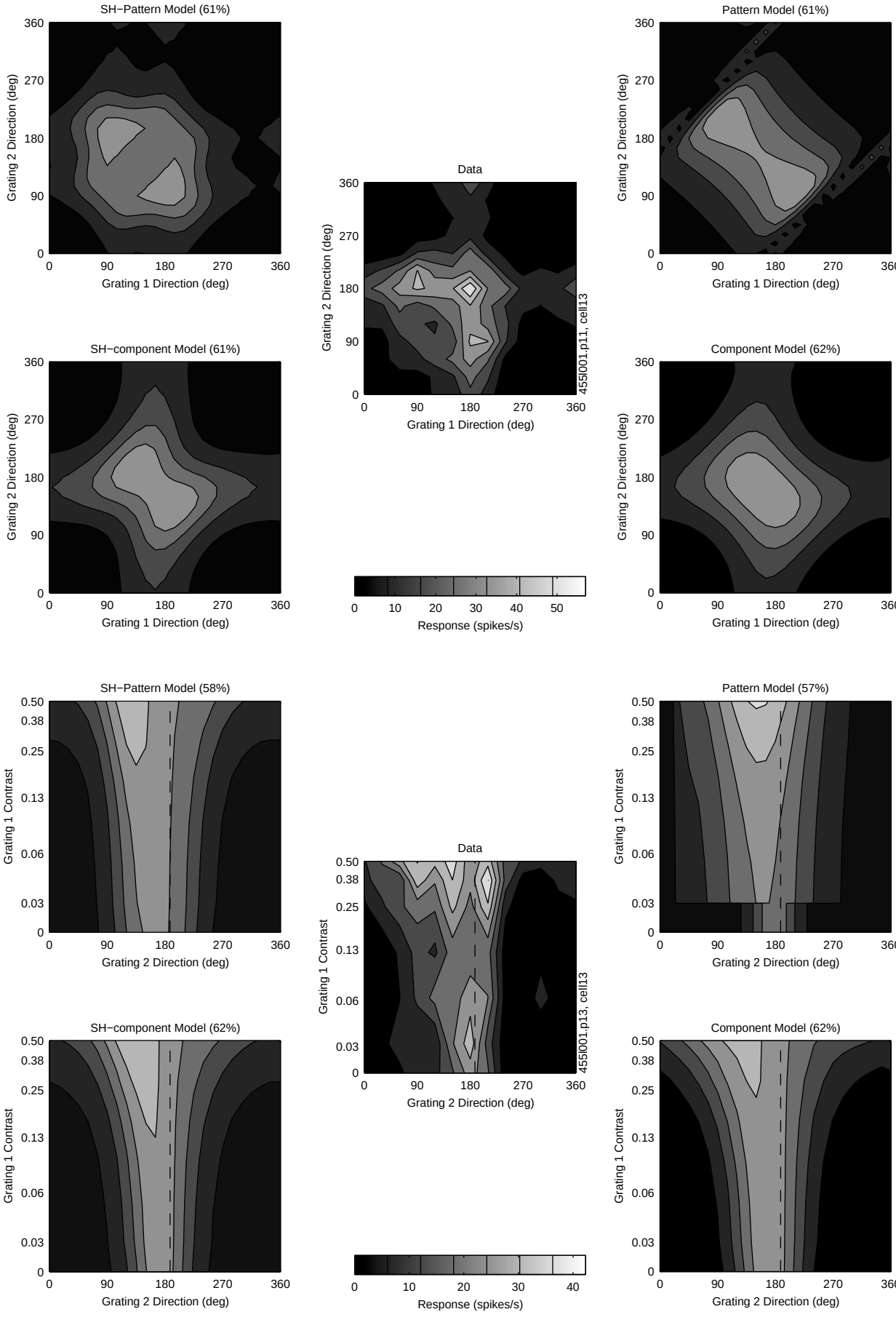
SH−Pattern Model (61%)
Pattern Model (61%)
Data
SH−component Model (61%)
Component Model (62%)
Grating 2 Direction (deg)
Grating 1 Direction (deg)
0
90
180
270
360
455l001.p11, cell13
0
10
20
30
40
50
Response (spikes/s)
SH−Pattern Model (58%)
Pattern Model (57%)
Data
SH−component Model (62%)
Component Model (62%)
Grating 1 Contrast
Grating 2 Direction (deg)
0.50
0.38
0.25
0.13
0.06
0.03
0
455l001.p13, cell13
0
10
20
30
40
Response (spikes/s)

Cell13

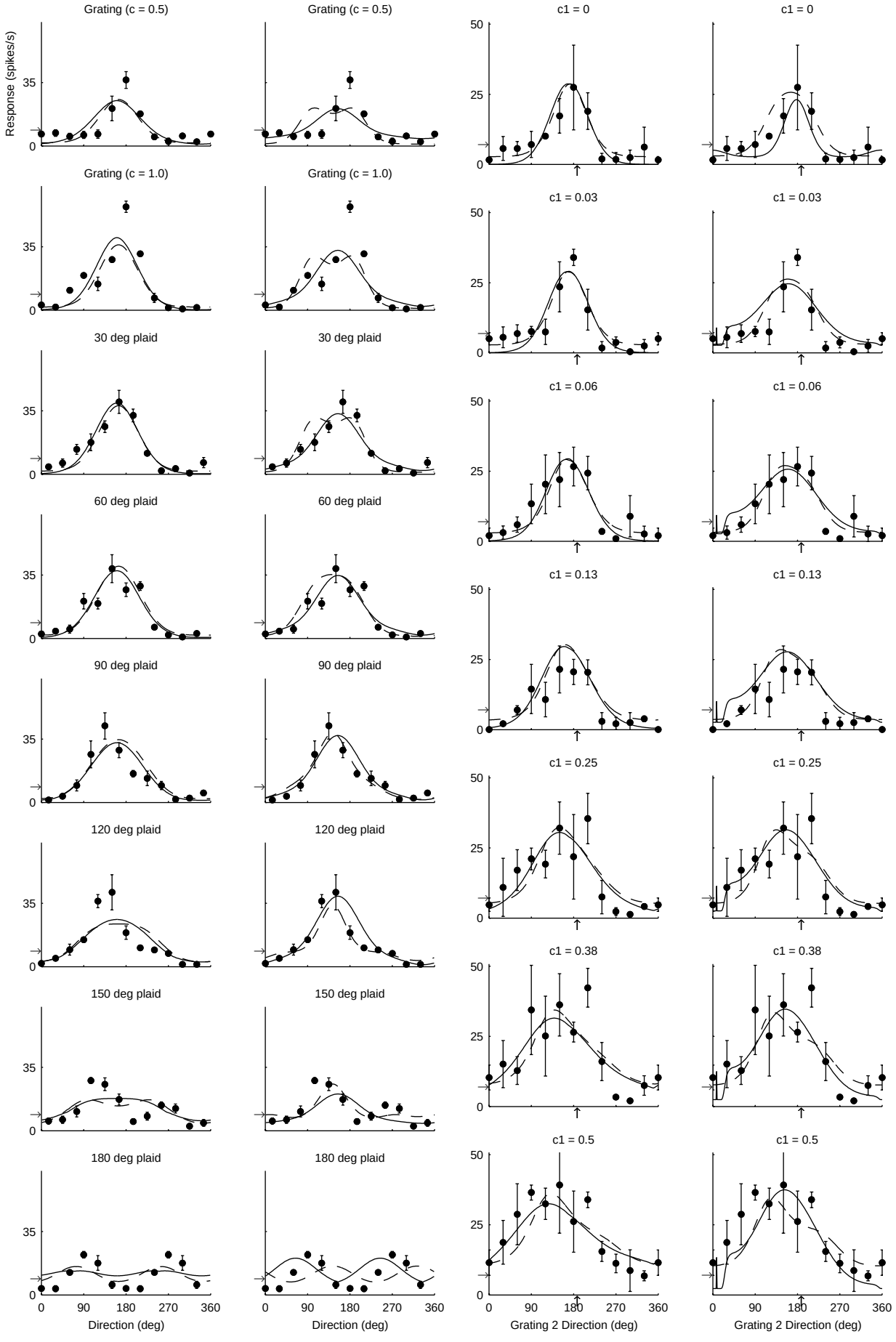

Component Model : 62%

SH−Component Model : 61%

Pattern Model : 61%

SH−Pattern Model : 61%

Component Model : 62%

SH−Component Model : 62%

Pattern Model : 57%

SH−Pattern Model : 58%

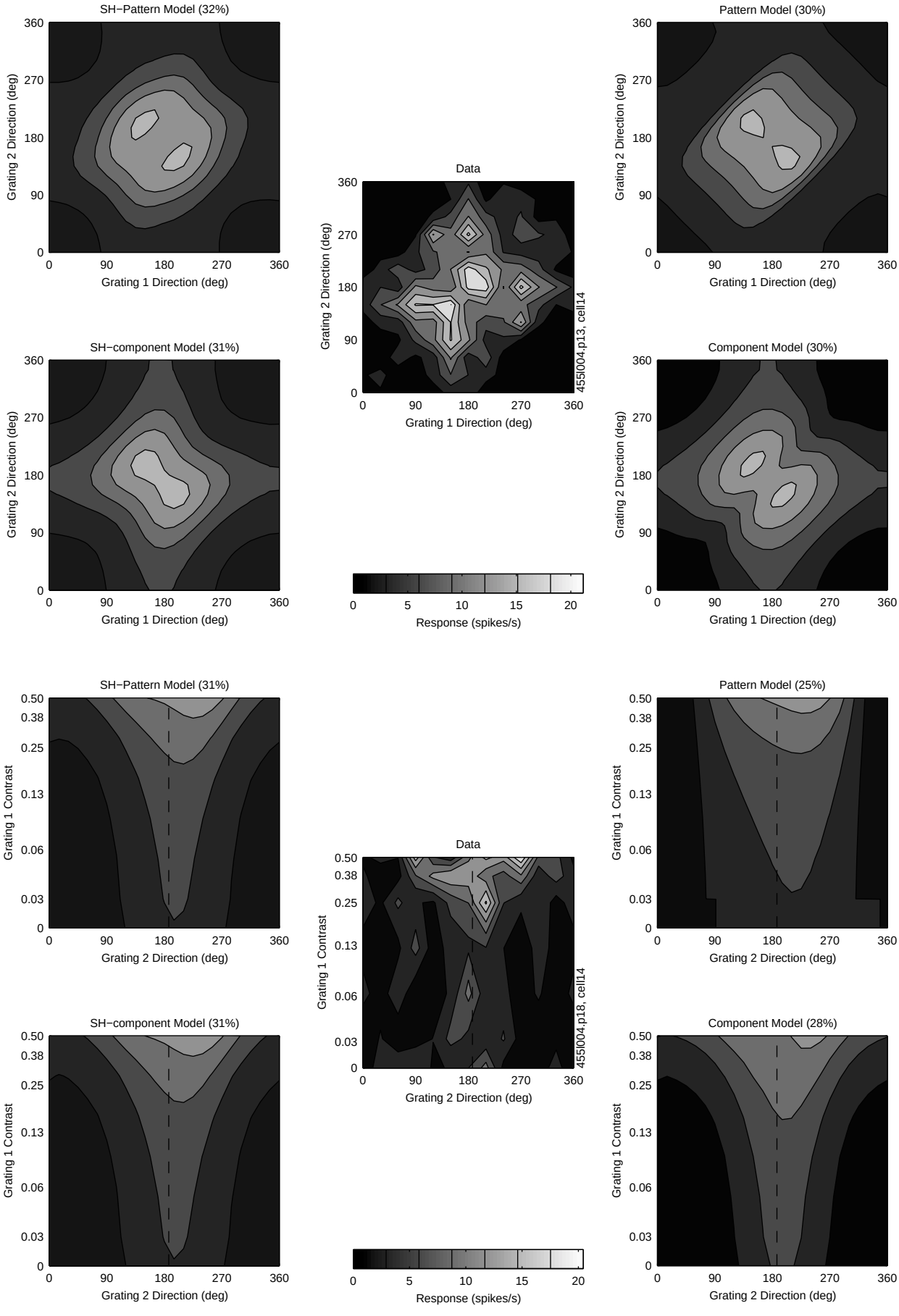
SH−Pattern Model (32%)
Data
Pattern Model (30%)
SH−component Model (31%)
Component Model (30%)
Grating 2 Direction (deg)
Grating 1 Direction (deg)
0
90
180
270
360
455l004.p13, cell14
Response (spikes/s)
0
5
10
15
20
SH−Pattern Model (31%)
Data
Pattern Model (25%)
SH−component Model (31%)
Component Model (28%)
Grating 1 Contrast
Grating 2 Direction (deg)
0.50
0.38
0.25
0.13
0.06
0.03
0
455l004.p18, cell14

Cell14

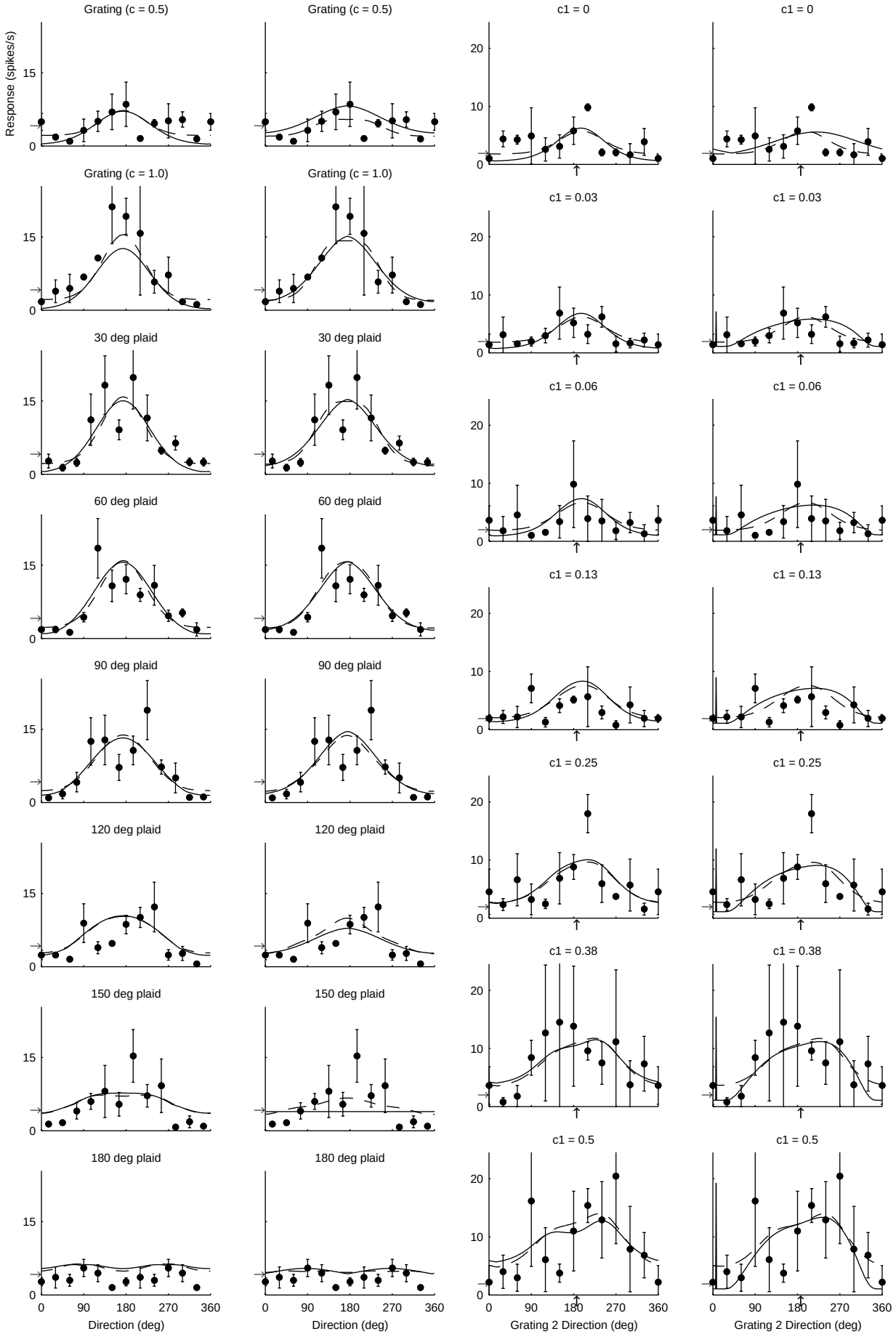

Component Model : 30%

SH−Component Model : 31%

Pattern Model : 30%

SH−Pattern Model : 32%

Component Model : 28%

SH−Component Model : 31%

Pattern Model : 25%

SH−Pattern Model : 31%

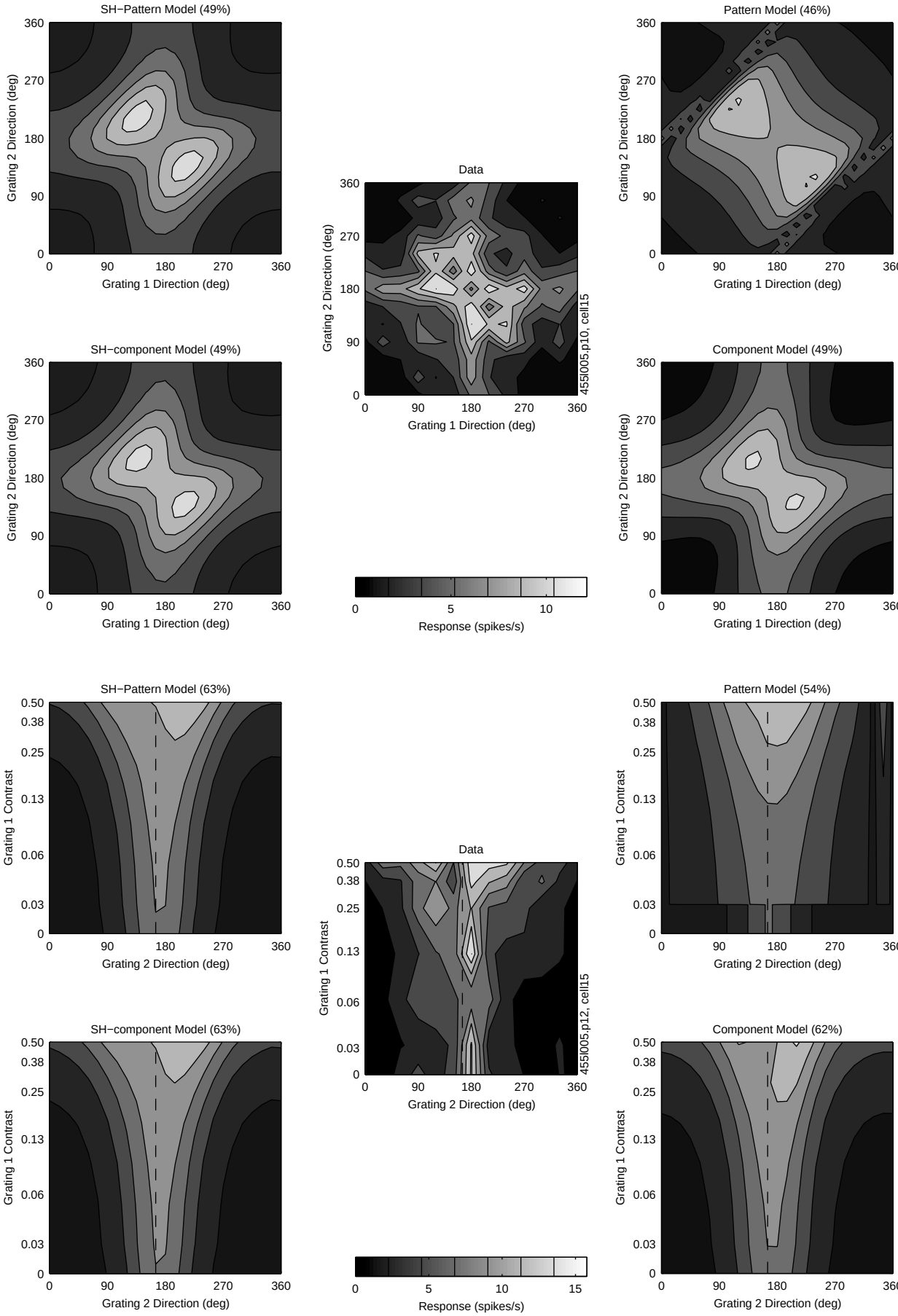
SH−Pattern Model (49%)
Data
Pattern Model (46%)
SH−component Model (49%)
Component Model (49%)
Grating 2 Direction (deg)
Grating 1 Direction (deg)
0
90
180
270
360
455l005.p10, cell15
0
5
10
Response (spikes/s)
SH−Pattern Model (63%)
Data
Pattern Model (54%)
SH−component Model (63%)
Component Model (62%)
Grating 1 Contrast
Grating 2 Direction (deg)
0.50
0.38
0.25
0.13
0.06
0.03
455l005.p12, cell15
0
5
10
15
Response (spikes/s)

Cell15

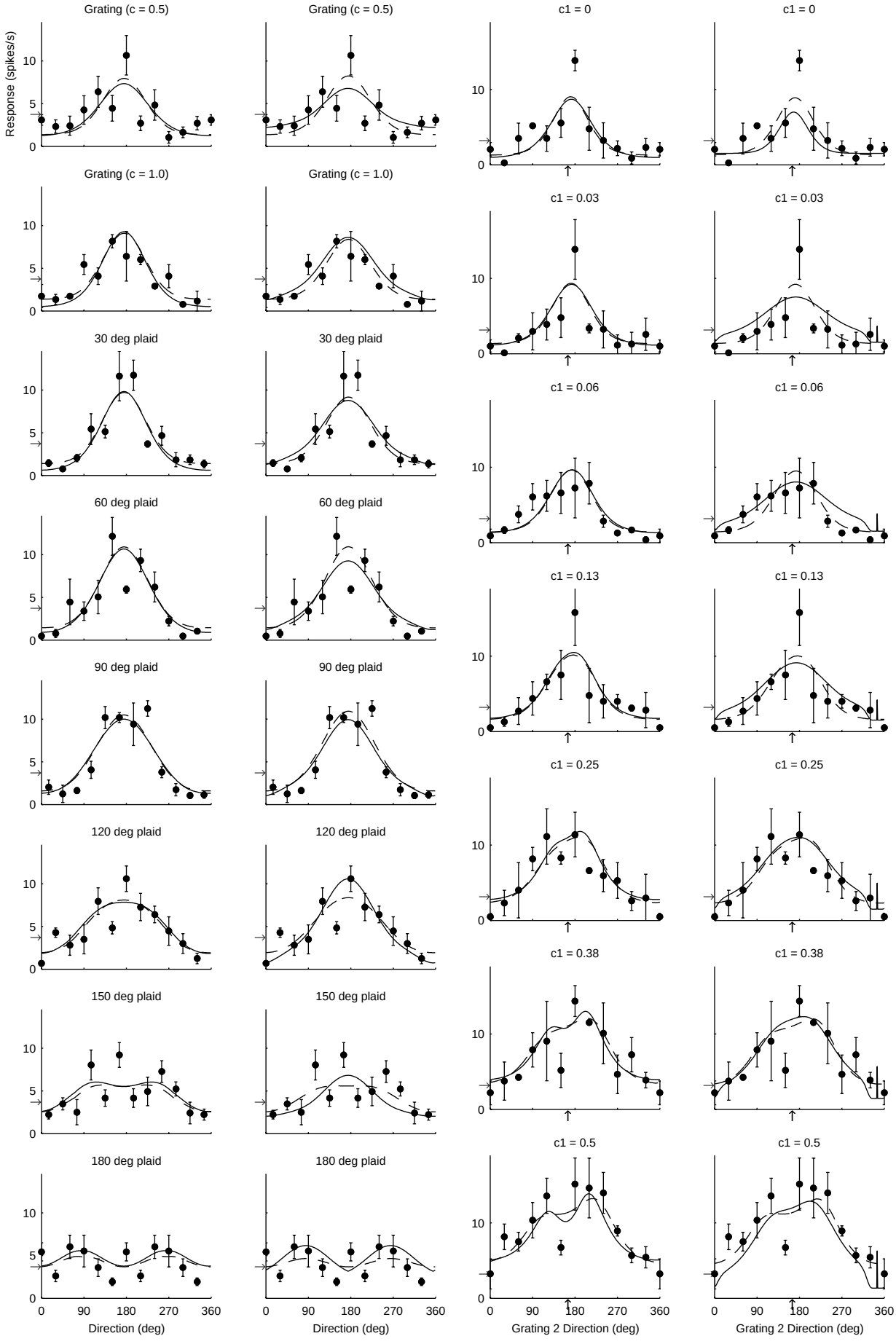

Component Model : 49%

SH−Component Model : 49%

Pattern Model : 46%

SH−Pattern Model : 49%

Component Model : 62%

SH−Component Model : 63%

Pattern Model : 54%

SH−Pattern Model : 63%

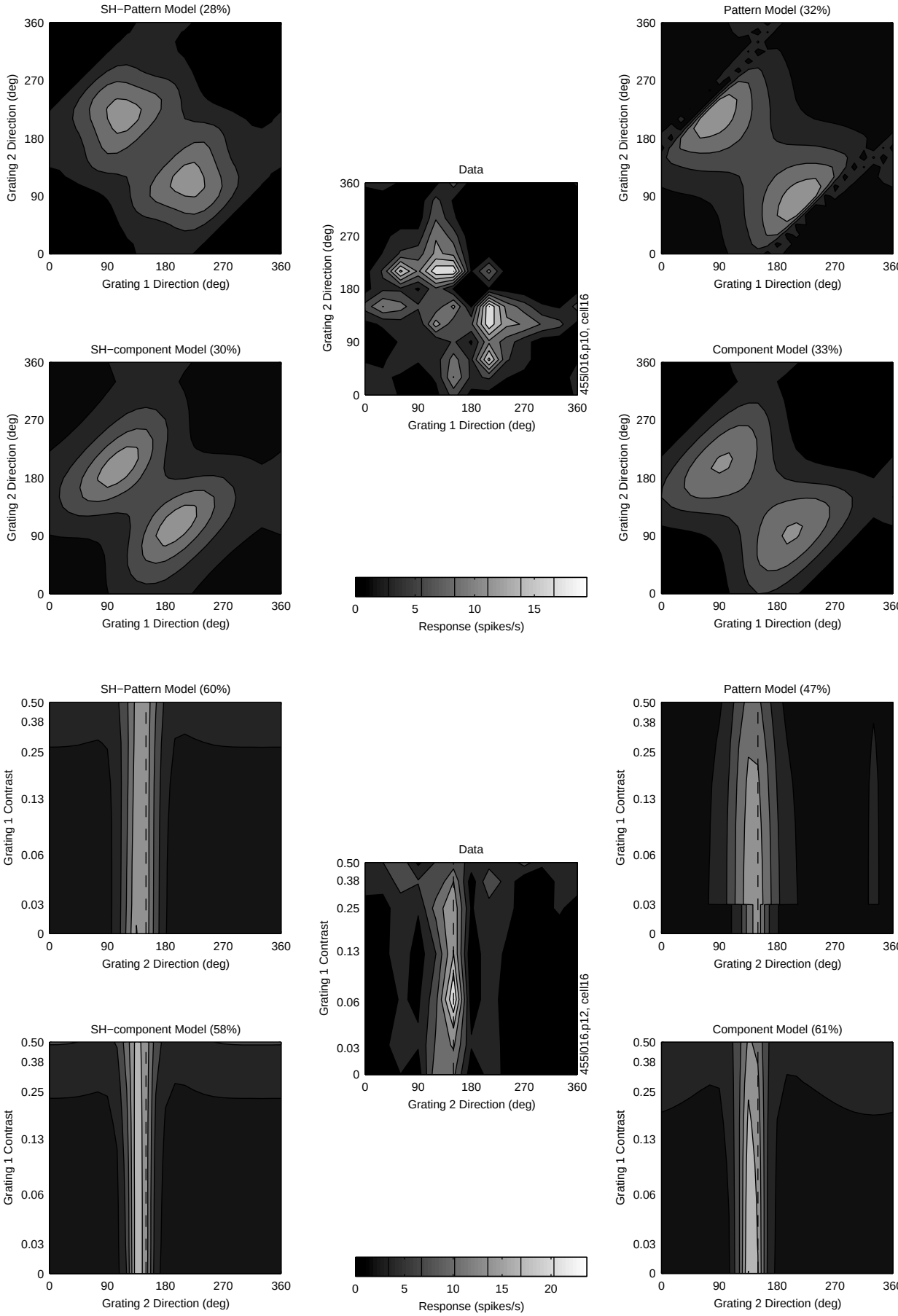
SH−Pattern Model (28%)
Pattern Model (32%)
Data
SH−component Model (30%)
Component Model (33%)
Grating 2 Direction (deg)
Grating 1 Direction (deg)
0
90
180
270
360
455l016.p10, cell16
0
5
10
15
Response (spikes/s)
SH−Pattern Model (60%)
Pattern Model (47%)
Data
SH−component Model (58%)
Component Model (61%)
Grating 1 Contrast
Grating 2 Direction (deg)
0.50
0.38
0.25
0.13
0.06
0.03
0
455l016.p12, cell16
0
5
10
15
20
Response (spikes/s)

Cell16

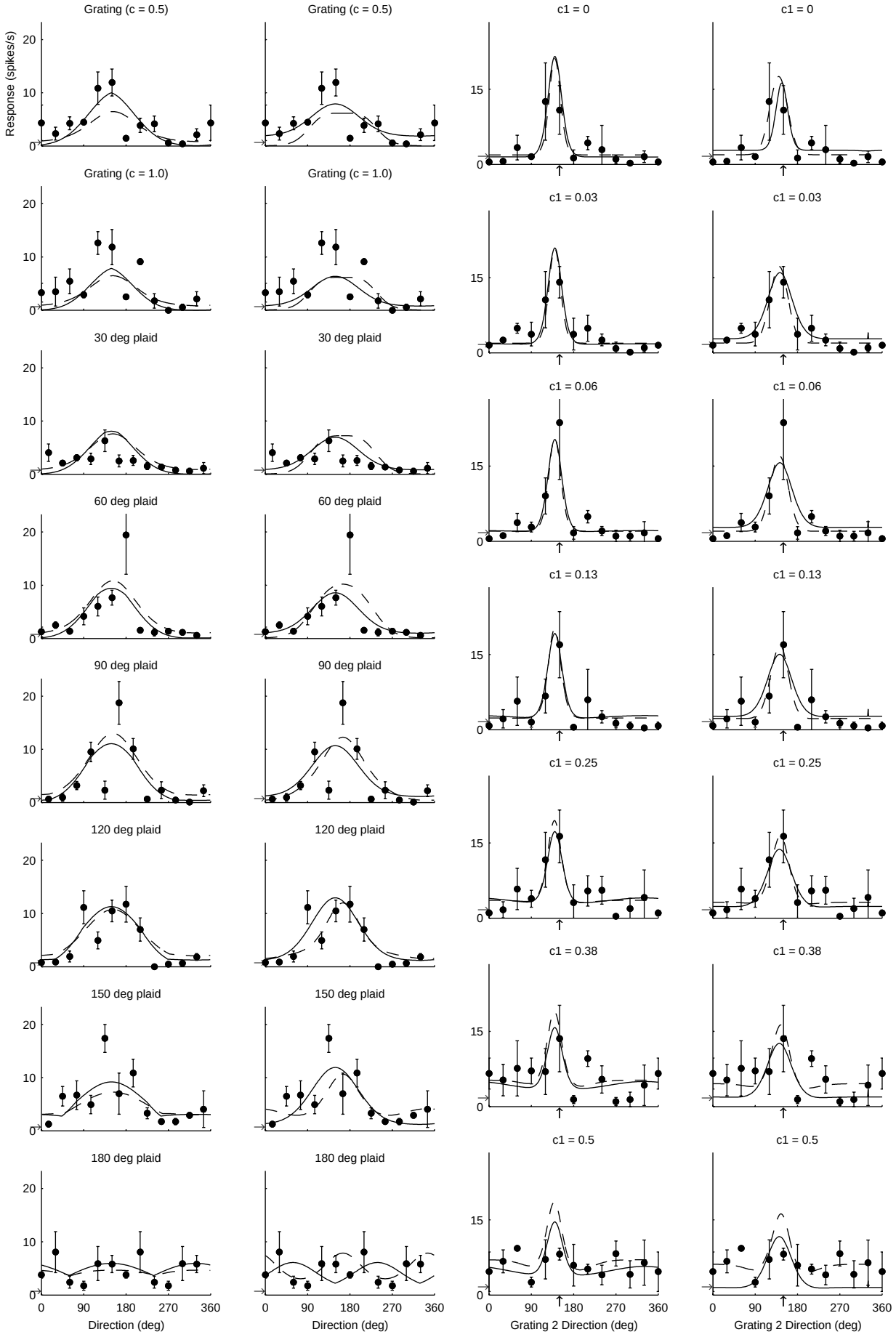

Component Model : 33%

SH−Component Model : 30%

Pattern Model : 32%

SH−Pattern Model : 28%

Component Model : 61%

SH−Component Model : 58%

Pattern Model : 47%

SH−Pattern Model : 60%

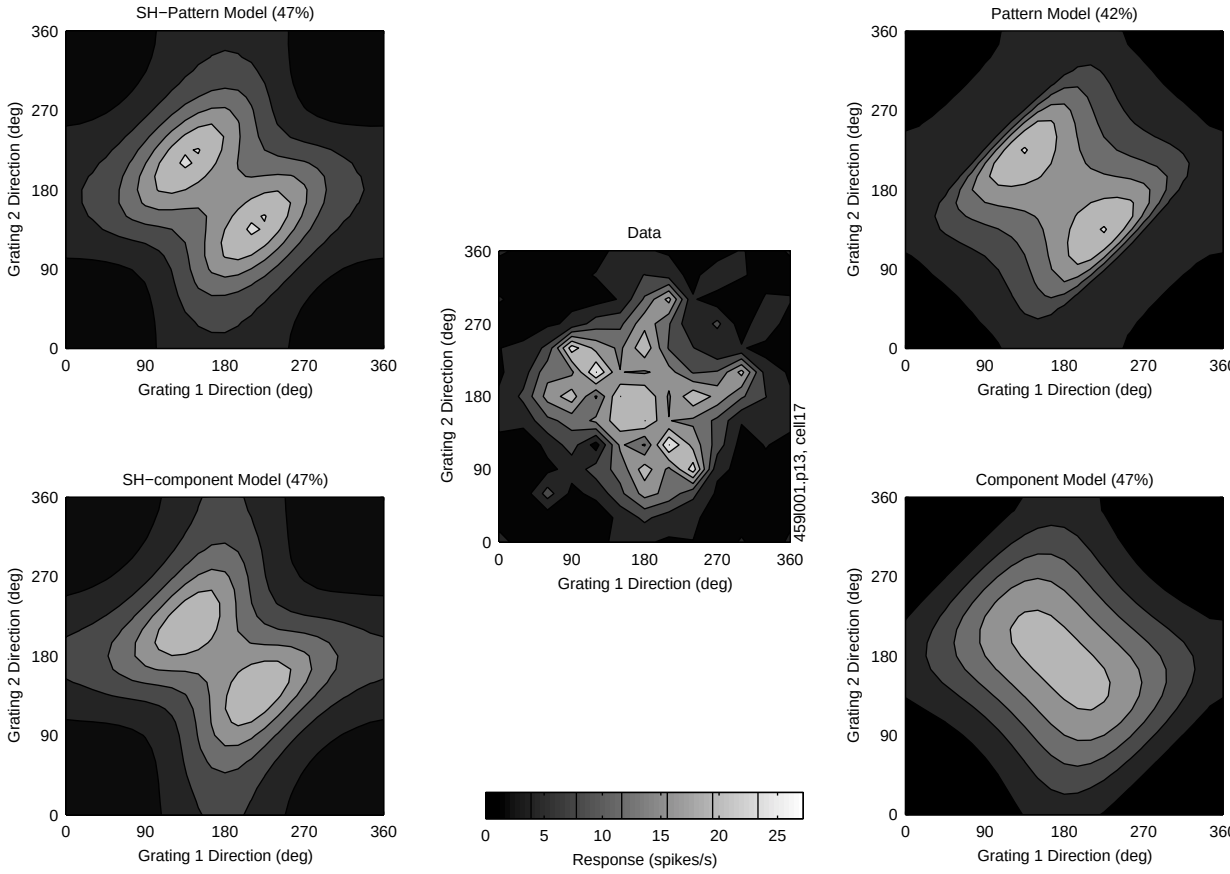
SH−Pattern Model (47%)
Data
Pattern Model (42%)
SH−component Model (47%)
Component Model (47%)
Grating 2 Direction (deg)
Grating 1 Direction (deg)
0
90
180
270
360
459l001.p13, cell17
0
5
10
15
20
25
Response (spikes/s)

Cell17

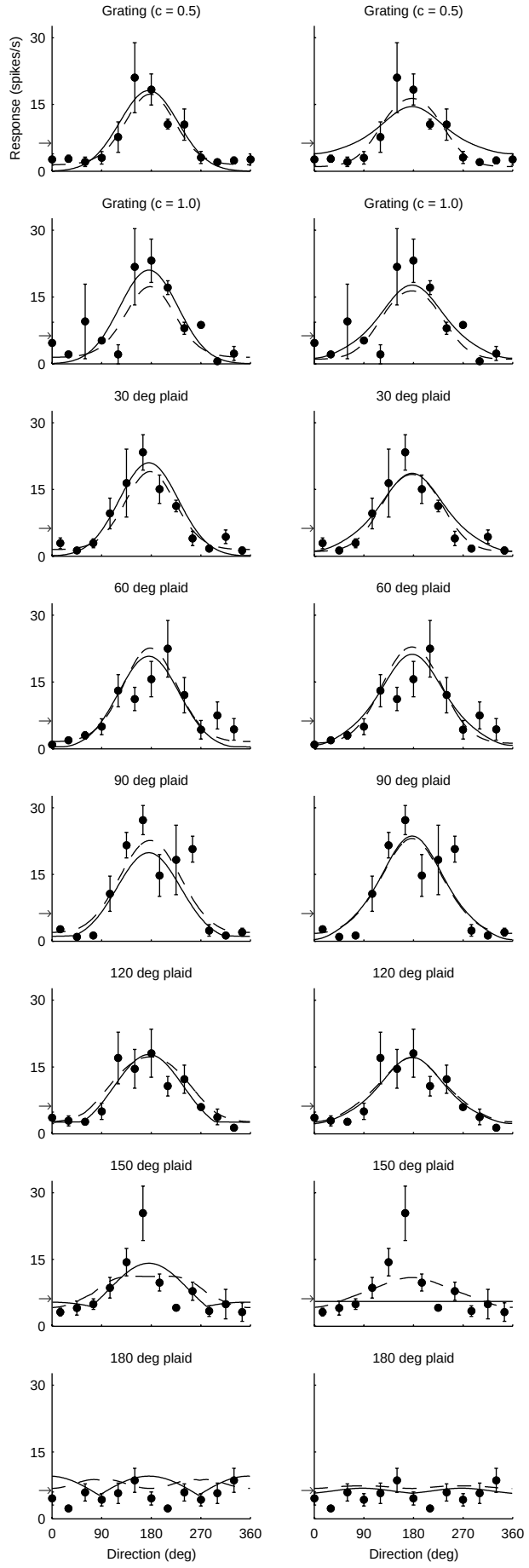

Component Model : 47%

SH−Component Model : 47%

Pattern Model : 42%

SH−Pattern Model : 47%

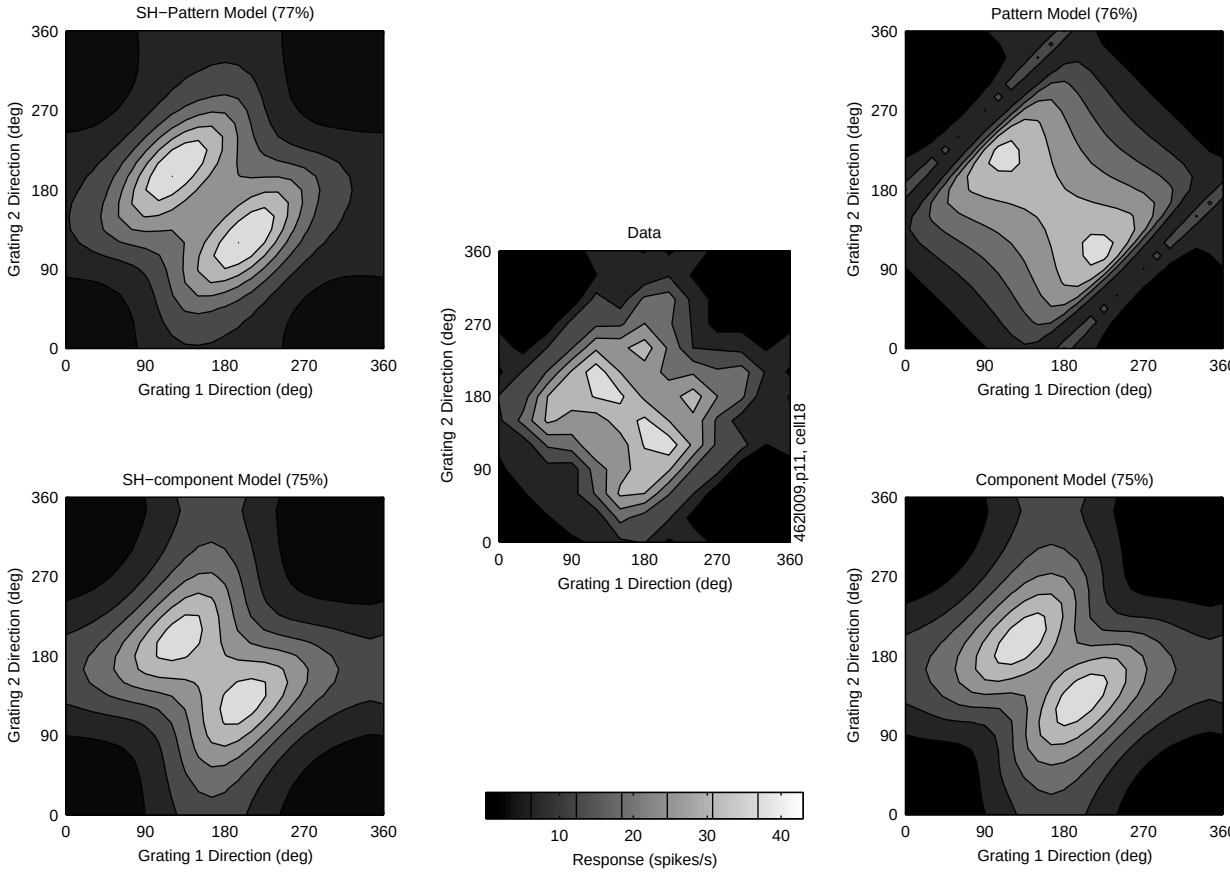
SH−Pattern Model (77%)
Pattern Model (76%)
Data
SH−component Model (75%)
Component Model (75%)
Grating 2 Direction (deg)
Grating 1 Direction (deg)
0
90
180
270
360
462l009.p11, cell18
10
20
30
40
Response (spikes/s)

Cell18

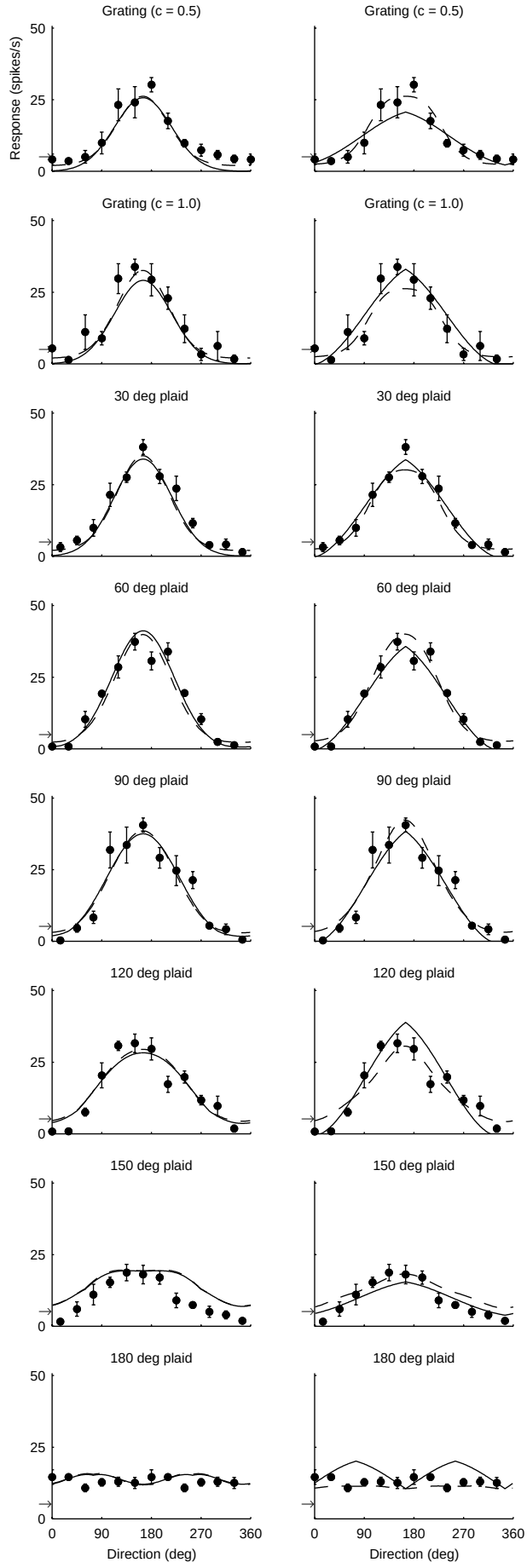

Component Model : 75%

SH−Component Model : 75%

Pattern Model : 76%

SH−Pattern Model : 77%

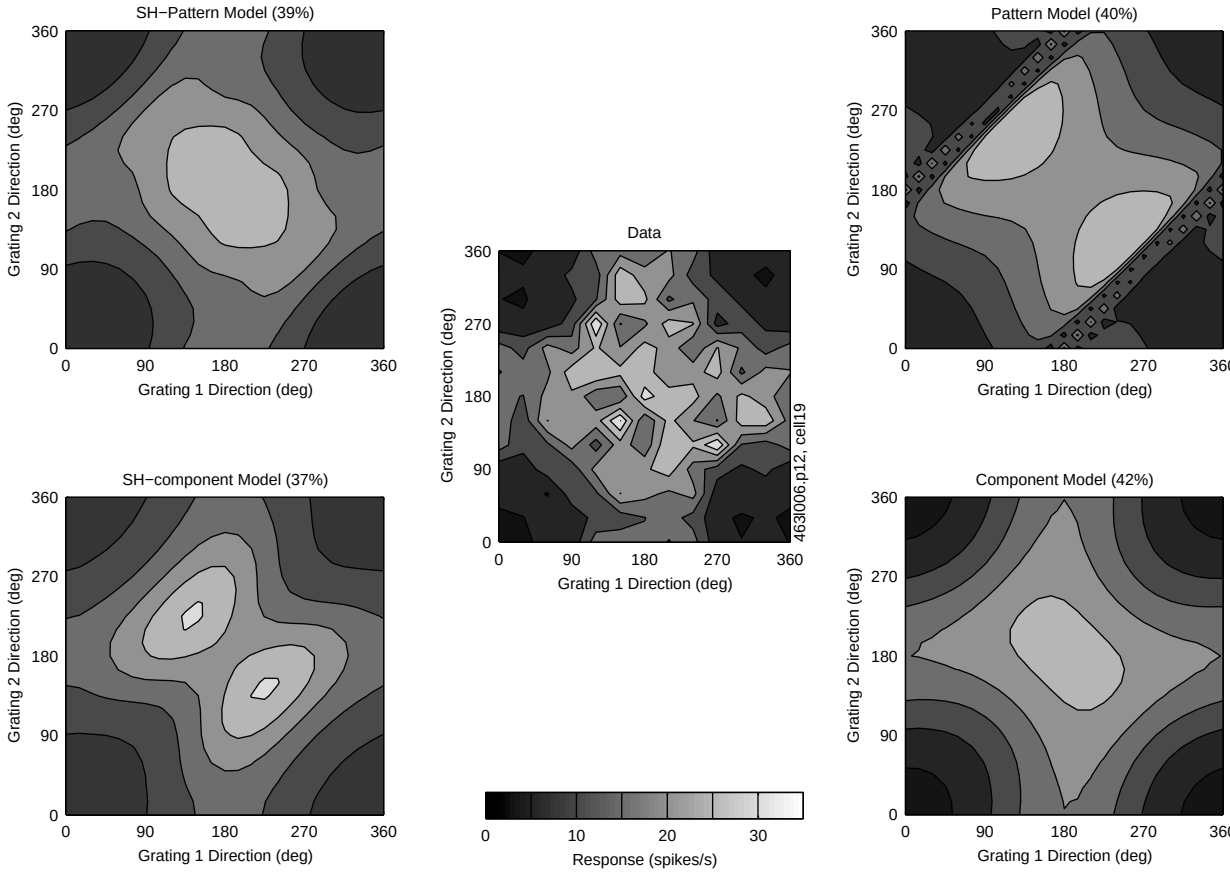
SH−Pattern Model (39%)
Pattern Model (40%)
Data
SH−component Model (37%)
Component Model (42%)
Grating 2 Direction (deg)
Grating 1 Direction (deg)
0
90
180
270
360
463l006.p12, cell19
Response (spikes/s)
10
20
30

Cell19

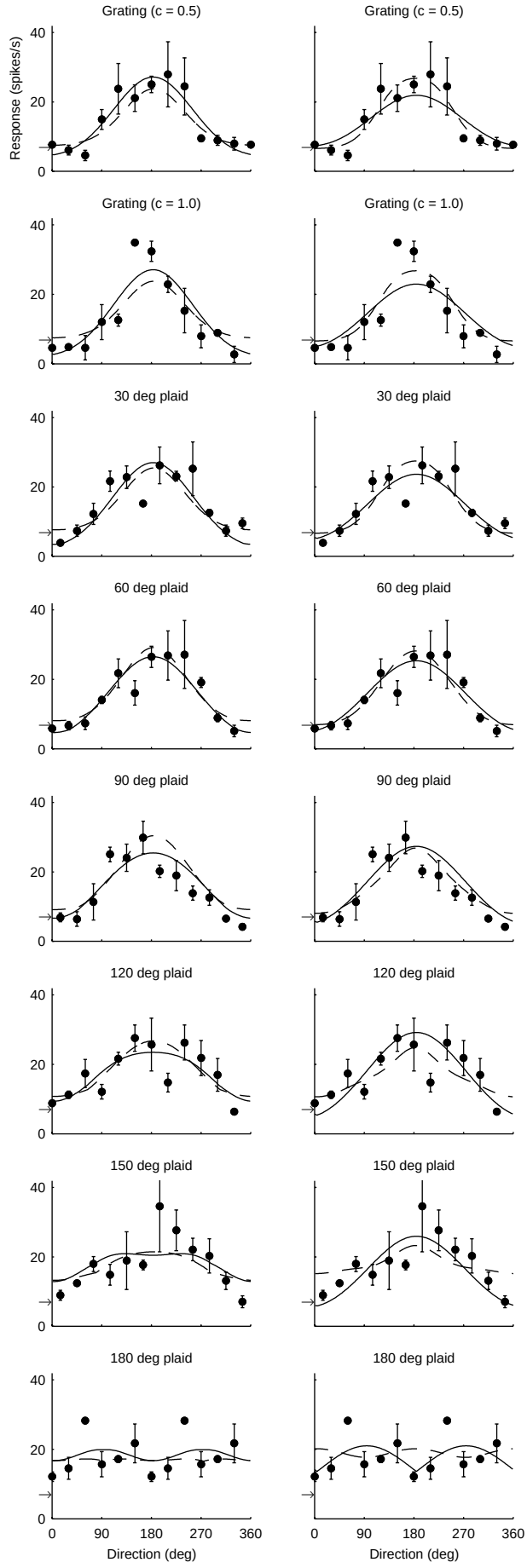

Component Model : 42%

SH−Component Model : 37%

Pattern Model : 40%

SH−Pattern Model : 39%